ESI for:

# *Sn,P*-coordinated Ru cation: A robust catalyst for aerobic oxidations of benzylamine and benzyl alcohol †

Michal Aman,[a] Libor Dostál ,[a] Aleš Růžička,[a] Jiří Tydlitát,[a] Jens Beckmann,[b] Jan Turek*[c] and Roman Jambor*[a]

*E-mail: roman.jambor@upce.cz

**Table of contents:**

## 1. Results and discussion

*Structure and NMR discussion in **2** – **4***

Ru(II) complexes **2** – **4** were characterized by NMR spectroscopy and X-ray diffraction analysis. Molecular structures of **2** – **4** confirmed substantial differences in the chelating behaviour of **1**. While the complex **2** consists of $\kappa^2$*Sn,P*-coordinated [($\kappa^2$-**1**)Ru($\eta^6$-cymene)Cl]$^+$ cation (**2**$^+$) that is compensated by Cl$^-$, compound **4** is a neutral $\kappa^2$*Sn,P*-coordinated complex [($\kappa^2$-**1**)Ru($\eta^5$-$C_5Me_5$)Cl] (Figure S1). Both compounds represent the typical octahedral three-legged piano stool structure.[S1] The Ru1-Cl1 bond distance (2.3936(6) Å) is shorter in **2** as compared to **4** (2.4692(12) Å) consistent with the cationic character of **2** (Ru1···Cl2 = 12.3739(9) Å). The Ru1-P1 (2.3293(6) Å) and Ru1-Sn1 (2.5953(4) Å) bond distances are, however, longer in **2** (*cf.* 2.2856(12) Å and 2.5503(4) Å in **4**). These values are comparable with those found in the related $\kappa^2$*Sn,P*-coordinated complex [($\kappa^2$*Sn,P*-SnCl($NCH_2P^tBu_2$)$_2C_6H_4$}Ru($\eta^6$-cymene)Cl].[S2] In contrast, compound **3** is a neutral $\kappa^1$*Sn*-coordinated complex [($\kappa^1$-**1**)$RuI_2$($\eta^6$-cymene)] with a similar octahedral arrangement of the Ru1 atom. The Ru1-P1 distance (4.936(3) Å) proved the absence of P→Ru coordination in **3**, while the Ru1-Sn1 bond length (2.6121(10) Å) is longer than in **2** and **4**. Nevertheless, all Ru-Sn bond lengths are comparable to those found in other Ru(II) complexes containing stannyl ligands.[S3]

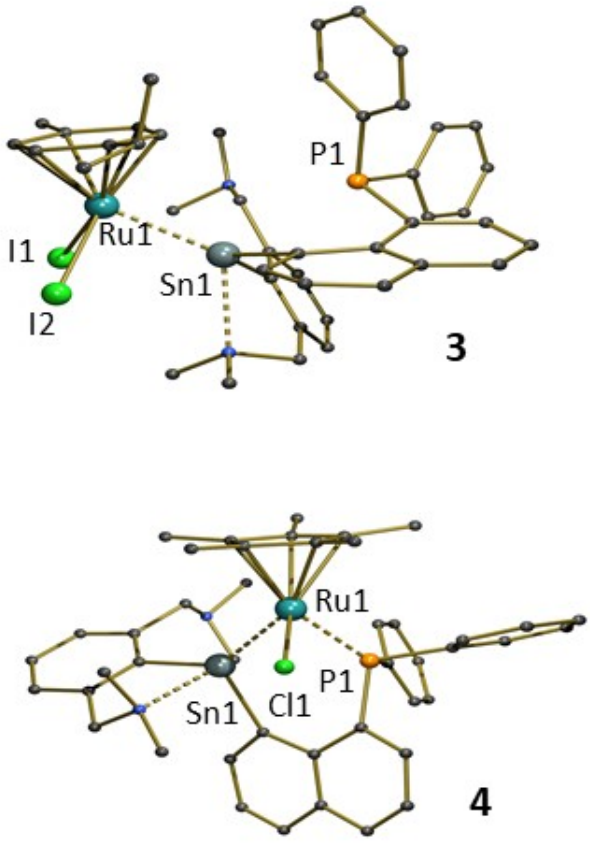


**Figure S1**. PovRay presentation of molecular structures of **3** and **4**

The $^{1}$H NMR spectra revealed one set of signals for all complexes. The $^{31}$P{$^{1}$H} NMR spectra of $\kappa^2$*Sn,P*-coordinated complexes showed signals at $\delta$ 36.2 ppm (for **2**) and 52.6 ppm (for **4**), shifted downfield in comparison with the starting **1** ($\delta$ -20.0 ppm). In contrast, the signal resonating at $\delta$ -19.4 ppm was observed in the $^{31}$P{$^{1}$H} NMR spectrum of **3**. This small shift, as compared to **1**, suggests the absence of the P→Ru coordination and confirms the $\kappa^1$*Sn*-coordination of **1** in solution. Similarly, the $^{119}$Sn{$^{1}$H} NMR spectra are a valuable tool to determine the coordination mode of **1**. The upfield shifted signals at $\delta$ 106.6 ppm with $J_{P,Sn}$ = 651 Hz and at $\delta$ 28.3 ppm with $J_{P,Sn}$ = 38 Hz were observed for **2** and **3,** respectively (*cf.* $\delta$ 158.0 ppm, $J_{P,Sn}$ = 572 Hz for **1**). The signal of **4**, on the other hand, appears downfield at $\delta$ 340.2 ppm with $J_{P,Sn}$ = 538 Hz. While the higher values of $J_{P,Sn}$ are similar to those found in $\kappa^2$*Sn,P*-coordinated complexes of Ru, Rh or Ir,[S4] a lower $J_{P,Sn}$ corroborates the $\kappa^1$*Sn*-coordination in **3**.

## 2. Theoretical studies

*Structure and bonding in **2 - 4***

Compounds **2** - **4** (Figure S2) were further investigated by using the natural bond orbital (NBO) analysis[S5] (Figure S3). The natural population analysis (NPA) charges[S5] and the Wiberg bond indices (WBI)[S6] are collected in Table S1 along with the most relevant geometrical parameters. The Ru-Sn interactions in all complexes show significant covalent character with the $WBI_{Ru-Sn}$ values around 0.7.

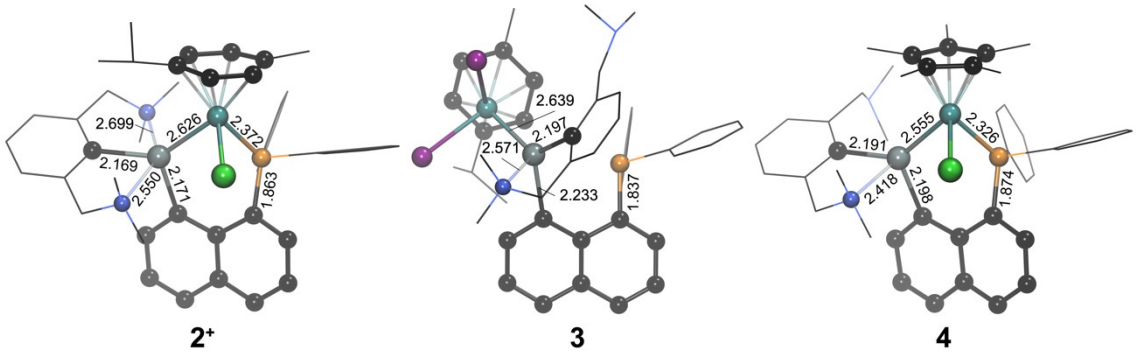


**Figure S2.** Optimized geometries of compounds **2**$^{+}$-**4** (hydrogen atoms are omitted for clarity) along with selected bond distances (in Å).

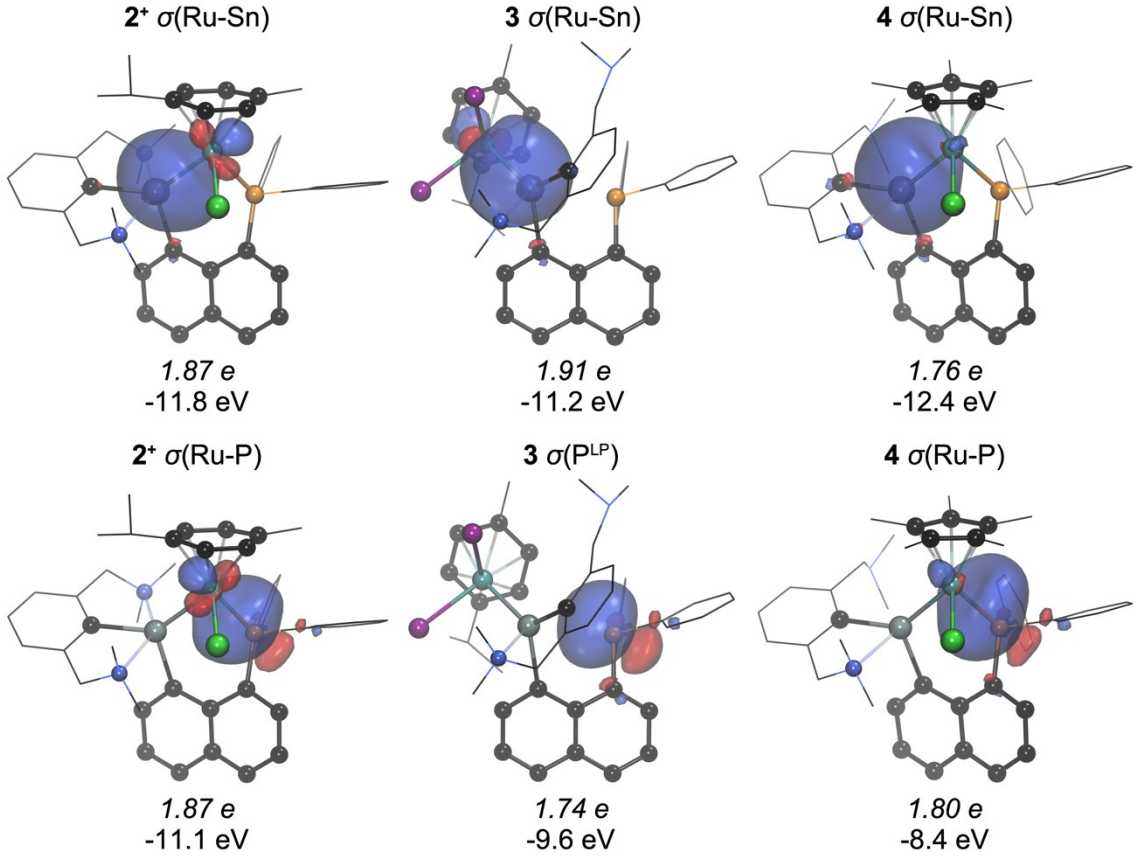


**Figure S3.** Relevant NBOs (isosurface 0.03 a.u.) involving P, Sn and Ru atoms in **2**$^{+}$-**4**. NBO populations and orbital energies are also displayed.

**Table S1.** Selected bond lengths (*d*; in Å), Wiberg bond indices (WBI), and NPA atomic charges (*q*; in *e*) for **2**-**4**.

| | **1** | **2** | **2Sn** | **2P** | **3** | **4** |
|---|---|---|---|---|---|---|
| $d_{Ru\text{-}Sn}$[a] | | 2.626<br>*2.595* | 2.633 | | 2.639<br>*2.612* | 2.555<br>*2.550* |
| $WBI_{Ru\text{-}Sn}$ | | 0.679 | 0.715 | | 0.740 | 0.782 |
| $d_{Ru\text{-}P}$[a] | | 2.372<br>*2.329* | | 2.428 | | |
| $WBI_{Ru\text{-}P}$ | | 0.711 | | 0.705 | | 0.712 |
| $d_{Sn\text{-}N}$[a] | 2.690<br>2.736<br>*2.525*<br>*2.659* | 2.550<br>2.699<br>*2.524*<br>*2.667* | 2.562 | 2.699<br>2.757 | 2.571<br><br>*2.454* | 2.418<br><br>*2.353* |
| $WBI_{Sn\text{-}N}$ | 0.145<br>0.119 | 0.135<br>0.114 | 0.147 | 0.135<br>0.121 | 0.142 | 0.162 |
| $q_{Ru}$ | | -1.08 | -0.78 | -0.55 | -1.10 | -1.13 |
| $q_{Sn}$ | 1.04 | 2.08 | 1.82 | 1.15 | 1.84 | 1.91 |
| $q_{P}$ | 0.88 | 1.33 | 0.92 | 1.27 | 0.92 | 1.29 |

[a]Experimental values in italics.

To shed more light on the formation of **2**, two plausible isomers **2Sn** ($\kappa^1$Sn coordination similar to **3**) and **2P** ($\kappa^1$P-coordinated complex) were also optimized (Figure S4). The thermodynamic data suggest an equilibrium between isomers **2** and **2Sn** with a relative Gibbs free energy difference of less than 2 kcal mol$^{-1}$, while **2P** was found to be 16.3 kcal mol$^{-1}$ higher in energy (Figure S4). These findings correlate well with the experimental data showing no evidence for the formation of the $\kappa^1$P-coordinated complex.

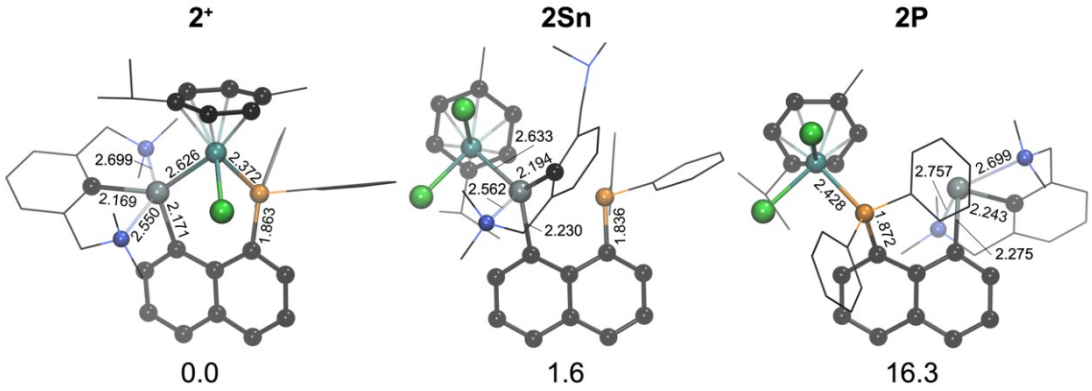


**Figure S4.** Optimized geometries of the three different isomers of **2** (hydrogen atoms are omitted for clarity) along with selected bond distances (in Å) and relative Gibbs free energies (in kcal mol$^{-1}$; calculated in benzene at the B3LYP-D3BJ/cc-pVTZ(-PP) level).

*Catalytic cycle*

**Table S2.** Gibbs free energy differences ($\Delta G$; in kcal mol$^{-1}$) for the consecutive steps of the suggested catalytic cycle.

| | $\Delta G$(DZ)[a] | $\Delta G$(TZ)[b] | $\Delta G^{solv}$(TZ)[c] |
|---|---|---|---|
| **2**$^+$ → **2**$^+$Int1A | -3.6 | -1.2 | |
| **2**$^+$Int1A → **2**$^+$Int2A | -2.3 | -9.2 | |
| **2**$^+$Int2A → **2**$^+$Int3 | 5.4 | -0.1 | |
| **2**$^+$Int3 → **2**$^+$ | -76.4 | -79.3 | |
| **2**$^+$ → **2**$^+$Int1B | 8.6 | 12.8 | 14.4 |
| **2**$^+$Int1B → **2**$^+$Int2B | -23.6 | -31.2 | -37.2 |
| **2**$^+$Int2B → **2**$^+$Int3 | 0.3 | -3.9 | -7.6 |
| **2**$^+$Int3 → **2**$^+$ | -76.4 | -79.3 | -75.2 |

[a]Calculated at the B3LYP-D3BJ/cc-pVDZ-PP level of theory; [b]Calculated at the B3LYP-D3BJ/cc-pVTZ-PP level of theory; [c]Calculated at the B3LYP-D3BJ/cc-pVTZ-PP level of theory in benzyl alcohol.

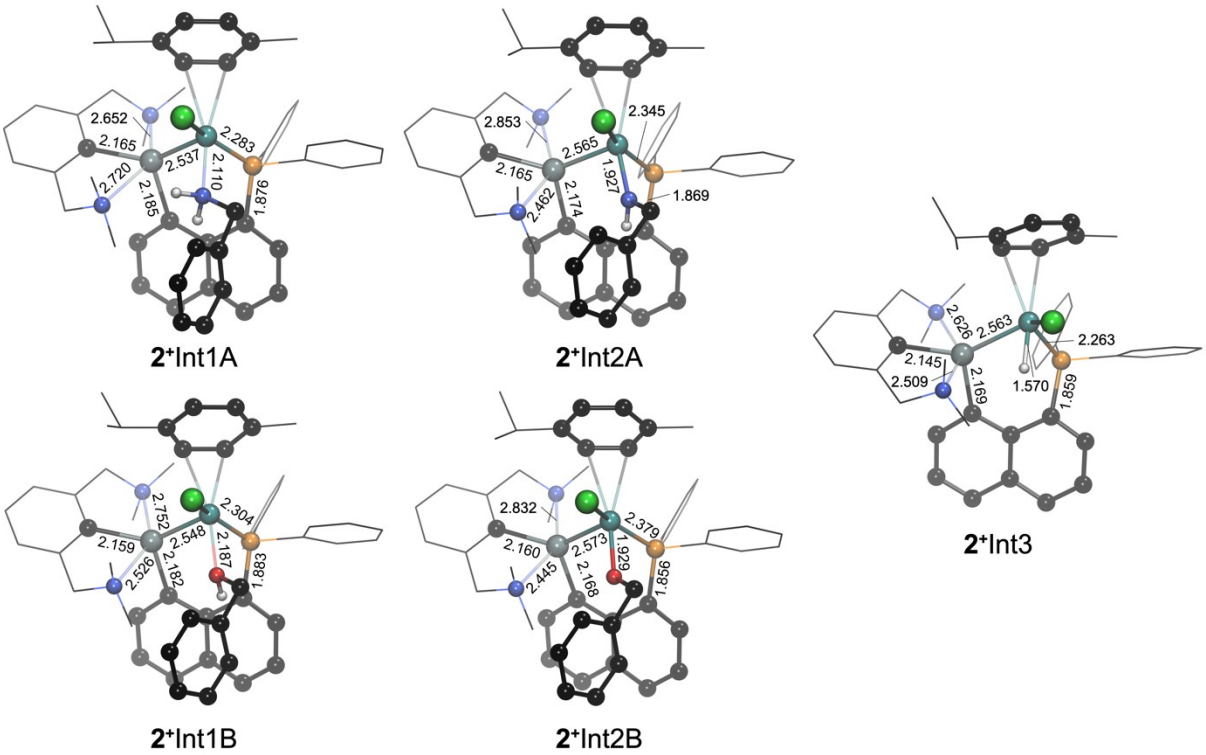


**Figure S5.** Optimized geometries of the three intermediates **2**$^+$Int1-3 involved in the suggested catalytic cycle (hydrogen atoms are omitted for clarity) along with selected bond distances (in Å).

**Table S3.** Selected bond lengths (*d*; in Å), Wiberg bond indices (WBI), and NPA atomic charges (*q*; in *e*) for intermediates **2**$^+$Int1-3.

| | **2**$^+$Int1A | **2**$^+$Int2A | **2**$^+$Int1B | **2**$^+$Int2B | **2**$^+$Int3 |
|---|---|---|---|---|---|
| $d_{\text{Ru-Sn}}$ | 2.537 | 2.565 | 2.548 | 2.573 | 2.563 |
| $\text{WBI}_{\text{Ru-Sn}}$ | 0.777 | 0.716 | 0.756 | 0.706 | 0.678 |
| $d_{\text{Ru-P}}$ | 2.283 | 2.345 | 2.304 | 2.379 | 2.263 |
| $\text{WBI}_{\text{Ru-P}}$ | 0.743 | 0.654 | 0.715 | 0.617 | 0.774 |
| $d_{\text{Ru-N/O/H}}$ | 2.110 | 1.927 | 2.187 | 1.929 | 1.570 |
| $\text{WBI}_{\text{Ru-N/O/H}}$ | 0.500 | 0.861 | 0.326 | 0.718 | 0.625 |
| $q_{\text{Ru}}$ | -0.75 | -0.53 | -0.69 | -0.32 | -0.66 |
| $q_{\text{Sn}}$ | 2.00 | 2.03 | 2.03 | 2.03 | 1.91 |
| $q_{\text{P}}$ | 1.26 | 1.24 | 1.26 | 1.22 | 1.33 |

*Alternative catalytic cycle*

The bimetallic nature of the studied complexes offers an alternative reaction pathway, which involves the Sn centre (Scheme S1, Figure S6). The coordination site on the tin atom is available thanks to the flexibility of the ligand L. Accordingly, a pre-reactive complex **2**$^+$Int0A' is formed after de-coordination of one of the amino groups and formation of weak NH···π and CH···π interactions. The former is between the $NH_2$ group of the benzylamine and the Ph group of the phosphine substituent while the latter concerns the phenyl ring of the benzylamine and the naphthalene core of **2**$^+$ (Figure S6). This step is slightly endergonic with a ΔG value of 5.4 kcal mol$^{-1}$ (Table S4). In the following step (ΔG = 1.6 kcal mol$^{-1}$) the benzylamine coordinates to the Sn centre through a relatively strong N→Sn interaction ($d_{\text{Sn-N}}$ = 2.562 Å; *cf.* $\sum_{\text{vdW}}$Sn,N = 4.08 Å) yielding complex **2**$^+$Int1A'. The reaction of **2**$^+$Int1A' with molecular oxygen gives a Ru(III) complex **2**$^+$Int2A'. This step is highly endergonic (ΔG = 39.1 kcal mol$^{-1}$), which contrasts with the ΔG value of -9.2 kcal mol$^{-1}$ found for the corresponding step in the Ru-catalyzed reaction. The newly formed Sn-N covalent bond causes a significant elongation of the Ru-Sn bond and a decrease of the corresponding $\text{WBI}_{\text{Ru-Sn}}$ value (Table S5). Furthermore, the N→Sn donor-acceptor stabilization of the Sn centre by the ligand L is much weaker than in **2**$^+$Int0A' and **2**$^+$Int1A' (Figure S6). Like the previous steps, the elimination of the benzalimine resulting in a formation of the tin hydride **2**$^+$Int3' is slightly endergonic (ΔG = 0.2 kcal mol$^{-1}$). The geometry of **2**$^+$Int3' with an elongated Ru-Sn bond and a very weak N→Sn intramolecular bond is analogous to that of **2**$^+$Int2A'. Finally, the catalytic cycle is closed by a highly exergonic $H_2$ elimination to regenerate **2**$^+$ (ΔG = -144.8 kcal mol$^{-1}$).

The oxidation of the benzyl alcohol follows an analogous catalytic mechanism revealing intermediates with a very similar molecular structure (Figure S6). However, the thermodynamics of the catalytic steps corresponding to the formation of **2**$^+$Int2B' and **2**$^+$Int3'

are slightly different (Table S4). Calculations performed in the presence of benzyl alcohol as a solvent showed no major differences in the ΔG values compared to the gas phase results (Table S4).

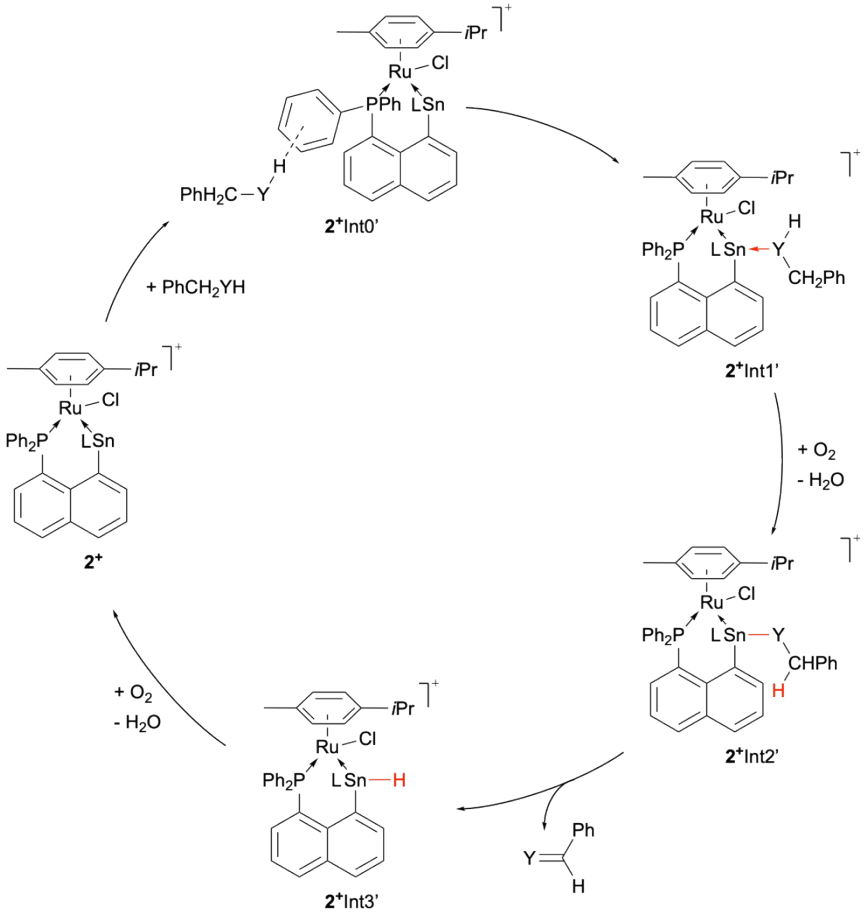


**Scheme S1.** Proposed alternative mechanism of aerobic oxidations catalysed by $\mathbf{2}^{+}$ (Y = NH or O).

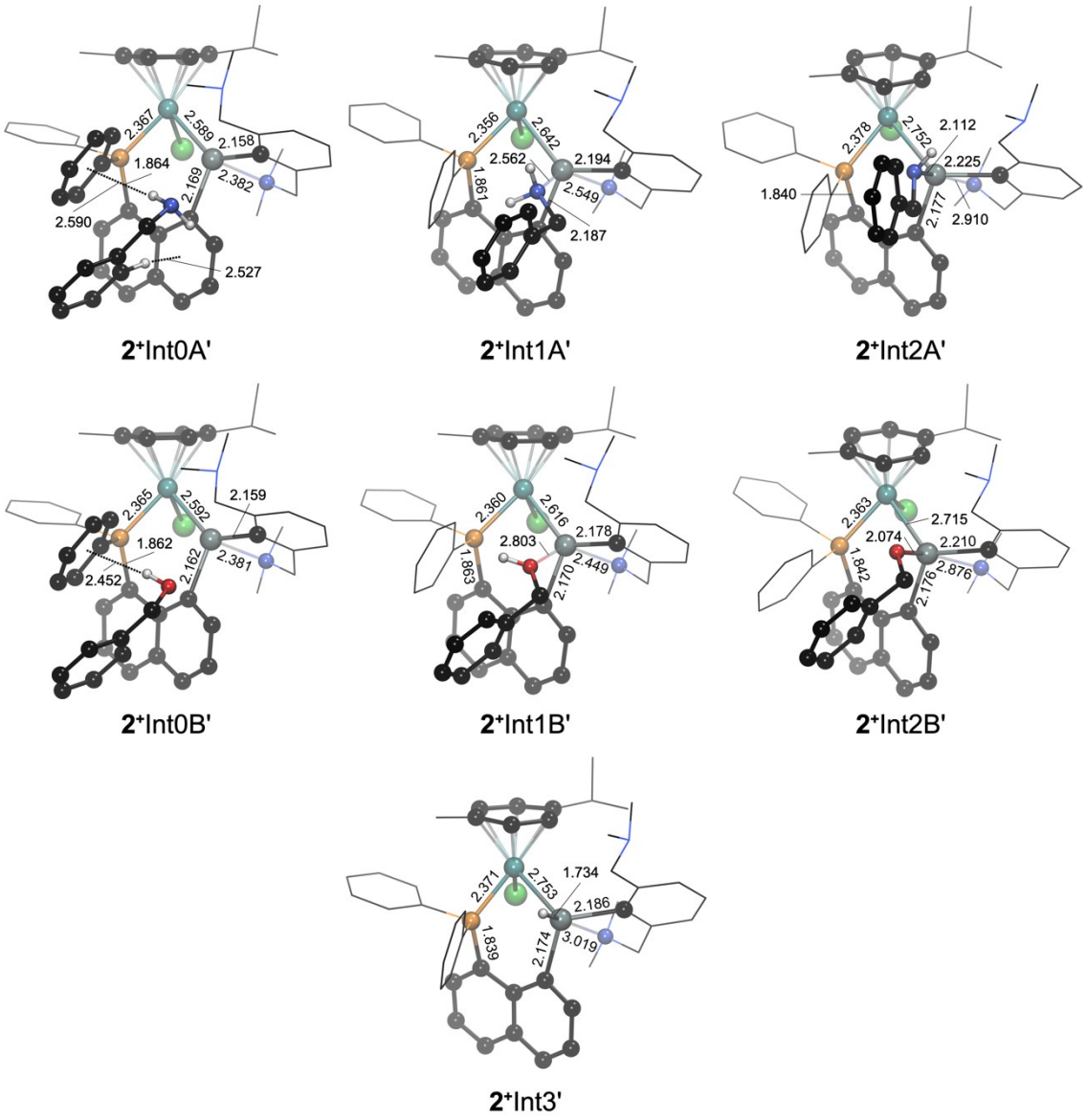


**Figure S6.** Optimized geometries of the four intermediates **2**$^{+}$Int0'-3' involved in the alternative catalytic cycle (hydrogen atoms are omitted for clarity) along with selected bond distances (in Å).

**Table S4.** Gibbs free energy differences ($\Delta G$; in kcal mol$^{-1}$) for the consecutive steps of the alternative catalytic cycle.

| | $\Delta G$(DZ)[a] | $\Delta G$(TZ)[b] | $\Delta G^{solv}$(TZ)[c] |
|---|---|---|---|
| **2**$^+$ → **2**$^+$Int0A’ | 3.5 | 5.4 | |
| **2**$^+$Int0A’ → **2**$^+$Int1A’ | 0.8 | 1.6 | |
| **2**$^+$Int1A’ → **2**$^+$Int2A’ | 49.6 | 39.1 | |
| **2**$^+$Int2A’ → **2**$^+$Int3’ | 3.5 | 0.2 | |
| **2**$^+$Int3’ → **2**$^+$ | -140.4 | -144.8 | |
| **2**$^+$ → **2**$^+$Int0B’ | 1.1 | 4.2 | 7.3 |
| **2**$^+$Int0B’ → **2**$^+$Int1B’ | 2.4 | 3.1 | 4.9 |
| **2**$^+$Int1B’ → **2**$^+$Int2B’ | 26.6 | 17.4 | 9.4 |
| **2**$^+$Int2B’ → **2**$^+$Int3’ | 12.3 | 10.1 | 6.6 |
| **2**$^+$Int3’ → **2**$^+$ | -140.4 | -144.8 | -145.4 |

[a]Calculated at the B3LYP-D3BJ/cc-pVDZ-PP level of theory; [b]Calculated at the B3LYP-D3BJ/cc-pVTZ-PP level of theory; [c]Calculated at the B3LYP-D3BJ/cc-pVTZ-PP level of theory in benzyl acohol.

**Table S5.** Selected bond lengths ($d$; in Å), Wiberg bond indices (WBI), and NPA atomic charges ($q$; in $e$) for the intermediates **2**$^+$Int0’-3’.

| | **2**$^+$Int0A’ | **2**$^+$Int1A’ | **2**$^+$Int2A’ | **2**$^+$Int0B’ | **2**$^+$Int1B’ | **2**$^+$Int2B’ | **2**$^+$Int3’ |
|---|---|---|---|---|---|---|---|
| $d_{Ru\text{-}Sn}$ | 2.589 | 2.642 | 2.752 | 2.592 | 2.616 | 2.715 | 2.753 |
| $WBI_{Ru\text{-}Sn}$ | 0.693 | 0.676 | 0.461 | 0.687 | 0.676 | 0.463 | 0.491 |
| $d_{Ru\text{-}P}$ | 2.367 | 2.356 | 2.378 | 2.365 | 2.360 | 2.363 | 2.371 |
| $WBI_{Ru\text{-}P}$ | 0.715 | 0.716 | 0.674 | 0.716 | 0.719 | 0.688 | 0.674 |
| $d_{Sn\text{-}N/O/H}$ | 4.291 | 2.562 | 2.112 | 4.071 | 2.803 | 2.074 | 1.734 |
| $WBI_{Sn\text{-}N/O/H}$ | 0.006 | 0.162 | 0.388 | 0.011 | 0.087 | 0.300 | 0.793 |
| $q_{Ru}$ | -1.10 | -1.06 | -0.70 | -1.10 | -1.10 | -0.75 | -0.64 |
| $q_{Sn}$ | 2.04 | 2.00 | 2.10 | 2.04 | 2.05 | 2.18 | 1.54 |
| $q_{P}$ | 1.33 | 1.34 | 1.31 | 1.33 | 1.33 | 1.32 | 1.31 |

## 3. Experimental section

### General Methods

The starting compound **1** was prepared according to the literature.[S7] All reactions were carried out under argon atmosphere using standard Schlenk techniques. Complexes $[(\eta^6\text{-cymene})RuCl]_2(\mu\text{-}Cl)_2$, $[(\eta^6\text{-cymene})RuI]_2(\mu\text{-}I)_2$ and $[(\eta^5\text{-}C_5Me_5)RuCl_2]_n$, silica gel 60 for column chromatography, aluminium oxide 90 active neutral for column chromatography 0.063-0.200 mm, benzylamine and benzyl alcohol were purchased from Sigma Aldrich. Solvents were dried by standard methods, distilled prior to use.

### Experimental details

*Solution NMR spectroscopy*

The $^1H$, $^{13}C\{^1H\}$, $^{31}P\{^1H\}$ and $^{119}Sn\{^1H\}$ NMR spectra were recorded at ambient temperature with a Bruker Avance 500 spectrometer. The chemical shifts $\delta$ are given in ppm and referenced to external $SiMe_4$ ($^1H$, $^{13}C$), and $SnMe_4$ ($^{119}Sn$).

*Gas chromatograph – Mass spectrometry (GC/MS)*

The mass spectra of $CH_2Cl_2$ solutions of prepared imines were measured on GC/MS configuration comprised of an Agilent Technologies—6890N gas chromatograph (HP-5MS column, length 30 m, I.D. 0.25 mm, film 0.25 lm) with He gas as mobile phase, equipped with a 5973 Network MS detector (EI 70 eV, mass range 33–550 Da).

*Synthesis of **2**.*

$[(\eta^6\text{-cymene})RuCl]_2(\mu\text{-}Cl)_2$ (0.10 g, 0.16 mmol) was added to a benzene solution of **1** (0.20 g, 0.32 mmol) at room temperature and stirred for 2 h. The resulting solution was evaporated to dryness and the yellow solid residue was washed with hexane and dried. Yield: 0.26 g (88%). Mp. 153-154 °C. Anal. Calc. for $C_{44}H_{48}PN_2Cl_2SnRu$ (926.52): C, 57.04; H, 5.22. Found: C, 57.3; H, 5.1. $^1H$ NMR (500 MHz, $CDCl_3$, 300K): δ 1.12 (d, 6H, $J$ = 7.2 Hz, $CH(CH_3)_2$), 1.61 (s, 6H, $NCH_3$), 1.71 (s, 6H, $NCH_3$), 1.93 (s, 3H, $CH_3$), 2.64 (h, 1H, $CH(CH_3)_2$) 3.09 (AX system, 1H, $J$ = 7.2 Hz, $CH_2N$), 3.38 (AX system, 1H, $J$ = 7.2 Hz, $CH_2N$), 3.42 (AX system, 1H, $J$ = 7.2 Hz, $CH_2N$), 4.44 (AX system, 1H, $J$ = 7.2 Hz, $CH_2N$), 5.70 (dd, 2H, $C_6H_4$), 5.87 (d, 1H, $J$ = 9.2 Hz, $C_6H_4$), 6.27 (d, 1H, $J$ = 9.2 Hz, $C_6H_4$), 6.81-6.86 (m, 1H), 7.00 (bs, 1H), 7.18-7.26 (m, 4H), 7.31-7.47 (m, 8H), 7.53 (bs, 2H), 7.59 (d, 1H, $J$ = 8.3 Hz), 7.93 (t, 2H, $J$ = 8.3 Hz). $^{13}C$ NMR (125 MHz, $CDCl_3$, 300K): δ 19.5 ($CH_3$), 22.7, 23.5 ($CH(CH_3)_2$), 31.1 ($CH(CH_3)_2$), 46.4, 47.1 ($NCH_3$), 64.9, 66.6 ($CH_2N$), 82.5, 82.8, 89.7, 93.6, 116.6, 117.8 ($C_6H_4$), 124.8, 125.1 (d, $J_{C,P}$ = 10 Hz), 125.3, 126.0, 127.5, 128.2, 128.7 (d, $J_{C,P}$ = 8 Hz), 129.0, 129.3 (d, $J_{C,P}$ = 10 Hz), 130.5, 131.0, 131.5 (d, $J_{C,P}$ = 42.25 Hz), 132.9, 133.7 (d, $J_{C,P}$ = 8 Hz), 134.7 (d, $J_{C,P}$ = 11 Hz), 135.8, 136.5 (d, $J_{C,P}$ = 4.76 Hz), 139.9 (d, $J_{C,P}$ = 11 Hz), 141.8 (d, $J_{C,P}$ = 9 Hz), 145.0 (d, $J_{C,P}$ = 104 Hz) (Ar$C$). $^{31}P\{^1H\}$ NMR (202 MHz, $CDCl_3$, 300K): δ 36.2 ppm, $J_{P,Sn}$ = 651 Hz. $^{119}Sn\{^1H\}$ NMR (186 MHz, $CDCl_3$,): δ 106.6 ppm, $J_{P,Sn}$ = 651 Hz.

*Synthesis of **3**.*

[($\eta^6$-cymene)RuI]$_2$($\mu$-I)$_2$ (0.16 g, 0.16 mmol) was added to a benzene solution of **1** (0.20 g, 0.32 mmol) at room temperature and stirred for 2 h. The resulting solution was evaporated to dryness and the red solid residue was washed with hexane and dried Yield: 0.31 g (87%). Mp. 141-142 °C. Anal. Calc. for $C_{44}H_{48}PN_2I_2SnRu$ (1109.43): C, 47.63; H, 4.36. Found: C, 47.3; H, 4.2. $^1$H NMR (500 MHz, $C_6D_6$, 300K): δ 0.98 (d, 3H, *J* = 7.3 Hz, CH(C*H*$_3$)), 1.22 (d, 3H, *J* = 7.3 Hz, CH(C*H*$_3$)), 2.01 (s, 3H, C*H*$_3$), 2.19 (s, 6H, NC*H*$_3$), 2.44 (s, 6H, NC*H*$_3$), 2.90 (AX system, 1H, *J* = 7.5 Hz, C*H*$_2$N), 3.14 (h, 1H, C*H*), 4.25 (AX system, 1H, *J* = 7.5 Hz, C*H*$_2$N), 5.05 (AX system, 2H, *J* = 7.5 Hz, C*H*$_2$N), 5.13 (d, 1H, *J* = 8.9 Hz, C$_6$*H*$_4$), 5.33 (d, 1H, *J* = 8.9 Hz, C$_6$*H*$_4$), 5.43 (d, 1H, *J* = 8.9 Hz, C$_6$*H*$_4$), 5.53 (d, 1H, *J* = 8.9 Hz, C$_6$*H*$_4$), 6.58 (t, 2H, *J* = 8.5 Hz), 6.68 (d, 1H, *J* = 8.5 Hz), 6.91-7.10 (m, 10H), 7.30 (m, 1H), 7.51 (m, 1H), 7.68 (m, 2H), 7.85 (d, 1H, *J* = 9.1 Hz), 9.26 (d, 1H, *J* = 9.1 Hz). $^{13}$C NMR (125 MHz, $C_6D_6$, 300K): δ 20.4 (*C*H$_3$), 22.3, 23.5 (CH(*C*H$_3$)$_2$), 31.0 (*C*H(CH$_3$)$_2$), 46.4 (NCH$_3$), 64.4 (d, $J_{C,P}$ = 12 Hz), 67.3 (*C*H$_2$N), 81.6, 82.3, 82.5, 82.9, 96.9, 107.9 (*C*$_6$H$_4$), 124.5, 125.2, 125.6, 127.1, 128.2 (d, $J_{C,P}$ = 6 Hz), 128.3, 128.6, 128.8, 128.9, 129.7 (d, $J_{C,P}$ = 3 Hz), 131.3, 132.3 (d, $J_{C,P}$ = 7 Hz), 132.4 (d, $J_{C,P}$ = 10 Hz), 133.4 (d, $J_{C,P}$ = 5 Hz), 134.6 (d, $J_{C,P}$ = 4 Hz), 135.1 (d, $J_{C,P}$ = 3 Hz), 135.1, 135.6 (d, $J_{C,P}$ = 8.90 Hz), 141.0 (d, $J_{C,P}$ = 3 Hz), 142.7 (d, $J_{C,P}$ = 7 Hz), 143.4 (d, $J_{C,P}$ = 24 Hz), 148.2, 150.1 (d, $J_{C,P}$ = 37 Hz), 151.4 (d, $J_{C,P}$ = 25 Hz) (Ar*C*). $^{31}$P{$^1$H} NMR (202 MHz, $C_6D_6$, 300K): δ -19.4 ppm, $J_{P,Sn}$ = 38. $^{119}$Sn{$^1$H} NMR (186 MHz, $C_6D_6$, 300K): δ 28.3 ppm, $J_{P,Sn}$ = 38 Hz.

*Synthesis of **4**.*

[($\eta^5$-C$_5$Me$_5$)RuCl$_2$]$_n$ (0.07 g, 0.24 mmol) was added to a benzene solution of **1** (0.22 g, 0.36 mmol) at room temperature and stirred for 2 h. The resulting solution was evaporated to dryness and the residue was extracted with 10 ml of benzene / hexane (1:1) to precipitate white solid. The suspension was filtered to obtain a clear red filtrate, which yields red crystals of **4** at room temperature. Yield: 0.19 g (89%). Mp. 227-228 °C. Anal. Calc. for $C_{44}H_{50}PN_2ClSnRu$ (893.08): C, 59.17; H, 5.64. Found: C, 59.3; H, 5.4. $^1$H NMR (500 MHz, $C_6D_6$, 300K): δ 1.66 (s, 15H, C*H*$_3$), 1.92 (s, 6H, NC*H*$_3$), 1.96 (s, 6H, NC*H*$_3$), 2.69 (AX system, 1H, *J* = 7.5 Hz, C*H*$_2$N), 3.30 (AX system, 1H, *J* = 7.5 Hz, C*H*$_2$N), 3.48 (AX system, 1H, *J* = 7.5 Hz, C*H*$_2$N), 3.92 (AX system, 1H, *J* = 7.5 Hz, C*H*$_2$N), 6.88-6.94 (m, 6H), 7.00 (m, 2H), 7.09 (m, 2H), 7.29 (m, 2H), 7.42 (d, 2H, *J* = 9.5 Hz), 7.54 (m, 3H), 7.65 (d, 1H, *J* = 8.5 Hz), 7.75 (m, 1H). $^{13}$C NMR (125 MHz, $C_6D_6$, 300K): δ 10.9 (*C*H$_3$), 45.1, 46.7 (NCH$_3$), 67.3, 68.4 (*C*H$_2$N), 86.9 (d, $J_{C,P}$ = 3 Hz), 124.3 (d, $J_{C,P}$ = 8 Hz), 124.5 (d, $J_{C,P}$ = 28 Hz), 128.1, 128.6 (d, $J_{C,P}$ = 33 Hz), 128.7, 130.2 (d, $J_{C,P}$ = 44 Hz), 133.7, 134.8 (d, $J_{C,P}$ = 5 Hz), 135.0 (d, $J_{C,P}$ = 6 Hz), 136.3 (d, $J_{C,P}$ = 39 Hz), 141.0 (d, $J_{C,P}$ = 37 Hz), 141.3 (d, $J_{C,P}$ = 19 Hz), 142.8 (d, $J_{C,P}$ = 9 Hz), 144.9, 147.9, 148.7 (d, $J_{C,P}$ = 8 Hz), 150.6 (d, $J_{C,P}$ = 3 Hz) (Ar*C*). $^{31}$P{$^1$H} NMR (202 MHz, $C_6D_6$, 300K): δ 52.6 ppm, $J_{P,Sn}$ = 538 Hz. $^{119}$Sn{$^1$H} NMR (186 MHz, $C_6D_6$, 300K): δ 340.2 ppm, $J_{P,Sn}$ = 538 Hz.

*Synthesis of **5.***

$[(\eta^5\text{-}C_5Me_5)RuCl_2]_n$ (0.07 g, 0.24 mmol) was added to a benzene solution of **1** (0.22 g, 0.36 mmol) at room temperature and stirred for 2 h. The resulting solution was evaporated to dryness and the residue was extracted with 10 ml of benzene / hexane (1:1) to precipitate white solid. The suspension was filtered and the white solid residue recrystallized from $CH_2Cl_2$ to yield white solid material of **5**. Yield: 0.07 g (85%). Mp. 243-245 °C. Anal. Calc. for $C_{34}H_{35}PN_2Cl_2Sn$ (692.24): C, 58.99; H, 5.10. Found: C, 59.2; H, 5.3. $^1$H NMR (500 MHz, $CDCl_3$, 300K): δ 1.90 (s, 12H, NC$H_3$), 4.09 (s, 4H, C$H_2$N), 7.18-7.28 (m, 6H), 7.33 (bs, 4H), 7.40 (bs, 2H), 7.55 (m, 3H), 7.73 (d, 1H, $J$ = 8.9 Hz), 8.02 (d, 1H, $J$ = 9.1 Hz), 8.09 (d, 1H, $J$ = 9.1 Hz), 8.84 (d, 1H, $J$ = 8.9 Hz). $^{13}$C NMR (125 MHz, $CDCl_3$, 300K): δ 45.0 (N$CH_3$), 62.8 ($CH_2$N), 125.2, 125.3 (d, $J_{C,P}$ = 5 Hz), 126.6 (d, $J_{C,P}$ =5 Hz), 128.1, 128.6 (d, $J_{C,P}$ = 9 Hz), 128.9, 129.5, 129.7, 130.4, 133.1 (d, $J_{C,P}$ = 13 Hz), 134.5 (d, $J_{C,P}$ = 6 Hz), 134.8 (d, $J_{C,P}$ = 8 Hz), 136.9, 137.7, 138.6 (d, $J_{C,P}$ = 20 Hz). $^{31}$P{$^1$H} NMR (202 MHz, $CDCl_3$, 300K): δ -42.9 ppm, $J_{P,Sn}$ = 1185 Hz. $^{119}$Sn{$^1$H} NMR (186 MHz, $CDCl_3$, 300K): δ 354 ppm, $J_{P,Sn}$ = 1185 Hz.

*Homogenous aerobic oxidations of benzylamine*

Typical procedure: Ru catalyst (from 1 to 0.001 mol%) was added to a two-necked round-bottom flask containing benzylamine (15 mmol), 4Å molecular sieves and a magnetic stirrer at room temperature. The resulting reaction mixture was heated at 100 °C for 1 to 24 h in an air or oxygen atmosphere. Next, the reaction mixture was extracted with $CH_2Cl_2$ (10 ml), filtered through the syringe filter and analysed by $^1$H NMR and GC/MS analysis.

*Synthesis of {($C_6H_4CH_2$)N=CH}-$C_6H_5$ via aerobic oxidation of benzylamine*

Compound **2** (0.00075 mmol, 0.005 mol%) was added to a two-necked round-bottom flask containing the benzylamine (1.6 ml, 15 mmol), 4Å molecular sieves and a magnetic stirrer at room temperature. The resulting reaction mixture was heated at 100 °C for 24 h in an air atmosphere. The progress of the reaction was monitored by $^1$H NMR spectroscopy. After completion of the reaction, the reaction mixture was extracted with diethyl ether (10 ml) and filtered through a short bed of active neutral aluminium oxide 90. Stripping out the solvent afforded pure {($C_6H_4CH_2$)N=CH}$C_6H_5$. Yield: 6.4 mmol (85%).

*Homogenous aerobic oxidations of benzyl alcohol*

Typical procedure: Ru catalyst (0.015 mmol, 0.1 mol%) was added to a two-necked round-bottom flask containing benzyl alcohol (15 mmol), 4Å molecular sieves and a magnetic stirrer at room temperature. The resulting reaction mixture was heated at 80 °C for 24 h in an air atmosphere. Next, the reaction mixture was extracted with $CH_2Cl_2$ (10 ml), filtered through the syringe filter and analysed by $^1$H NMR and GC/MS analysis.

*Synthesis of $C_6H_4COH$ by the aerobic oxidation of benzyl alcohol*

Compound **2** (0.15 mmol, 1 mol%) was added to a two-necked round-bottom flask containing benzyl alcohol (1.6 ml, 15 mmol), 4Å molecular sieves and a magnetic stirrer at room

temperature. The resulting reaction mixture was heated at 80 °C for 24 h in an air atmosphere. The progress of the reaction was monitored by $^{1}$H NMR spectroscopy. After completion of the reaction, the reaction mixture was extracted with diethyl ether (10 ml) and filtered through a short bed of active neutral aluminium oxide 90. Stripping out the solvent afforded pure $C_6H_4COH$. Yield: 13.5 mmol (90%).

*NMR experiments for mechanistic studies of aerobic oxidations of benzylamine*

Compound **2** (6 mg) and benzylamine (0.1 ml) were dissolved in toluene-d8 and the solution was added to an NMR tube in an air atmosphere. The NMR tube was heated at 80 °C for 8 or 14 h in an air atmosphere. The resulting solution was analysed by $^{31}$P NMR spectroscopy.

In a Young valve NMR tube, compound **2** (6 mg) and benzylamine (0.1 ml) were dissolved in toluene-d8 under the argon atmosphere. The resulting reaction mixture was heated at 80 °C for 8 h in an NMR tube and analysed by $^{31}$P NMR spectroscopy.

*Stability of 2*

Compound **2** (30 mg) was dissolved in $CD_3OD$ and the solution was stirred in an air atmosphere for 1 and 24 h at r.t. The solution was transferred to an NMR tube and analyzed by $^{1}$H, $^{31}$P and $^{119}$Sn NMR spectroscopy.

Compound **2** (30 mg) and benzyl alcohol (0.01 mL) were dissolved in $CDCl_3$ and the solution was stirred in an air atmosphere for 24 h at r.t. The solution was transferred to an NMR tube and analyzed by $^{1}$H, $^{31}$P and $^{119}$Sn NMR spectroscopy.

Compound **2** (30 mg) and benzyl alcohol (0.01 mL) were dissolved in $CDCl_3$ and the solution was stirred in an air atmosphere for 2 h at 50°C. The solution was transferred to an NMR tube and analyzed by $^{1}$H, $^{31}$P and $^{119}$Sn NMR spectroscopy.

Compound **2** (30 mg) and benzylamine (0.01 mL) were dissolved in $CDCl_3$ and the solution was stirred in an air atmosphere for 24 h at r.t. The solution was transferred to an NMR tube and analyzed by $^{1}$H, $^{31}$P and $^{119}$Sn NMR spectroscopy.

In a Schlenk flask, compound **2** (30 mg) was dissolved in THF, the solution was frozen in liquid nitrogen. The flask was evacuated, filled with $O_2$ and warmed to r.t. The resulting solution was heated at 60°C for 24 h. The solution was evaporated, the residue dissolved in $CDCl_3$ and analyzed by $^{1}$H and $^{31}$P spectroscopy.

*Computational details*

All calculations were carried out by using DFT as implemented in the Gaussian16 quantum chemistry program.[S8] Geometry optimizations were carried out at the B3LYP-D3BJ[S9]/cc-pVDZ[S10] level of theory including Grimme DFT-D3 empirical dispersion with the Becke Johnson damping function (cc-pVDZ-PP[S11] basis set including small-core relativistic

pseudopotentials that account also for relativistic effects was used for Ru, Sn and I). The electronic energies of the optimized structures were re-evaluated by additional single-point calculations on each of the optimized geometries by using the triple-ζ quality cc-pVTZ(-PP) basis set.[S10,S11] Analytical vibrational frequencies within the harmonic approximation were computed with the cc-pVDZ(-PP) basis set to confirm a proper convergence to well-defined minima or saddle points on the potential energy surface. Subsequently, an NBO analysis[S5] and calculations of the Wiberg bond indices[S6] were performed at the B3LYP-D3BJ/cc-pVTZ(-PP) level of theory. The Gibbs free energies $G^{solv}$(cc-pVTZ) used to calculate the energy differences reported in this article were computed by using Equations (1)-(4)

$$G^{solv}(\text{cc-pVTZ}) = G(\text{cc-pVTZ}) + \text{SC} \quad (1)$$

$$G(\text{cc-pVTZ}) = E(\text{cc-pVTZ}) + \text{TC} \quad (2)$$

$$\text{TC} = G(\text{cc-pVDZ}) - E(\text{cc-pVDZ}) \quad (3)$$

$$\text{SC} = E^{solv}(\text{cc-pVDZ}) - E(\text{cc-pVDZ}) \quad (4)$$

in which $E$(x) is the self-consistent field electronic energy derived from the cc-pVDZ or cc-pVTZ basis sets, TC is the thermal correction to the energy calculated with the cc-pVDZ basis set, $G$(cc-pVDZ) is the free energy at 298.15 K for the double-ζ quality basis set, SC is the solvent correction for $E^{solv}$(cc-pVDZ), which is the self-consistent field energy in the implicit Solvation Model based on Density (SMD)[S12] using benzene (ε = 2.2706) or benzyl alcohol (ε = 12.457) as solvent, calculated with the cc-pVDZ basis set.

*Crystallographic details*

Single crystalline material of yellow crystals **2**·2($H_2O$), red crystals of **3**·2($C_6H_6$) and orange crystals of **4** suitable for X ray structure determination was obtained by slow evaporation of THF or benzene molecule from the parent solutions of **2** - **4.** Full-sets of diffraction data for **2**·2($H_2O$), **3**·2($C_6H_6$) and **4** were collected at 150(2)K with a Bruker D8-Venture diffractometer equipped with Cu (Cu/$K_\alpha$ radiation; λ =1.54178 Å) or Mo (Mo/$K_\alpha$ radiation; λ = 0.71073 Å) microfocus X-ray (IμS) sources, Photon CMOS detector and Oxford Cryosystems cooling device was used for data collection. The frames were integrated with the Bruker SAINT software package using a narrow-frame algorithm. Data were corrected for absorption effects using the Multi-Scan method (SADABS). Obtained data were treated by XT-version 2018/1 and SHELXL-2017/1 software implemented in APEX3 v2016.5-0 (Bruker AXS) system.[S13] Hydrogen atoms were mostly localized on a difference Fourier map, however to ensure uniformity of treatment of crystal, all hydrogen atoms were recalculated into idealized positions (riding model) and assigned temperature factors $H_{iso}$(H) = 1.2 $U_{eq}$ (pivot atom) or of 1.5$U_{eq}$ (methyl). H atoms in methyl, methylene, methine and hydrogen atoms in aromatic rings were placed with C-H distances of 0.99, 0.98, 0.97 and 0.95Å, respectively, and 0.82Å for OH. Disordered parts of structure **3** were fixed with appropriate distances and refined by standard methods implemented in SHELXL software. There is disordered solvent (benzene) in the structure of **3**. Attempts were made to model this disorder

or split it into two positions, but were unsuccessful. PLATON /SQUEZZE[S14] was used to correct the data for the presence of disordered solvent. A potential solvent volume of 562 $Å^3$ was found. 231 electrons per unit cell worth of scattering were located in the void. The calculated stoichiometry of solvent was calculated to be four additional benzene molecules per unit cell, which results in 168 electrons per unit cell. Crystallographic data for structural analysis have been deposited with the Cambridge Crystallographic Data Centre, CCDC no. 2041511 (**3**), 2041512 (**2**), 2041513 (**4**), respectively. Copies of this information may be obtained free of charge from The Director, CCDC, 12 Union Road, Cambridge CB2 1EY, UK (fax: +44-1223-336033; e-mail: deposit@ccdc.cam.ac.uk or www: http://www.ccdc.cam.ac.uk).

## 4. NMR spectra of studied compounds

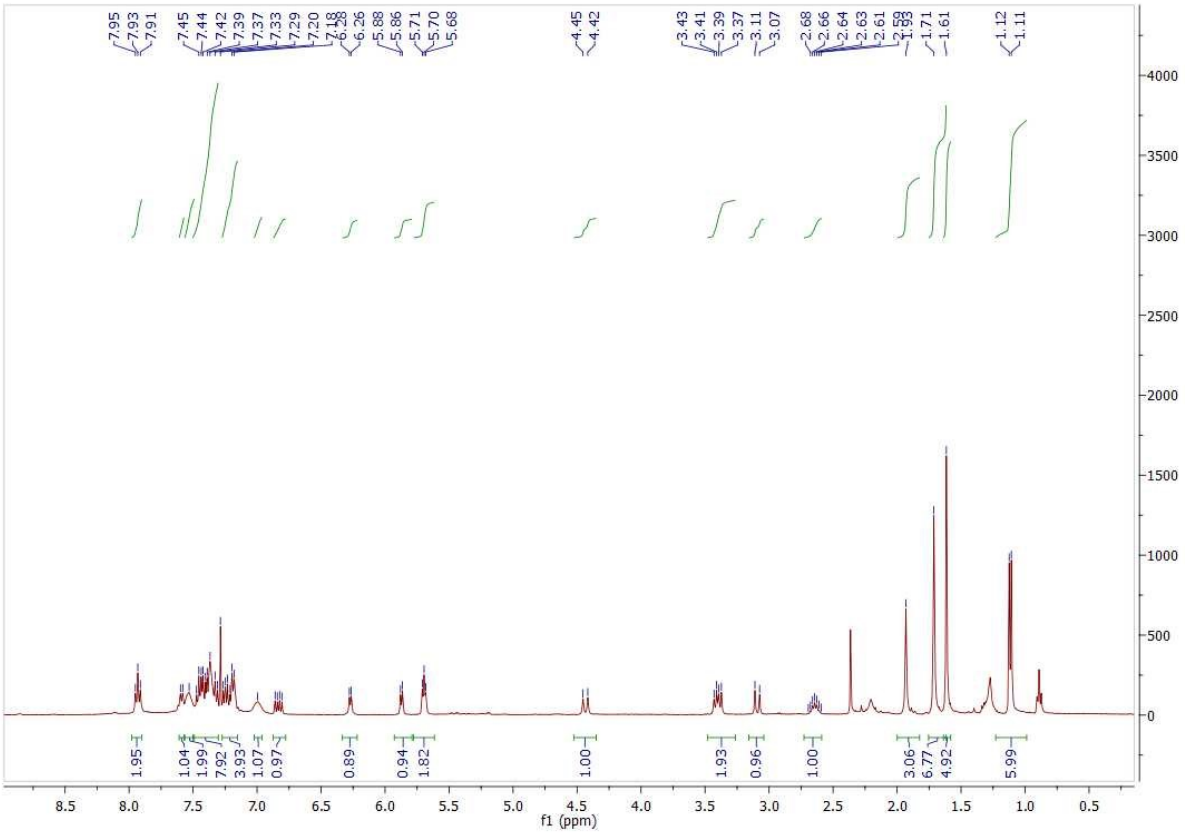


**Figure S7.** $^{1}H$ NMR ($CDCl_3$, 500MHz) of **2.**

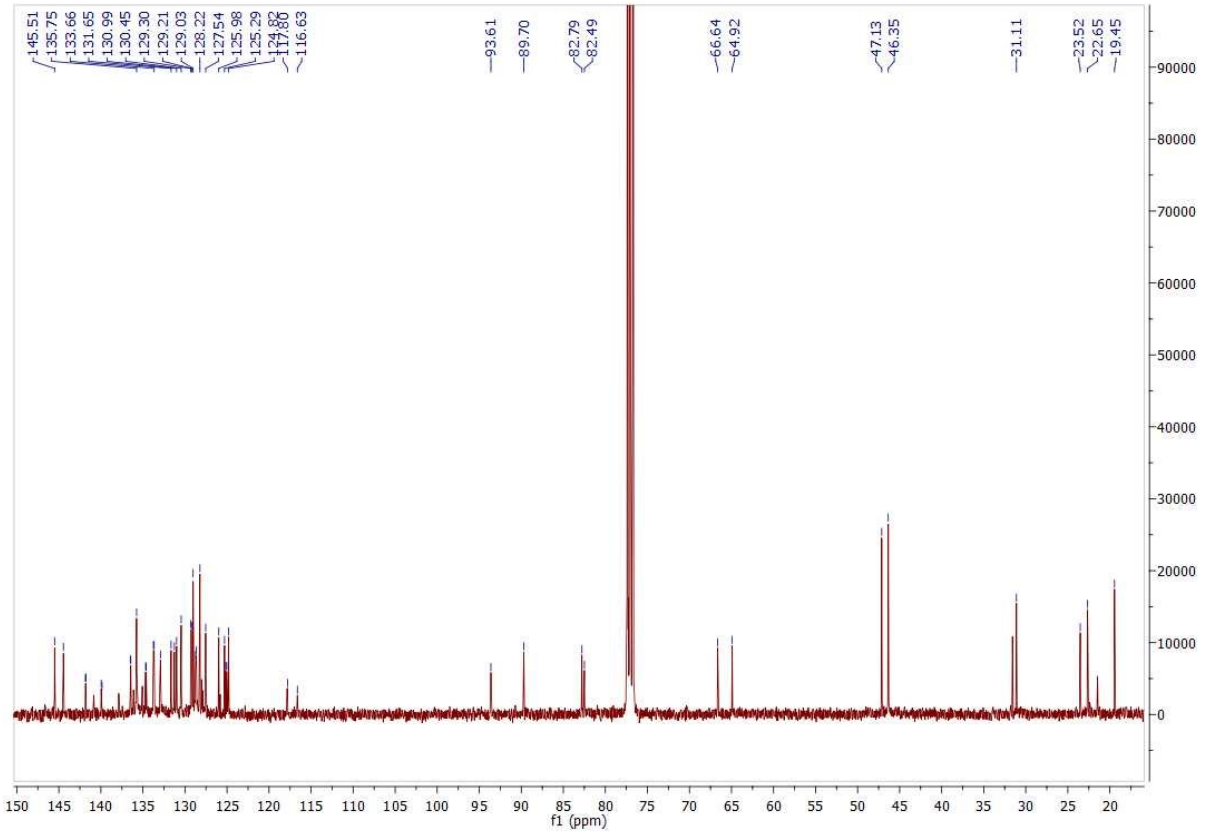


**Figure S8.** $^{13}C\{^{1}H\}$ NMR ($CDCl_3$, 125MHz) of **2.**

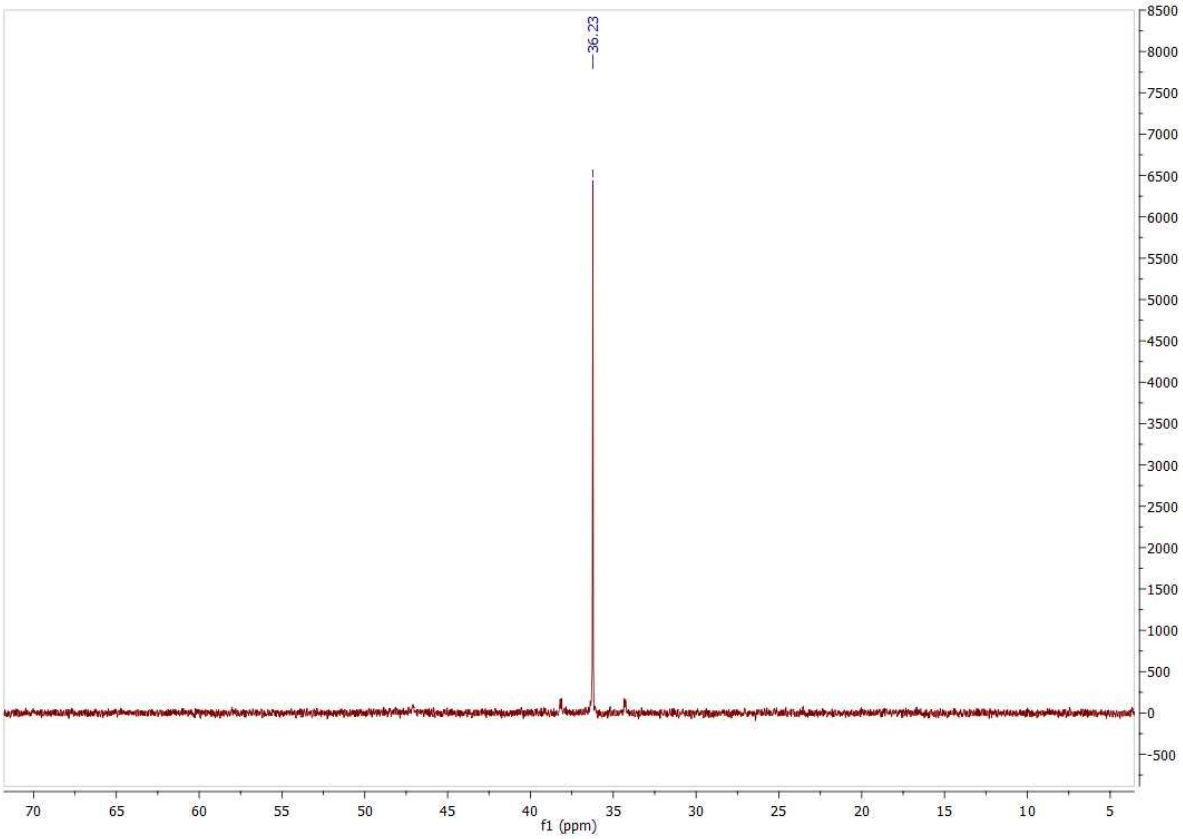


**Figure S9.** $^{31}P\{^{1}H\}$ NMR ($CDCl_3$, 202 MHz) of **2.**

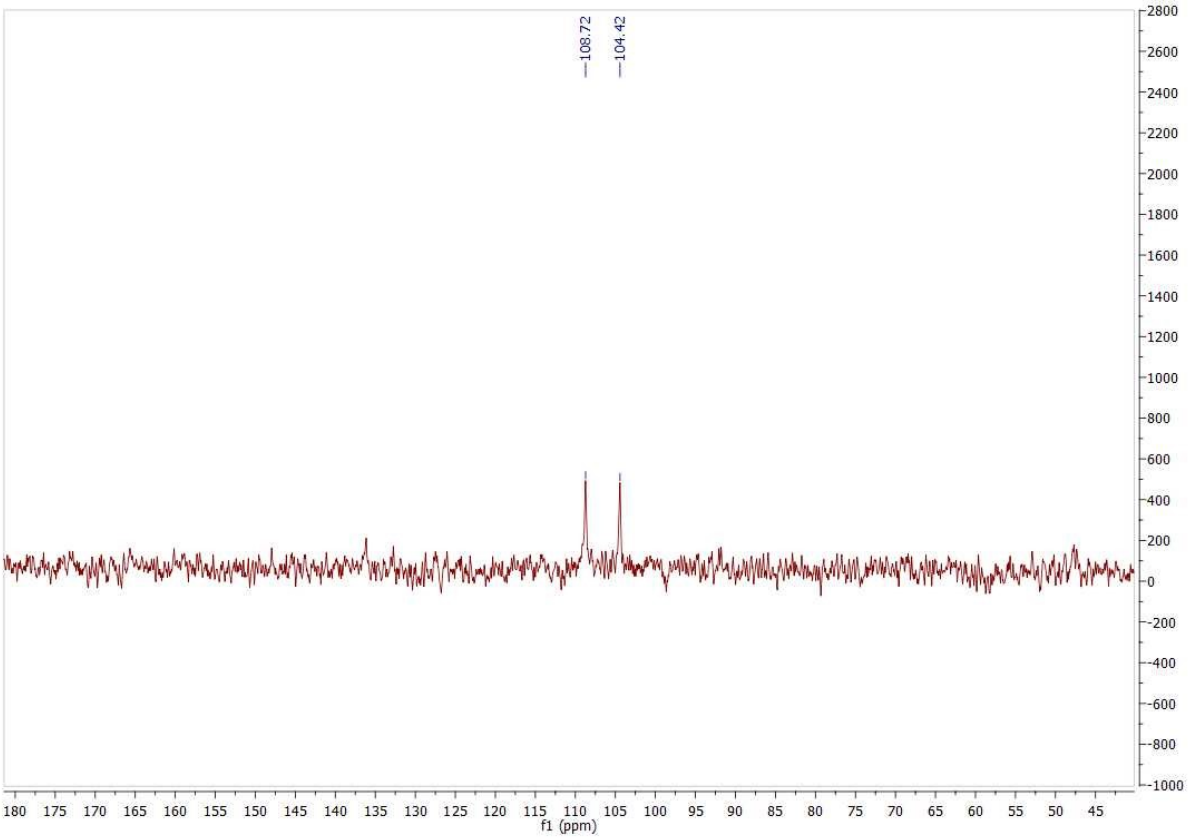


**Figure S10.** $^{119}Sn\{^{1}H\}$ NMR ($CDCl_3$, 186MHz) of **2.**

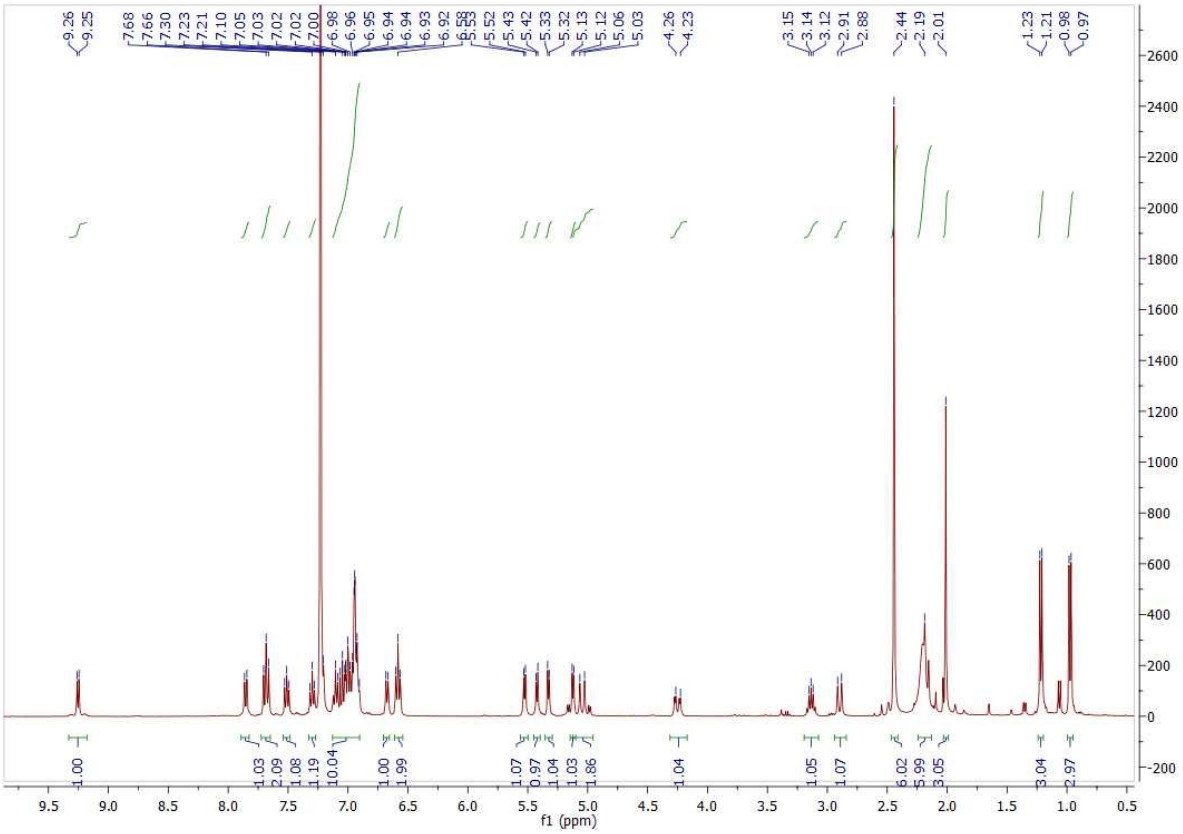


**Figure S11.** $^{1}H$ NMR ($C_6D_6$, 500MHz) of **3.**

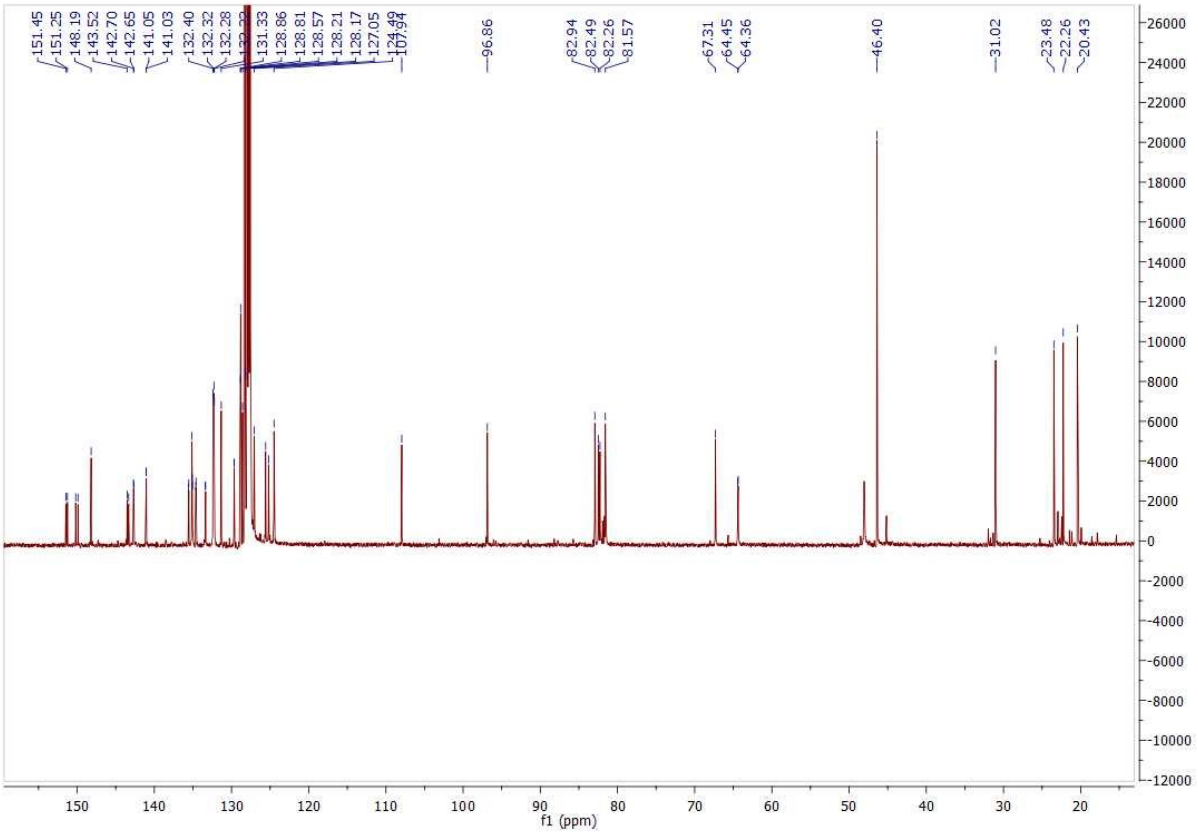


**Figure S12.** $^{13}C\{^{1}H\}$ NMR ($C_6D_6$, 125MHz) of **3.**

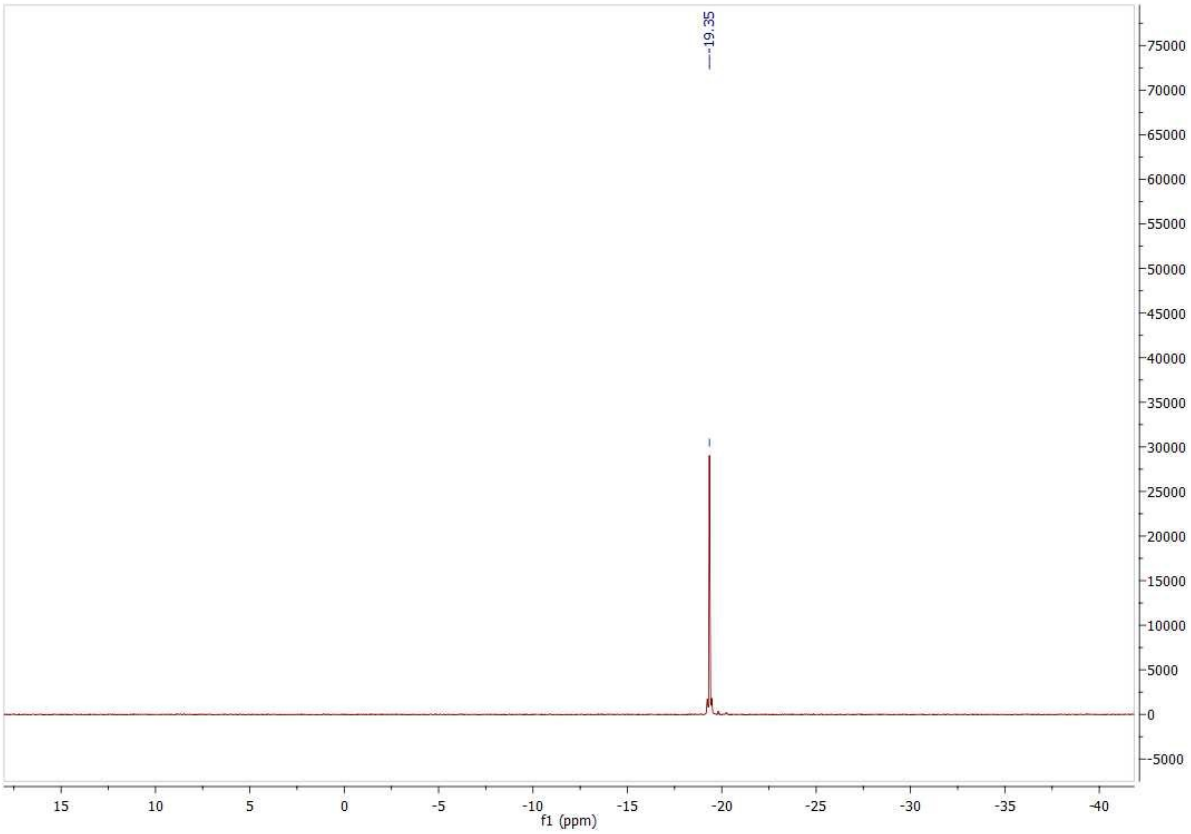


**Figure S13.** $^{31}P\{^{1}H\}$ NMR ($C_6D_6$, 202 MHz) of **3.**

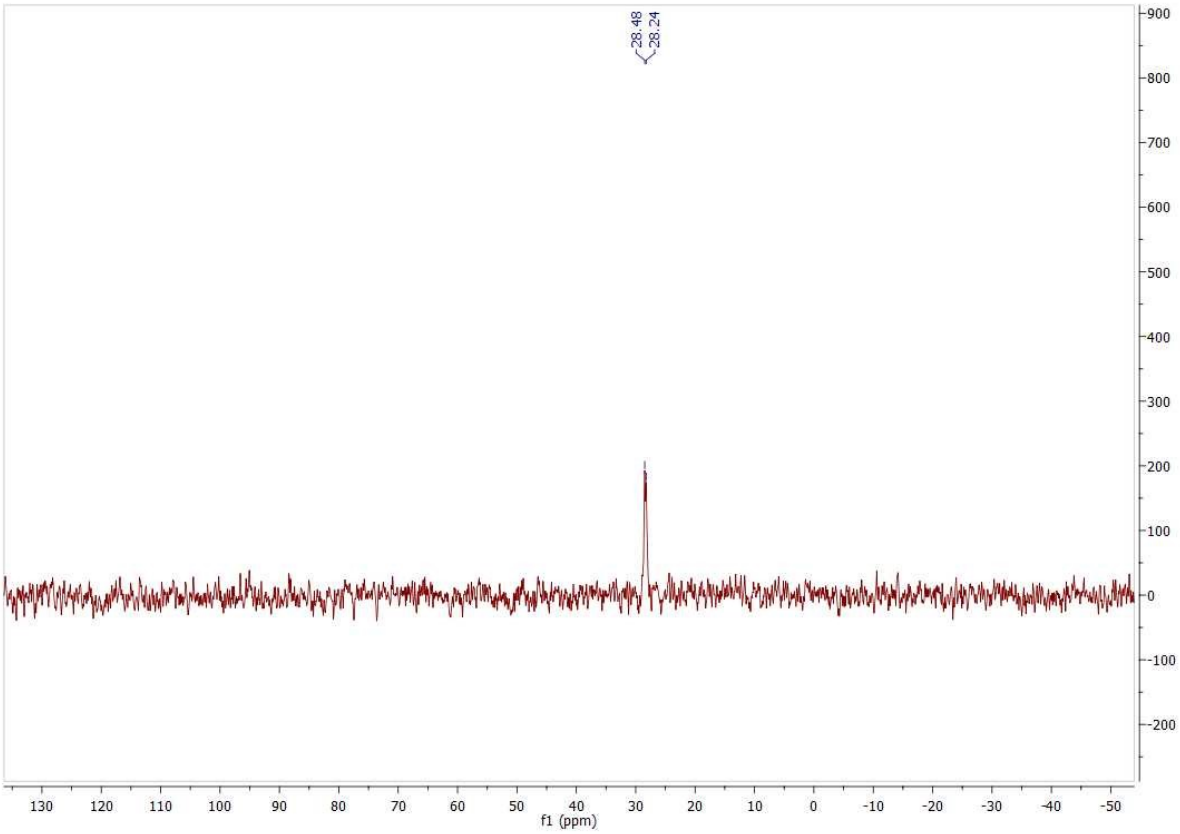


**Figure S14.** $^{119}Sn\{^{1}H\}$ NMR ($C_6D_6$, 186MHz) of **3**.

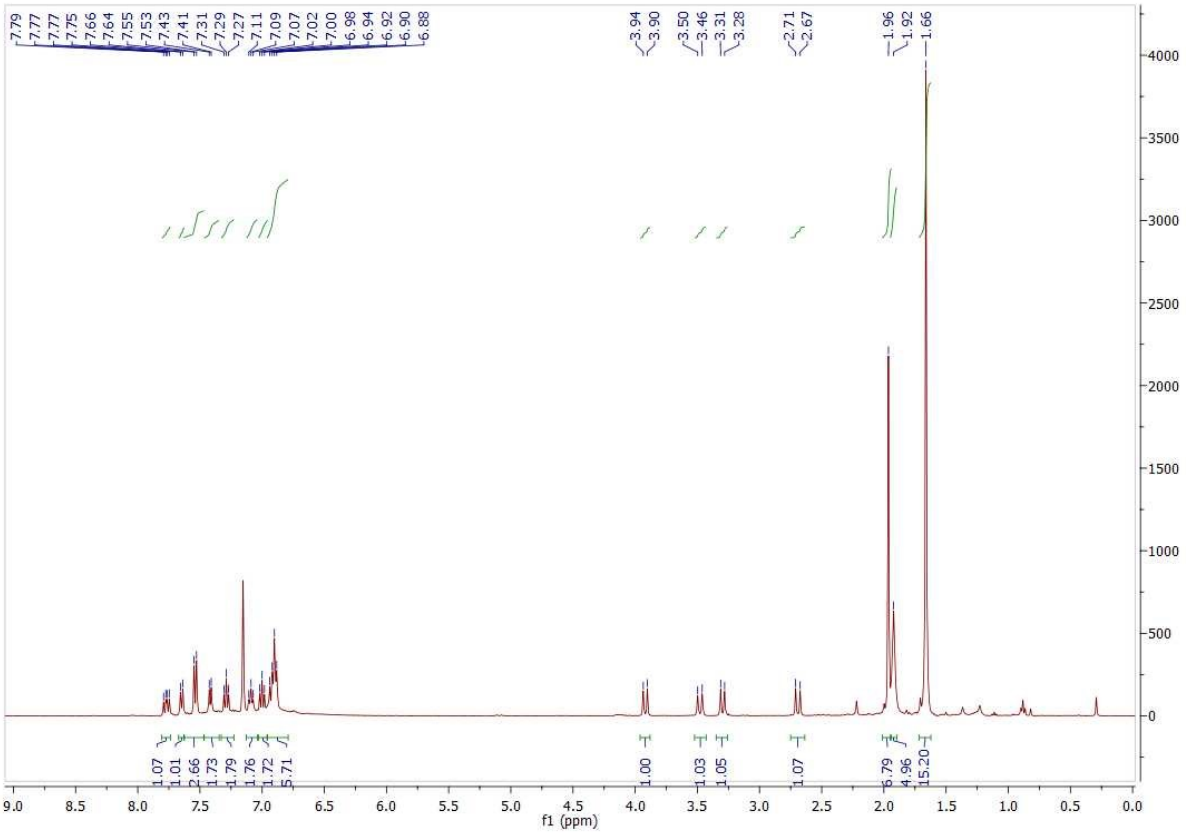


**Figure S15.** $^{1}H$ NMR ($C_6D_6$, 500MHz) of **4.**

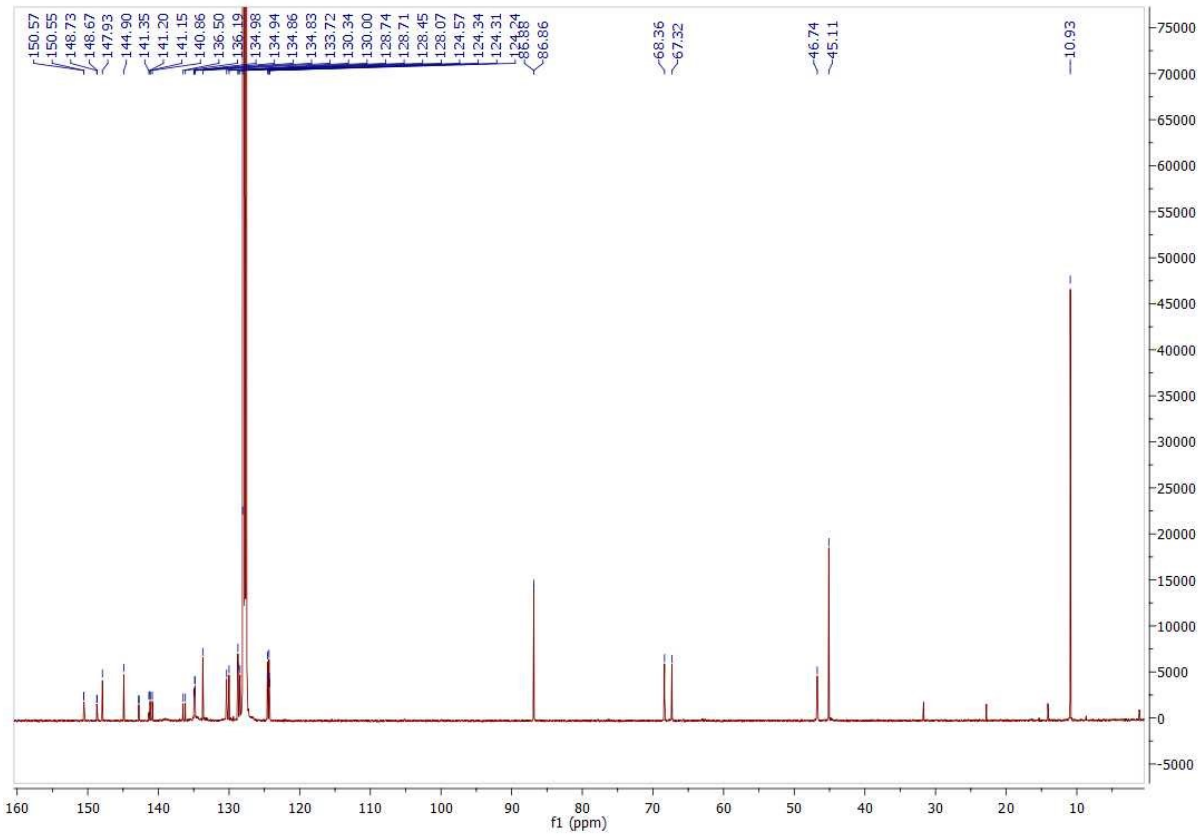


**Figure S16.** $^{13}C\{^{1}H\}$ NMR ($C_6D_6$, 125MHz) of **4.**

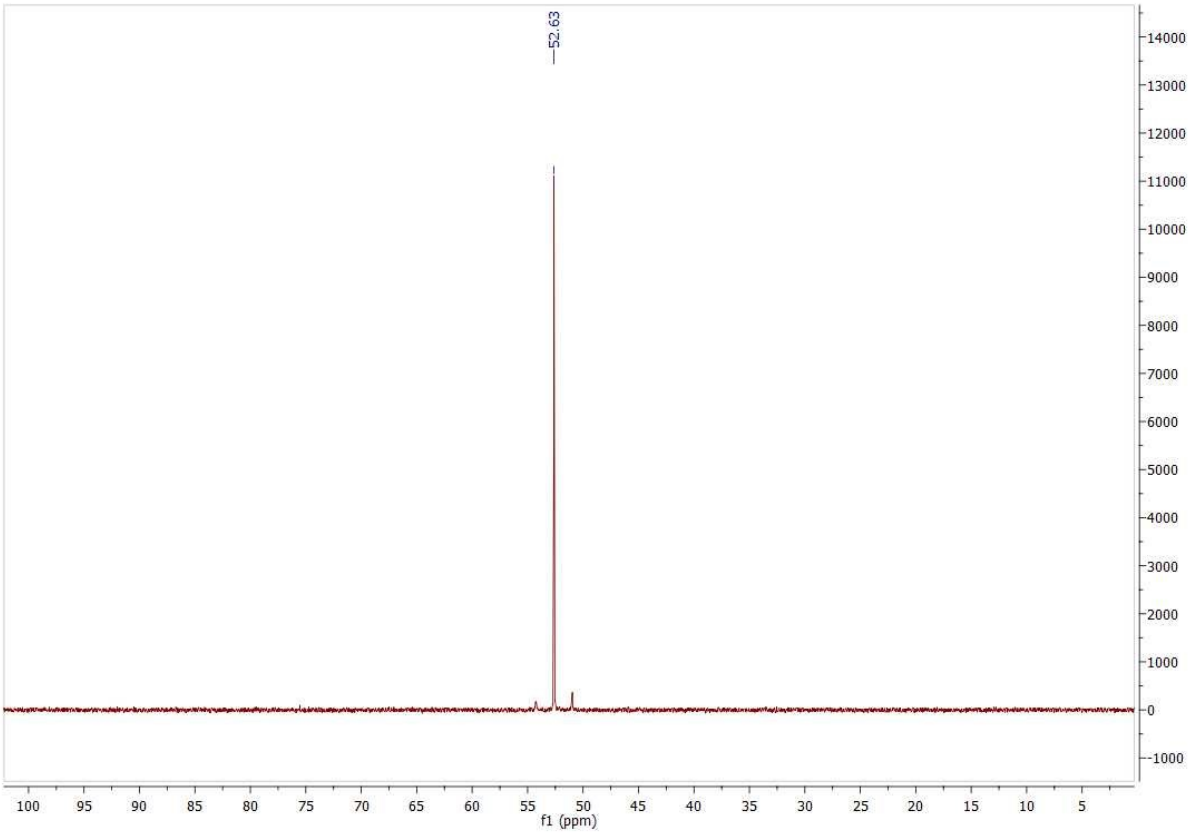


**Figure S17.** $^{31}P\{^{1}H\}$ NMR ($C_6D_6$, 202 MHz) of **4.**

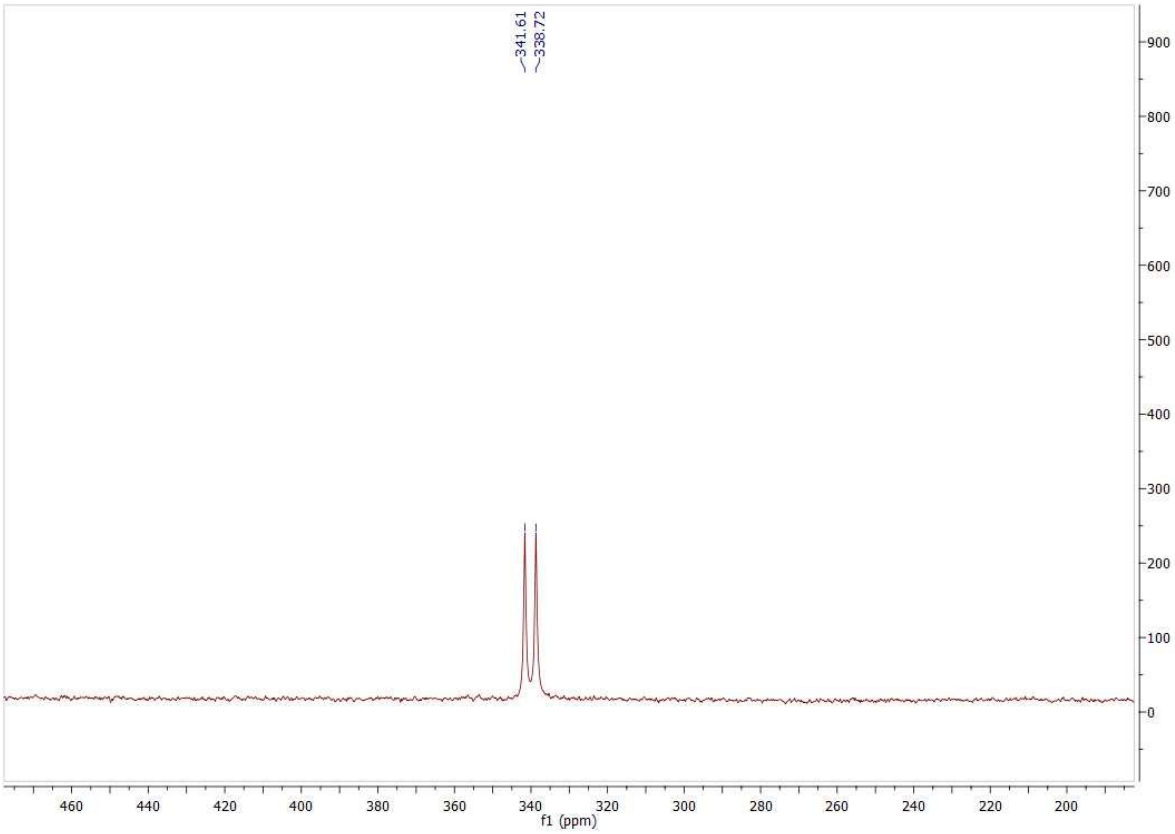


**Figure S18.** $^{119}Sn\{^{1}H\}$ NMR ($C_6D_6$, 186MHz) of **4.**

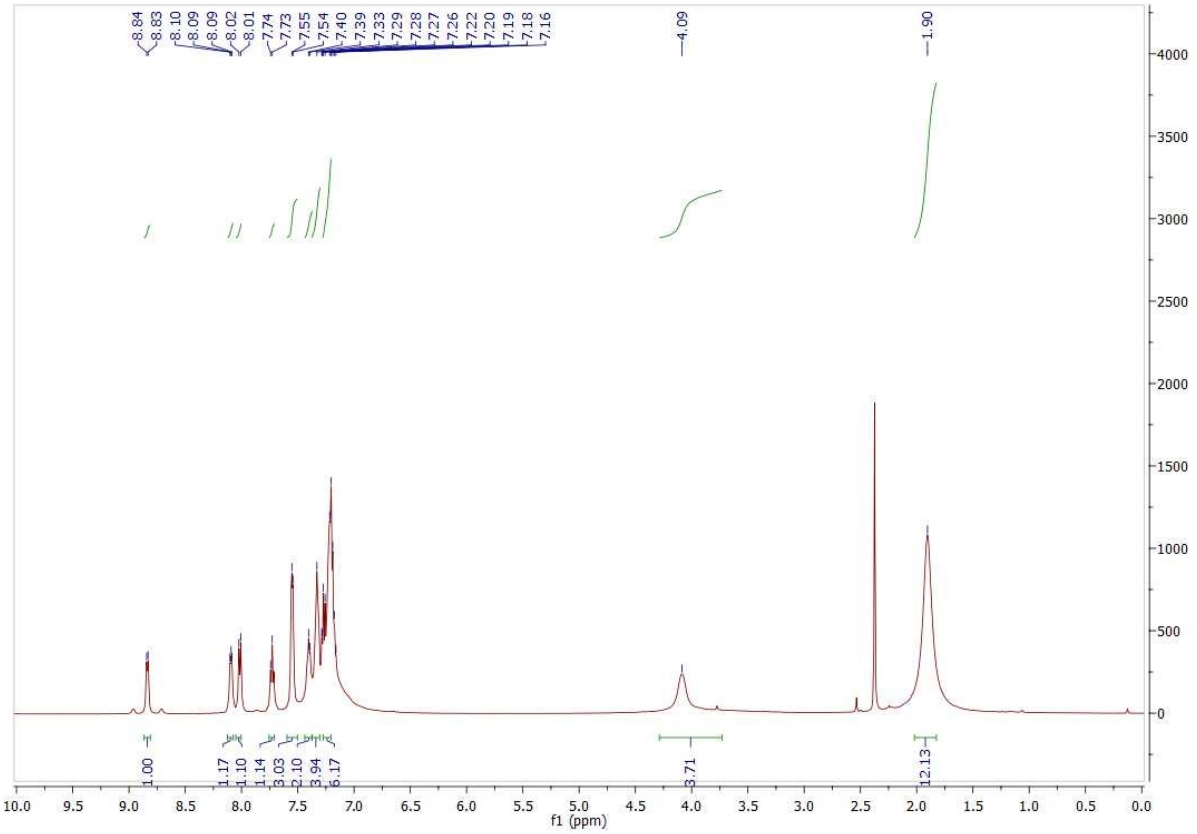


**Figure S19.** $^{1}$H NMR ($CDCl_3$, 500MHz) of **5.**

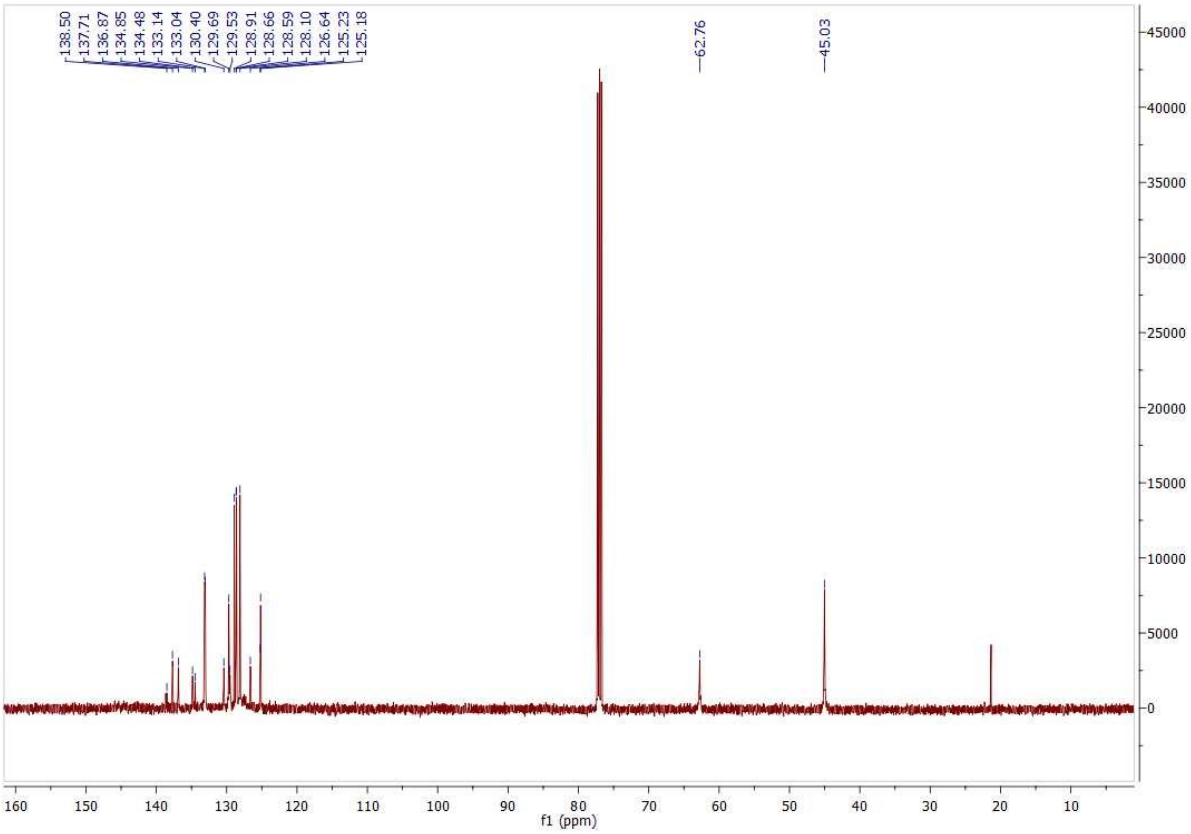


**Figure S20.** $^{13}C\{^{1}H\}$ NMR ($CDCl_3$, 125MHz) of **5.**

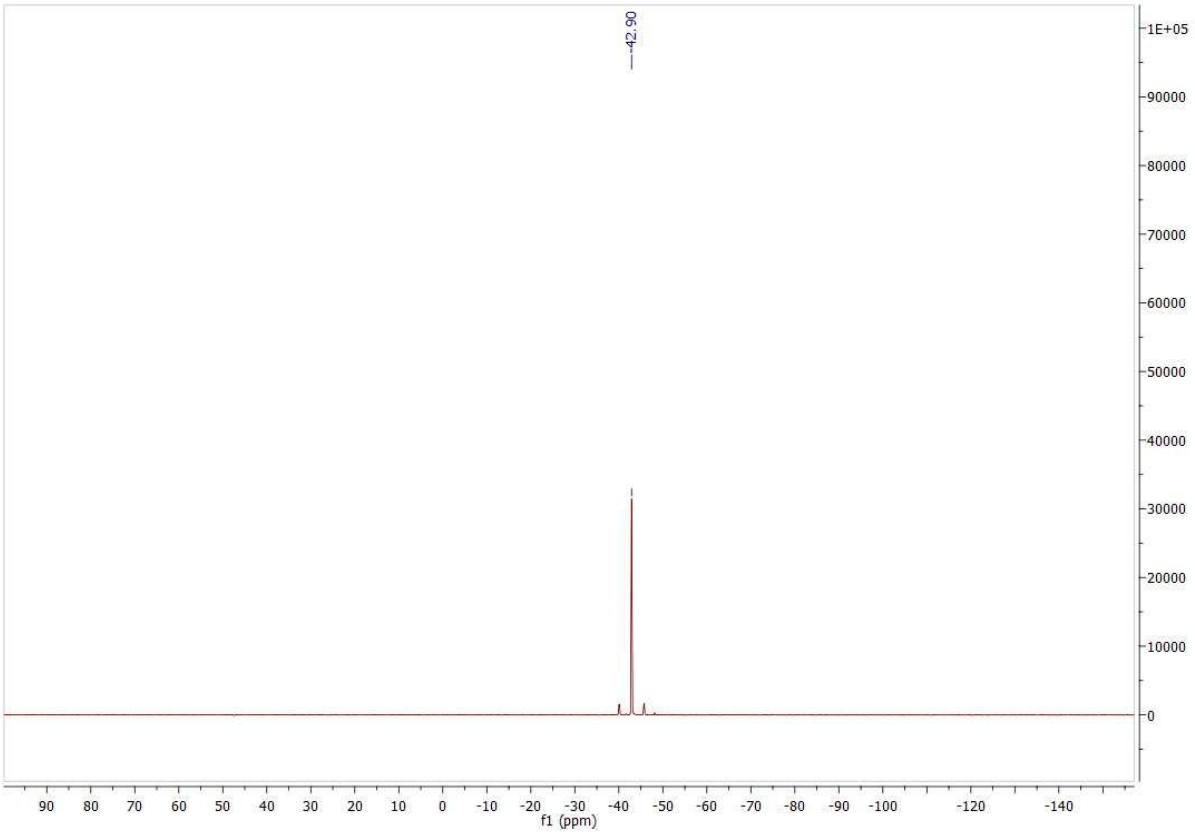


**Figure S21.** $^{31}P\{^{1}H\}$ NMR ($CDCl_3$, 202 MHz) of **5.**

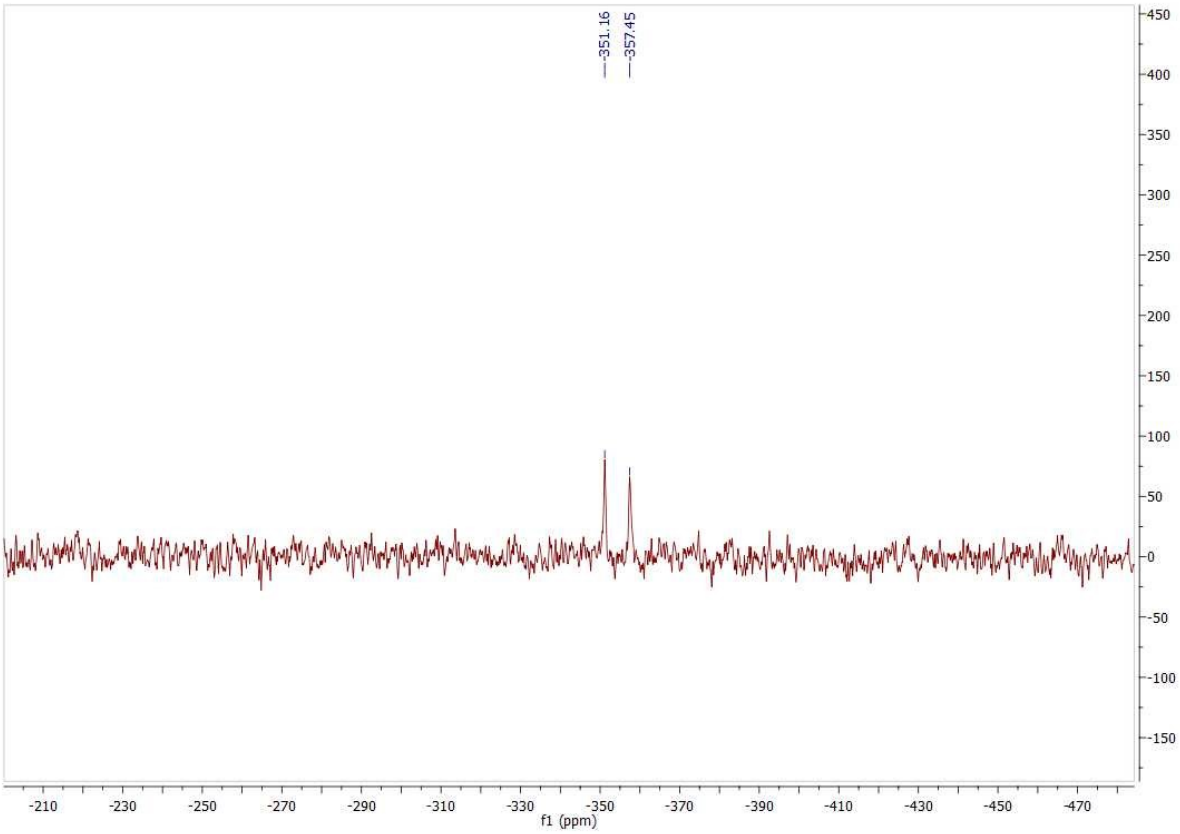


**Figure S22.** $^{119}Sn\{^{1}H\}$ NMR ($CDCl_3$, 186MHz) of **5.**

## 5. Catalytic tests together with NMR and GC MS analysis

*Synthesis of {($C_6H_4CH_2$)N=CH}-$C_6H_5$ via aerobic oxidation of benzylamine catalysed by 0.005 % mmol of* ***2***

**Physical data:** $^1$H NMR (500.13 MHz, $CDCl_3$): δ 8.46 (s, 1H, N=C*H*), 7.89 (m, 2H, Ar*H*), 7.49 (m, 3H, Ar*H*), 7.44 (d, 4H, Ar*H*), 7.35 (m, 1H, Ar*H*), 4.91 (s, 2H, $CH_2$N). $^{13}$C NMR (125.77 MHz, $CDCl_3$): δ 162.0 (CH=N), 139.4 (ArC), 136.2 (ArC), 130.8 (ArC), 128.7 (ArC), 128.6 (ArC), 128.3 (ArC), 128.0 (ArC), 127.0 (ArC), 65.0 ($CH_2$N). EI-MS (70 eV) *m/z* (rel. int.): 195 ($M^+$, 45), 194 (47), 117 (10), 91 (100), 65 (15)

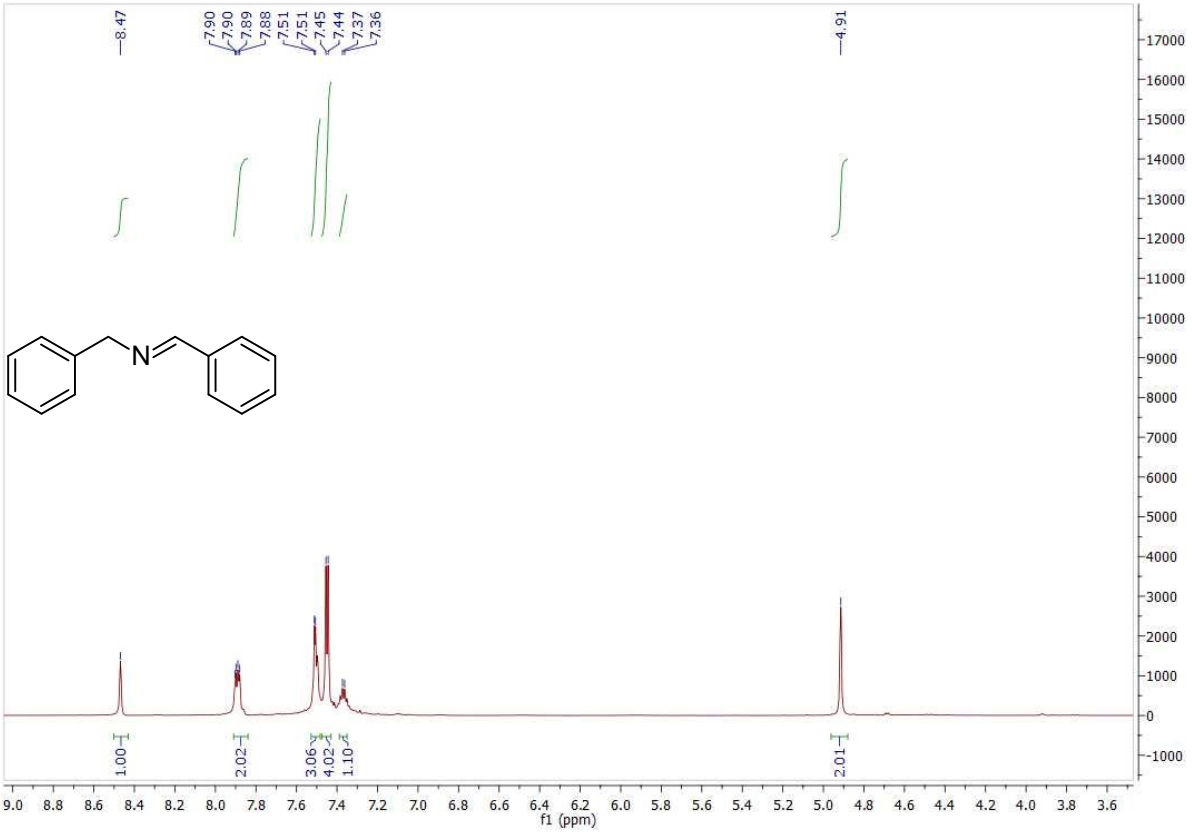


**Figure S23.** $^1$H NMR ($CDCl_3$, 500MHz) of {($C_6H_4CH_2$)N=CH}-$C_6H_5$.

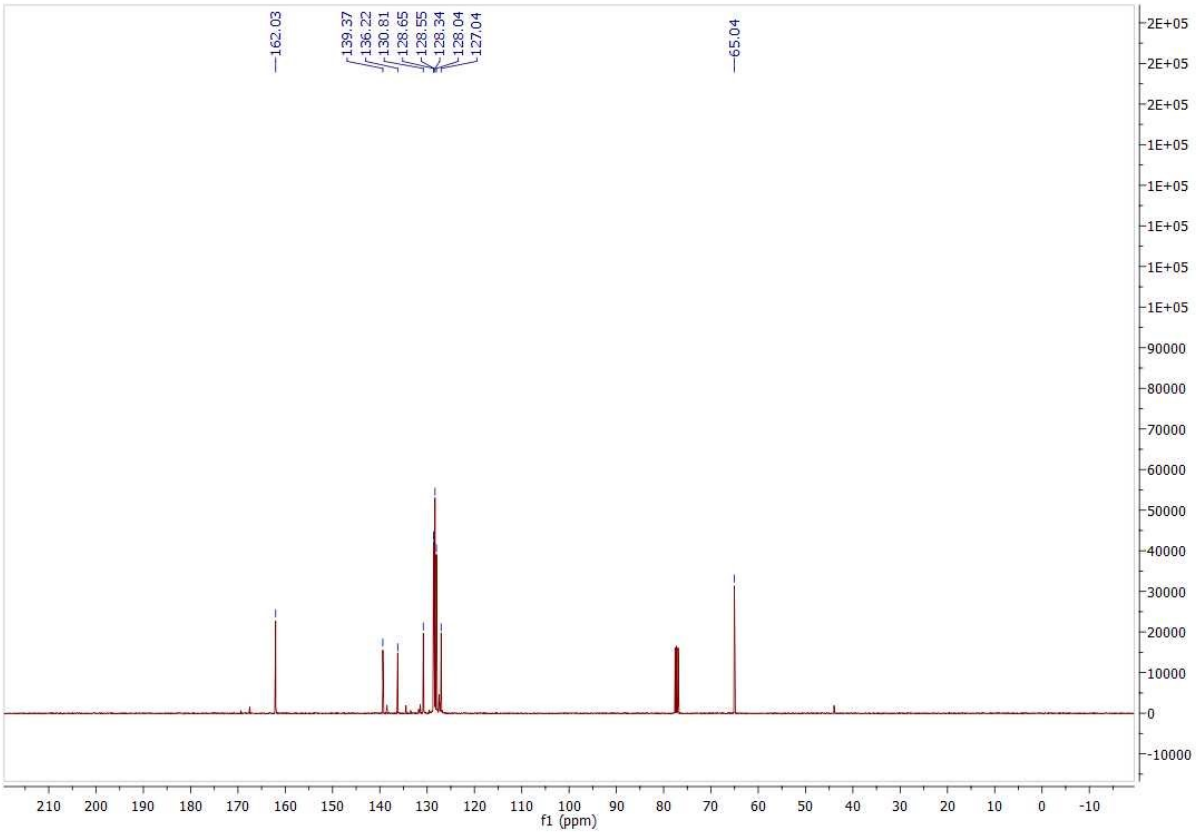


**Figure S24.** $^{13}C\{^{1}H\}$ NMR ($CDCl_3$, 125MHz) of $\{(C_6H_4CH_2)N{=}CH\}\text{-}C_6H_5$.

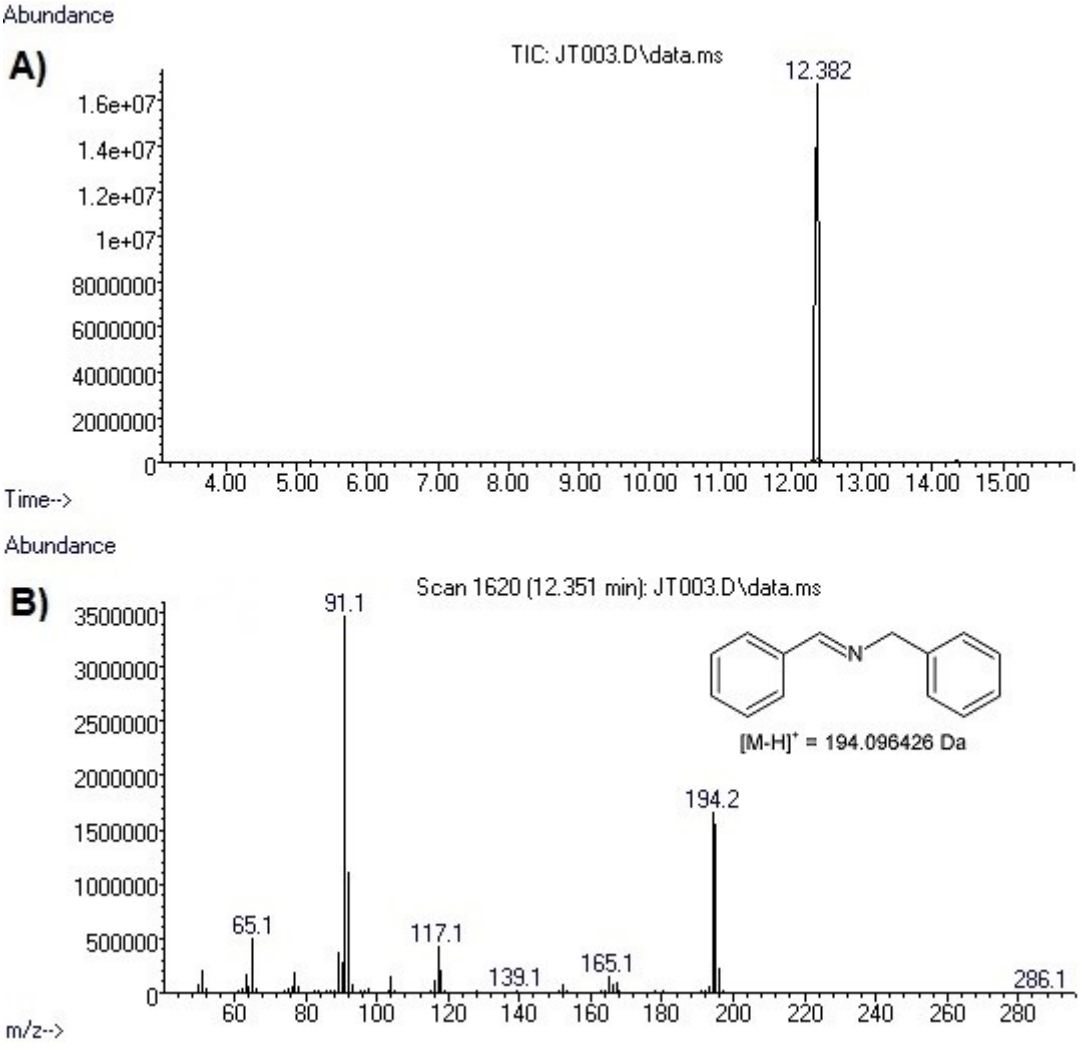


**Figure S25.** A) GC chromatograph of the reaction mixture after 24 h and B) EI-MS spectrum of $\{(C_6H_5CH_2)N{=}CH\}\text{-}C_6H_5$ ($R_t$ ~ 12.3-12.4 min).

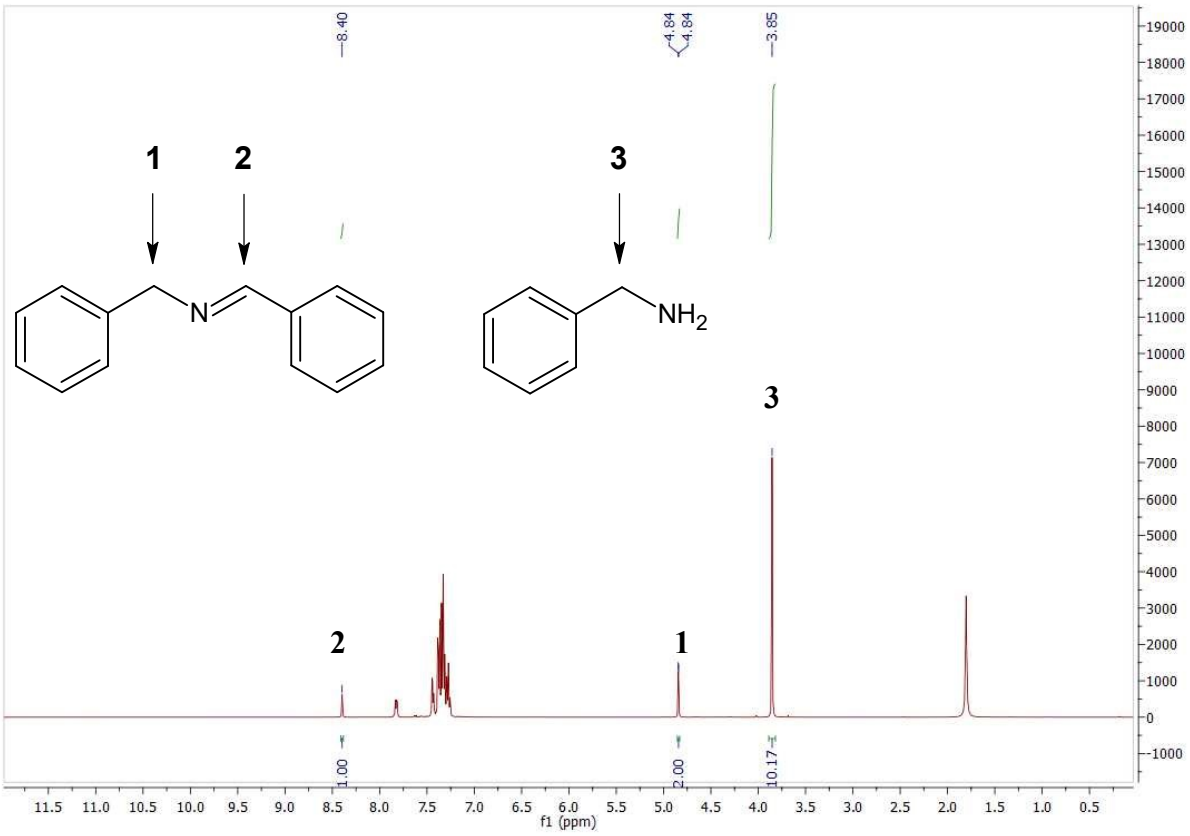


**Figure S26.** $^{1}$H NMR ($CDCl_{3,}$ 500MHz) of the reaction mixture *of the aerobic oxidation of benzylamine catalysed by 0.001 % mmol of* ***2.***

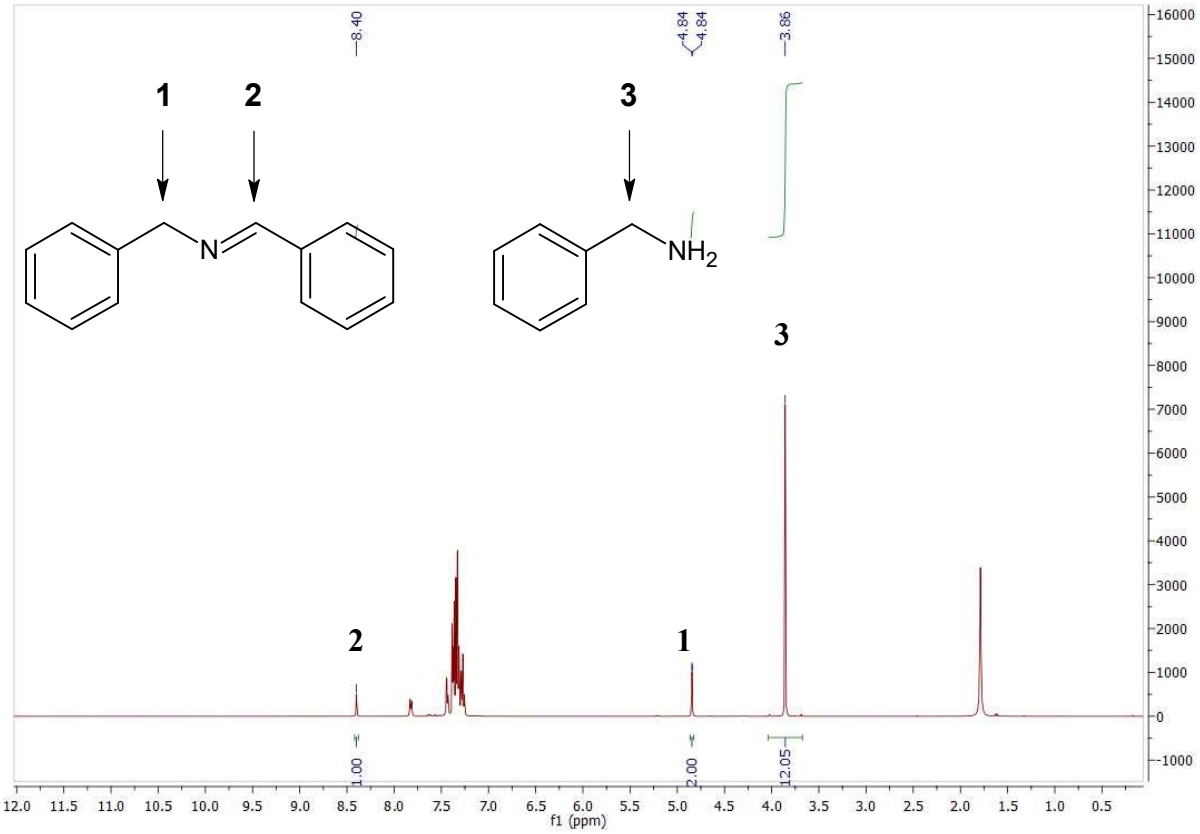


**Figure S27.** $^{1}$H NMR ($CDCl_{3,}$ 500MHz) of the reaction mixture *of the aerobic oxidation of benzylamine catalysed by 0.001 % mmol of **3.***

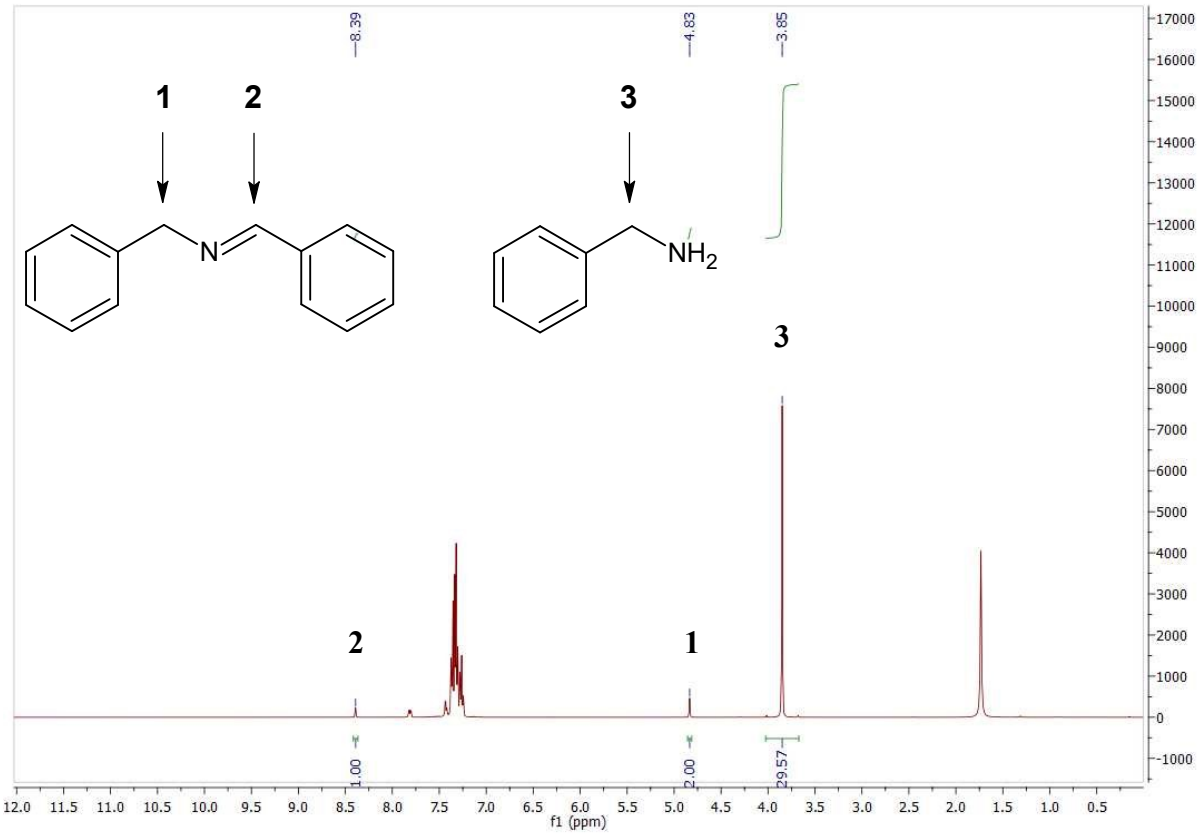


**Figure S28.** $^{1}$H NMR ($CDCl_{3,}$ 500MHz) of the reaction mixture *of the aerobic oxidation of benzylamine catalysed by 0.001 % mmol of* ***4.***

*Synthesis of $C_6H_4CHO$ via aerobic oxidation of benzyl alcohol catalysed by 1 % mmol of* ***2***

**Physical data:** $^1$H NMR (500.13 MHz, $CDCl_3$, 300K): δ 7.39 (s, 1H, Ar*H*), 7.46 (s, 1H, Ar*H*), 7.54 (m, 1H, Ar*H*), 7.80 (s, 1H, Ar*H*), 8.05 (s, 1H, Ar*H*), 9.94 (s, 1H, C*H*=O). EI-MS (70 eV) *m/z* (rel. int.): 106 ($M^+$, 100), 105 (98), 77 (85), 51 (28)

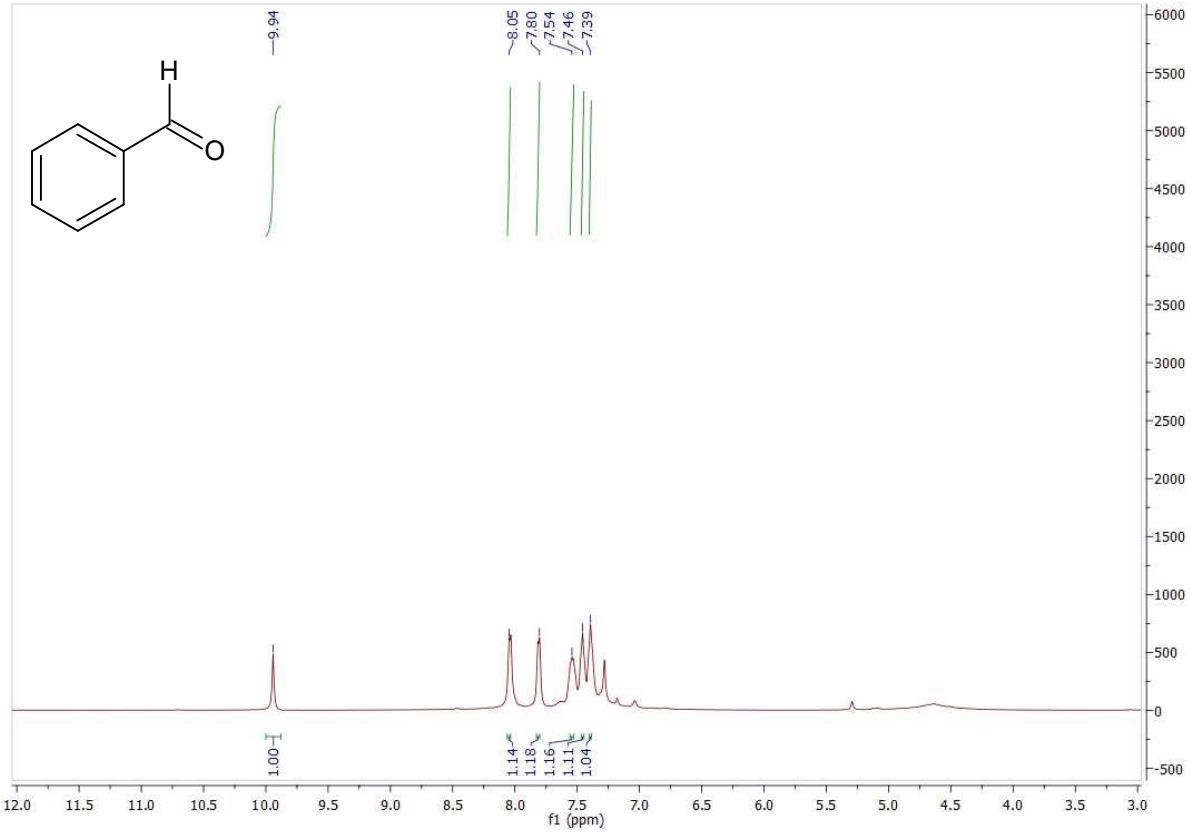


**Figure S29.** $^1$H NMR ($CDCl_3$, 500MHz) of *$C_6H_4CHO$*.

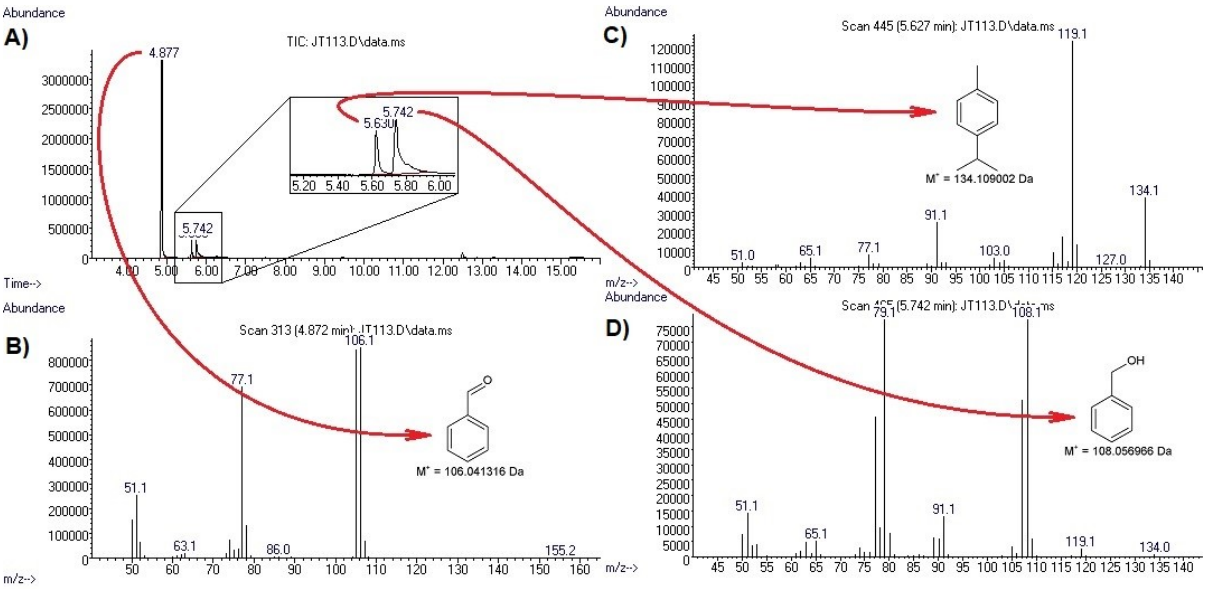


**Figure S30.** A) GC chromatograph of the reaction mixture after 24 h; B) EI-MS spectrum of ($C_6H_5CHO$) ($R_t$ ~ 4.8-4.9 min); C) EI-MS spectrum of *p*-cymene ($R_t$ ~ 5.5-5.7 min); D) EI-MS spectrum of benzyl alcohol ($R_t$ ~ 5.7-5.8 min).

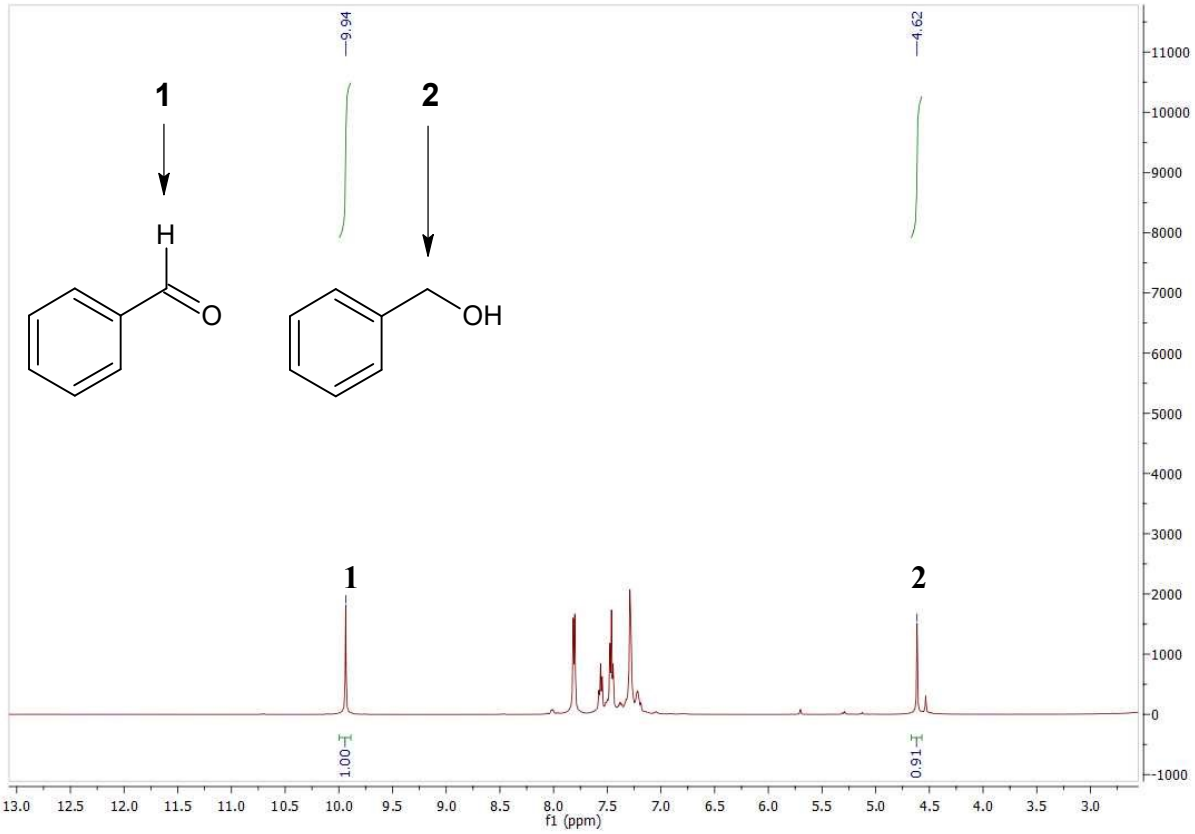


**Figure S31.** $^{1}H$ NMR ($CDCl_3$, 500MHz) of the reaction mixture *of the aerobic oxidation of benzyl alcohol catalysed by 0.1 % mmol of* ***2.***

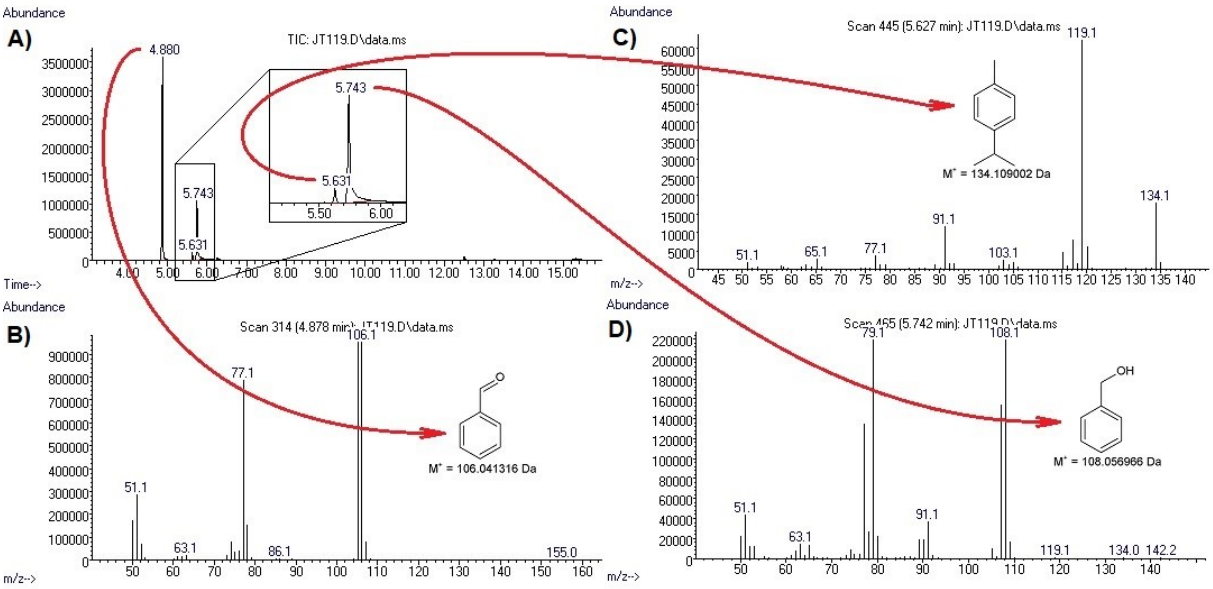


**Figure S32.** A) GC chromatograph of the reaction mixture obtained by the oxidation of *benzyl alcohol catalysed by 0.1 % mmol of* ***2*** after 24 h; B) EI-MS spectrum of ($C_6H_5CHO$) ($R_t$ ~ 4.8-4.9 min); C) EI-MS spectrum of *p*-cymene ($R_t$ ~ 5.6-5.7 min); D) EI-MS spectrum of benzyl alcohol ($R_t$ ~ 5.7-5.8 min).

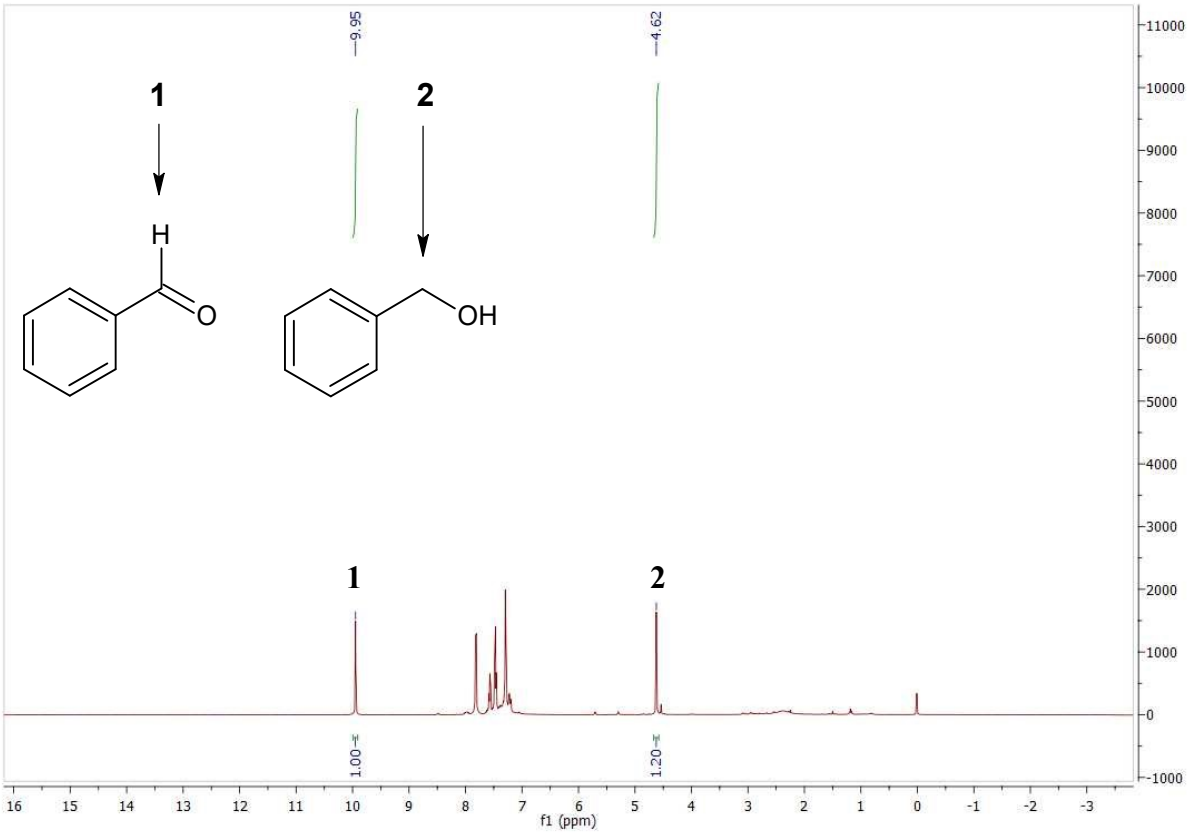


**Figure S33.** $^{1}H$ NMR ($CDCl_3$, 500MHz) of the reaction mixture *of the aerobic oxidation of benzyl alcohol catalysed by 0.1 % mmol of* ***3.***

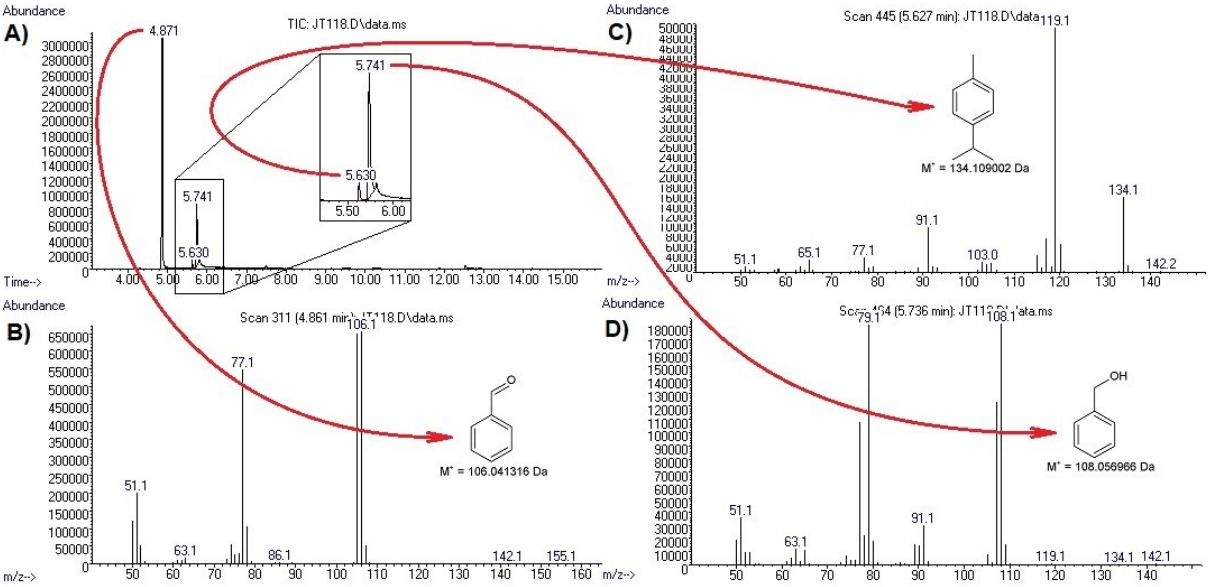


**Figure S34.** A) GC chromatograph of the reaction mixture obtained by the oxidation of *benzyl alcohol catalysed by 0.1 % mmol of **3*** after 24 h; B) EI-MS spectrum of ($C_6H_5CHO$) ($R_t$ ~ 4.8-4.9 min); C) EI-MS spectrum of *p*-cymene ($R_t$ ~ 5.6-5.7 min); D) EI-MS spectrum of benzyl alcohol ($R_t$ ~ 5.7-5.8 min).

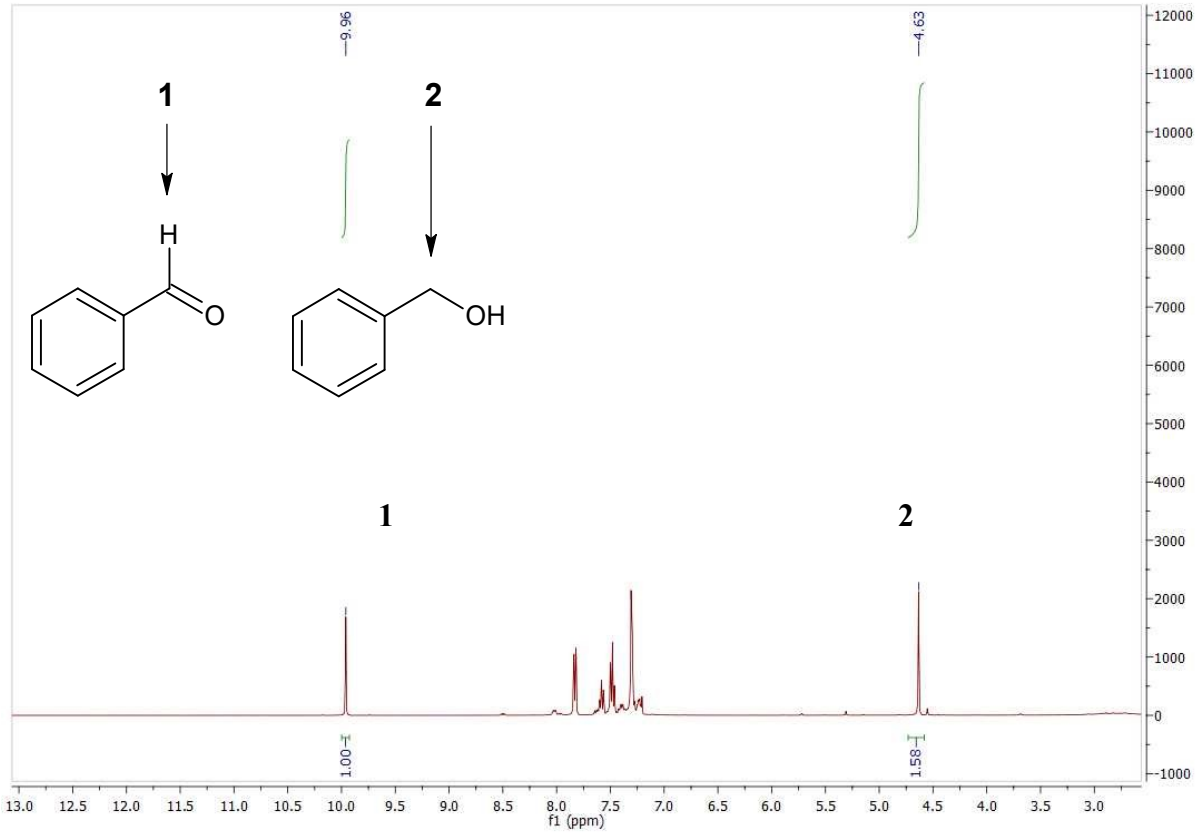


**Figure S35.** $^{1}H$ NMR ($CDCl_3$, 500MHz) of the reaction mixture *of the aerobic oxidation of benzyl alcohol catalysed by 0.1 % mmol of* ***4.***

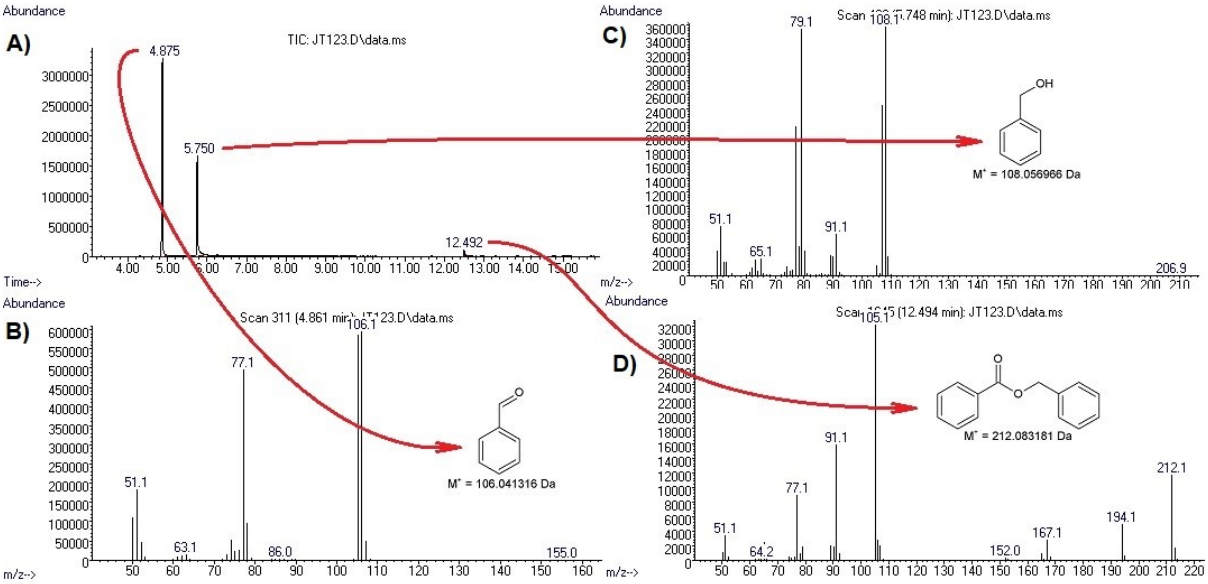


**Figure S36.** A) GC chromatograph of the reaction mixture obtained by the oxidation of *benzyl alcohol catalysed by 0.1 % mmol of **4*** after 24 h; B) EI-MS spectrum of ($C_6H_5CHO$) ($R_t$ ~ 4.8-4.9 min); C) EI-MS spectrum of benzyl alcohol ($R_t$ ~ 5.7-5.8 min); D) EI-MS spectrum of benzyl benzoate ($R_t$ ~ 12.4-12.5 min).

**Table S6.** Catalytic tests for aerobic oxidation of benzylamine with different catalysts.

| Catalyst | Loading (mol% ) | Substrate | Yield (%)[a] |
|---|---|---|---|
| $[\{RuCl_2(\eta^6\text{-cymene})\}_2]$ | 1 | Benzylamine | 71 |
| $[\{RuCl_2(\eta^6\text{-cymene})\}_2]$ + L | 1 | Benzylamine | 24 |
| $[\{RuCl_2(\eta^6\text{-cymene})\}_2]$ + 1-$PPh_2$-8-Br-$C_{10}H_6$ | 1 | Benzylamine | 59 |
| $[\{RuCl_2(\eta^6\text{-cymene})\}_2]$ + L + 1-$PPh_2$-8-Br-$C_{10}H_6$ | 1 | Benzylamine | 50 |
| $[\{RuCl_2(\eta^5\text{-}C_5Me_5)\}_2]$ | 1 | Benzylamine | 73 |
| $[\{RuCl_2(\eta^5\text{-}C_5Me_5)\}_2]$ + L | 1 | Benzylamine | 24 |
| $[\{RuCl_2(\eta^5\text{-}C_5Me_5)\}_2]$ + 1-$PPh_2$-8-Br-$C_{10}H_6$ | 1 | Benzylamine | 39 |
| $[\{RuCl_2(\eta^5\text{-}C_5Me_5)\}_2]$ + L + 1-$PPh_2$-8-Br-$C_{10}H_6$ | 1 | Benzylamine | 81 |
| compound **1** | 1 | Benzylamine | 0 |
| compound **2** | 1 | propylamine | 0 |
| compound **2** | 1 | oleyamine | 0 |

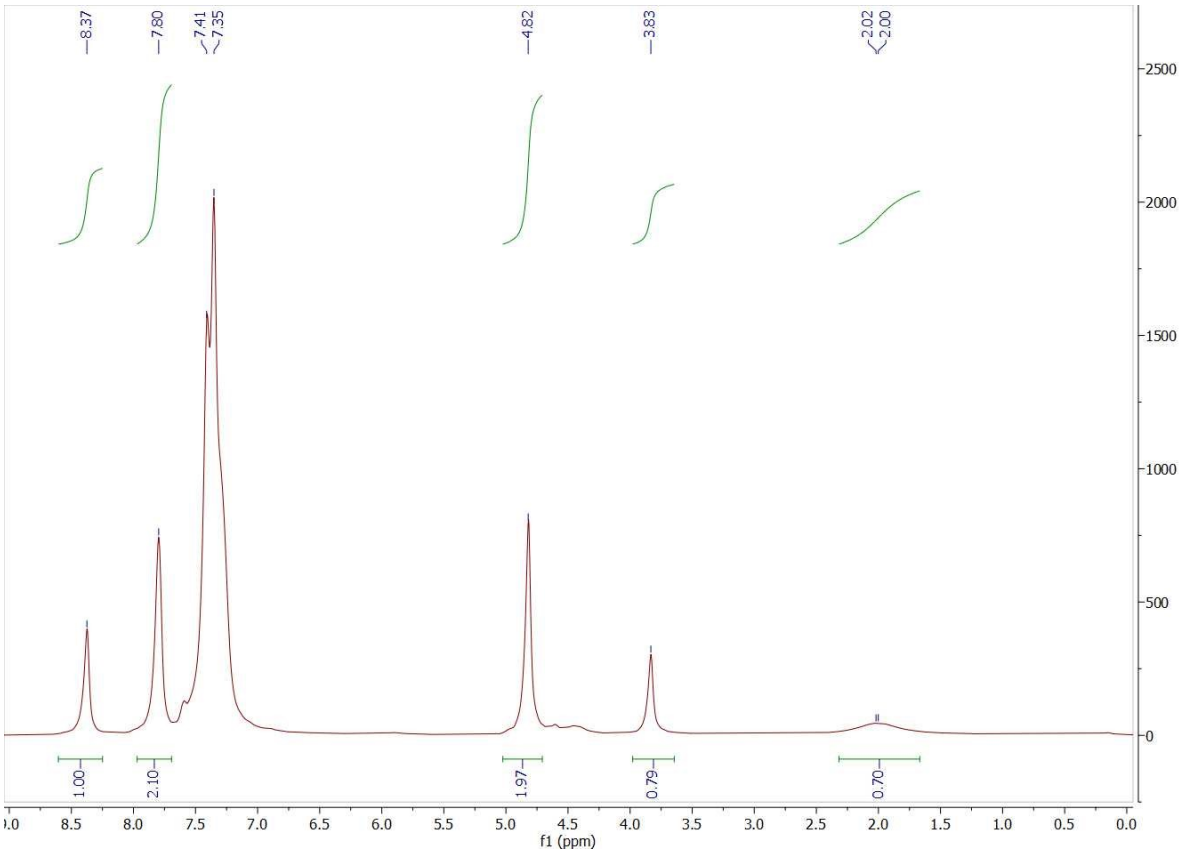


**Figure S37.** $^{1}H$ NMR ($CDCl_3$, 500MHz) of the reaction mixture *of the aerobic oxidation of benzylamine catalysed by 1 % mmol of [{$RuCl_2(\eta^6$-cymene)}$_2$].*

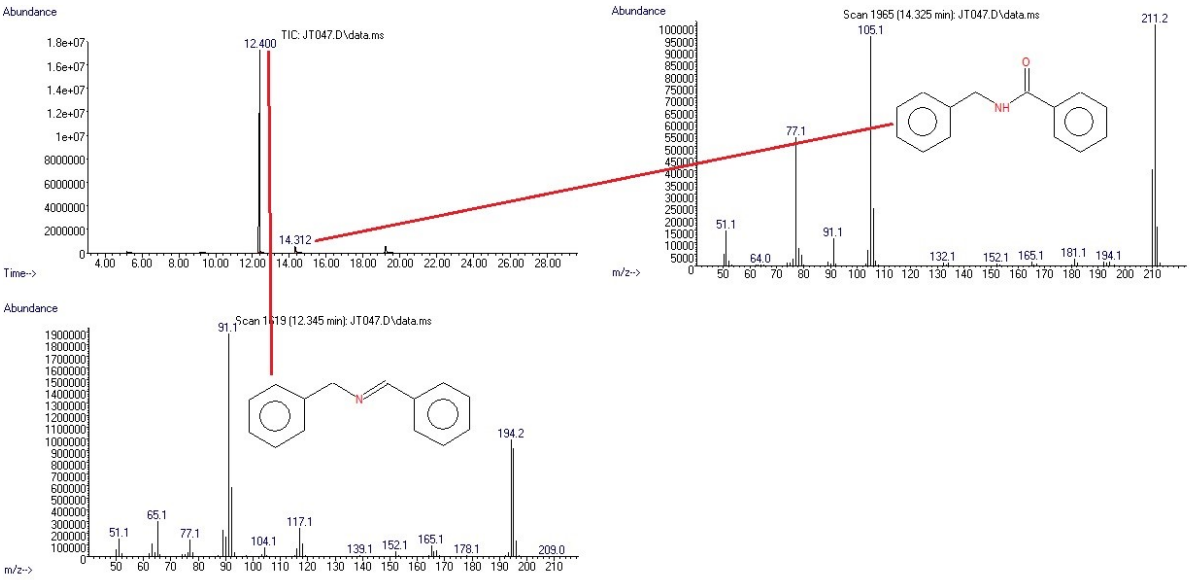


**Figure S38.** A) GC chromatograph of the reaction mixture obtained by the *aerobic oxidation of benzylamine catalysed by 1 % mmol of [{RuCl$_2$($\eta^6$-cymene)}$_2$]* after 24 h; B) EI-MS spectrum of {($C_6H_5CH_2$)N=CH}-$C_6H_5$ ($R_t$ ~ 12.3-12.4 min); C) EI-MS spectrum of {($C_6H_5CHO$)NH$CH_2$}-$C_6H_5$ ($R_t$ ~ 14.3-14.4 min).

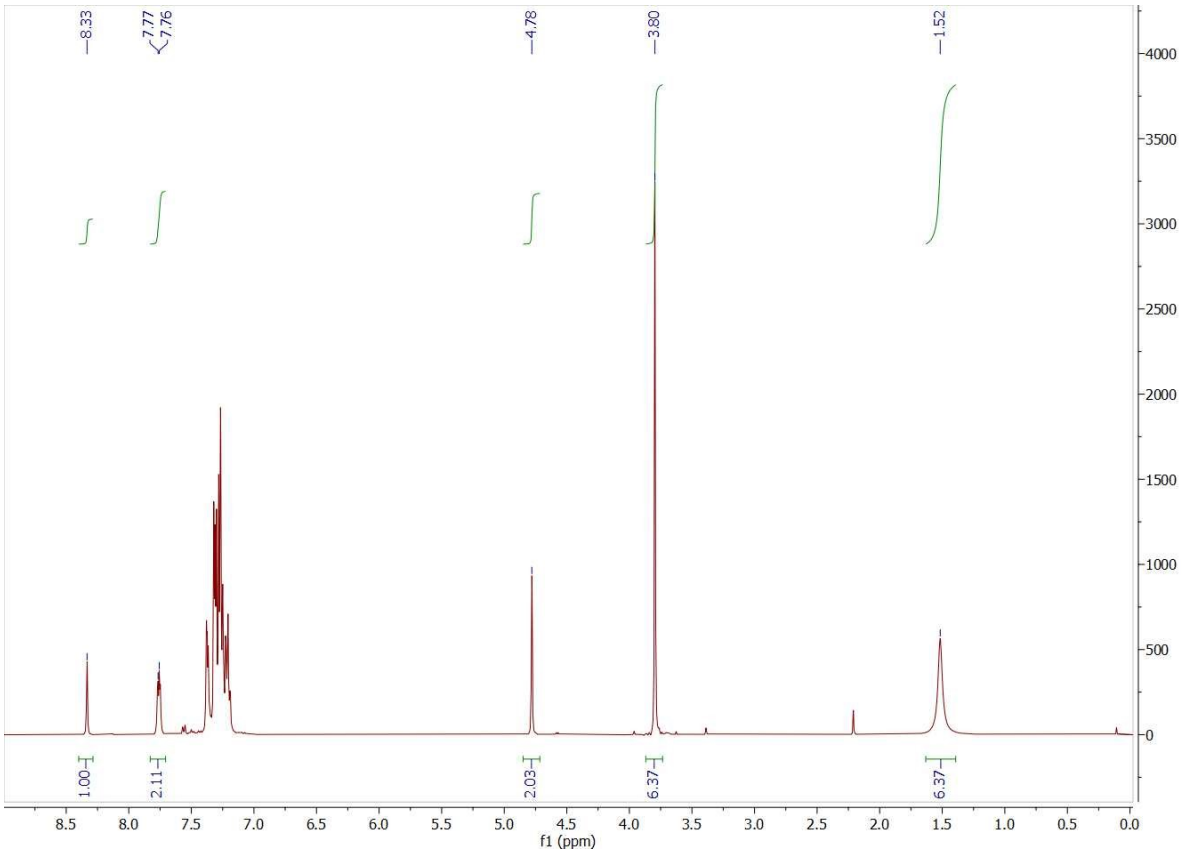


**Figure S39.** $^{1}$H NMR ($CDCl_3$, 500MHz) of the reaction mixture *of the aerobic oxidation of benzylamine catalysed by 1 % mmol of [{$RuCl_2(\eta^6$-cymene)}$_2$] + L.*

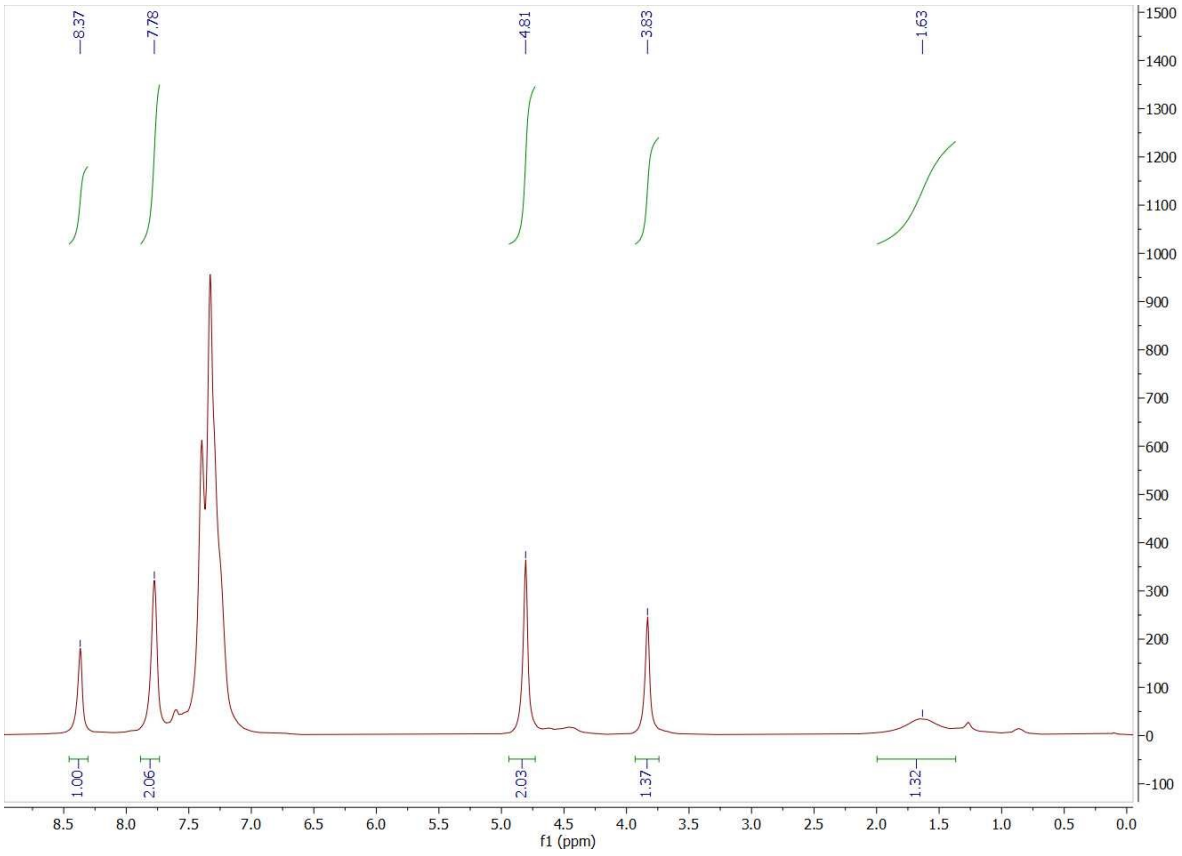


**Figure S40**. $^{1}$H NMR ($CDCl_3$, 500MHz) of the reaction mixture *of the aerobic oxidation of benzylamine catalysed by 1 % mmol of [{$RuCl_2(\eta^6$-cymene)}$_2$] + 1-$PPh_2$-8-Br-$C_{10}H_6$.*

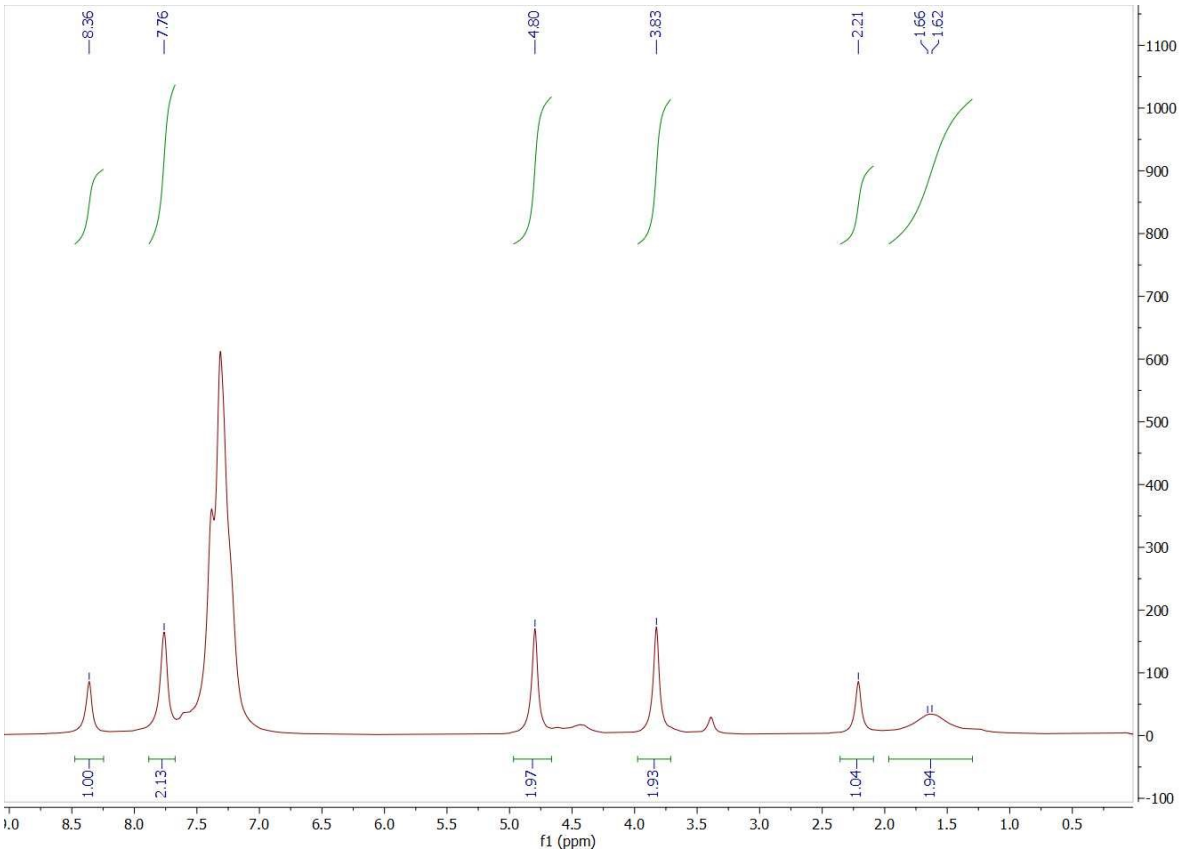


**Figure S41.** $^{1}$H NMR ($CDCl_3$, 500MHz) of the reaction mixture *of the aerobic oxidation of benzylamine catalysed by 1 % mmol of [{$RuCl_2(\eta^6$-cymene)}$_2$] + L + 1-$PPh_2$-8-Br-$C_{10}H_6$.*

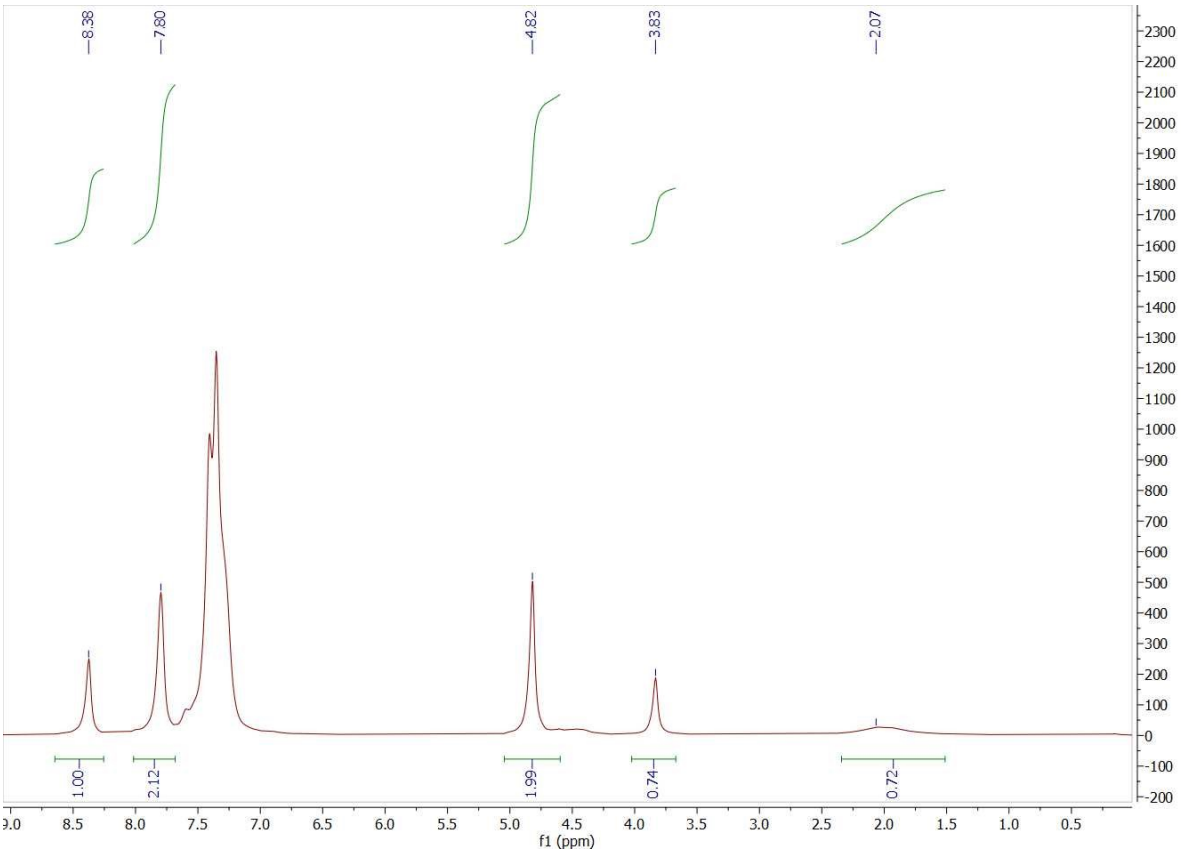


**Figure S42.** $^{1}$H NMR ($CDCl_3$, 500MHz) of the reaction mixture *of the aerobic oxidation of benzylamine catalysed by 1 % mmol of [{$RuCl_2(\eta^5\text{-}C_5Me_5)$}$_2$].*

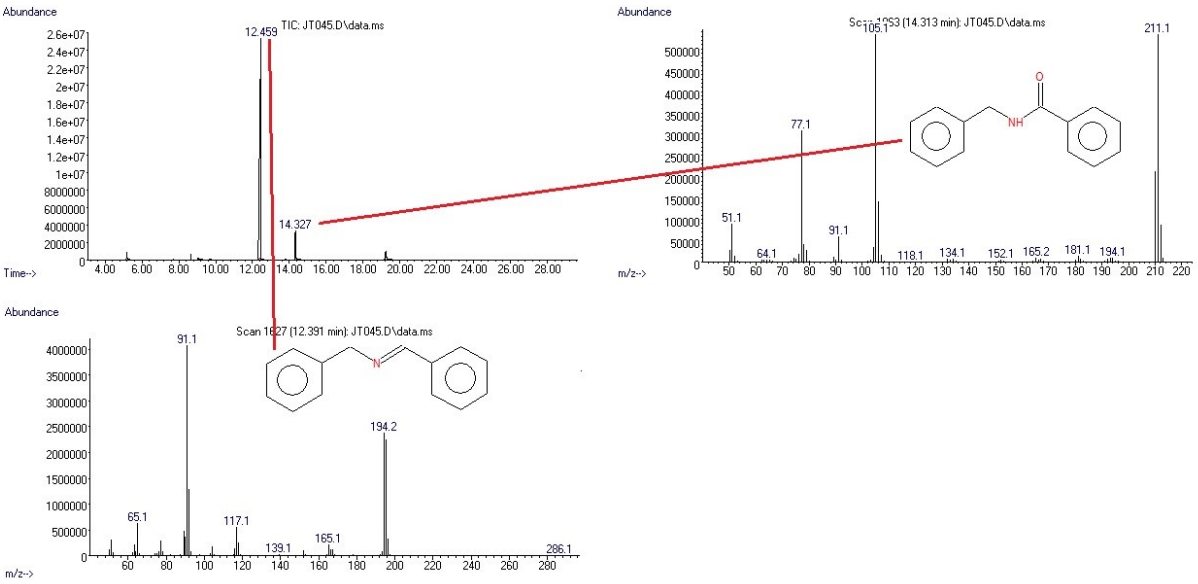


**Figure S43.** A) GC chromatograph of the reaction mixture obtained by the *aerobic oxidation of benzylamine catalysed by 1 % mmol of* $[\{RuCl_2(\eta^5\text{-}C_5Me_5)\}_2]$ after 24 h; B) EI-MS spectrum of $\{(C_6H_5CH_2)N{=}CH\}\text{-}C_6H_5$ ($R_t$ ~ 12.3-12.4 min); C) EI-MS spectrum of $\{(C_6H_5CHO)NHCH_2\}\text{-}C_6H_5$ ($R_t$ ~ 14.3-14.4 min).

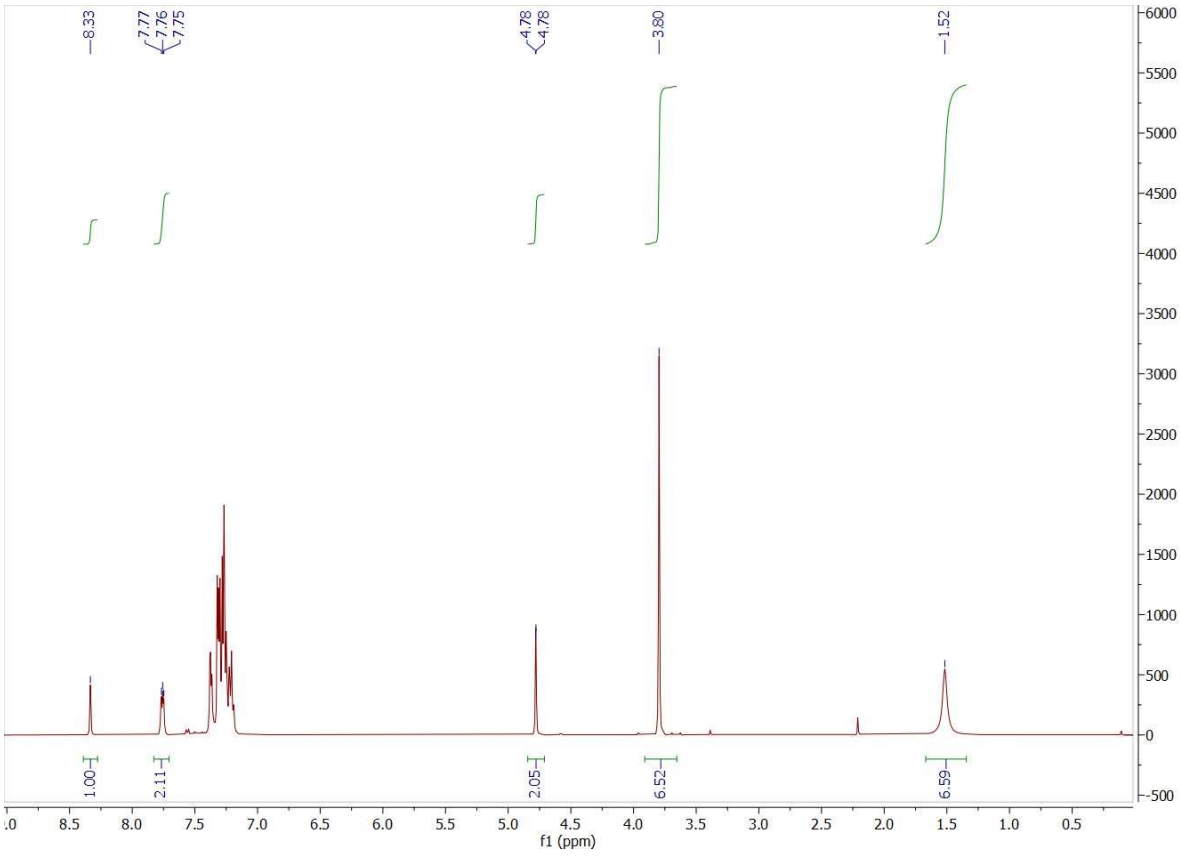


**Figure S44.** $^{1}$H NMR ($CDCl_3$, 500MHz) of the reaction mixture *of the aerobic oxidation of benzylamine catalysed by 1 % mmol of [{$RuCl_2(\eta^5\text{-}C_5Me_5)$}$_2$] + L.*

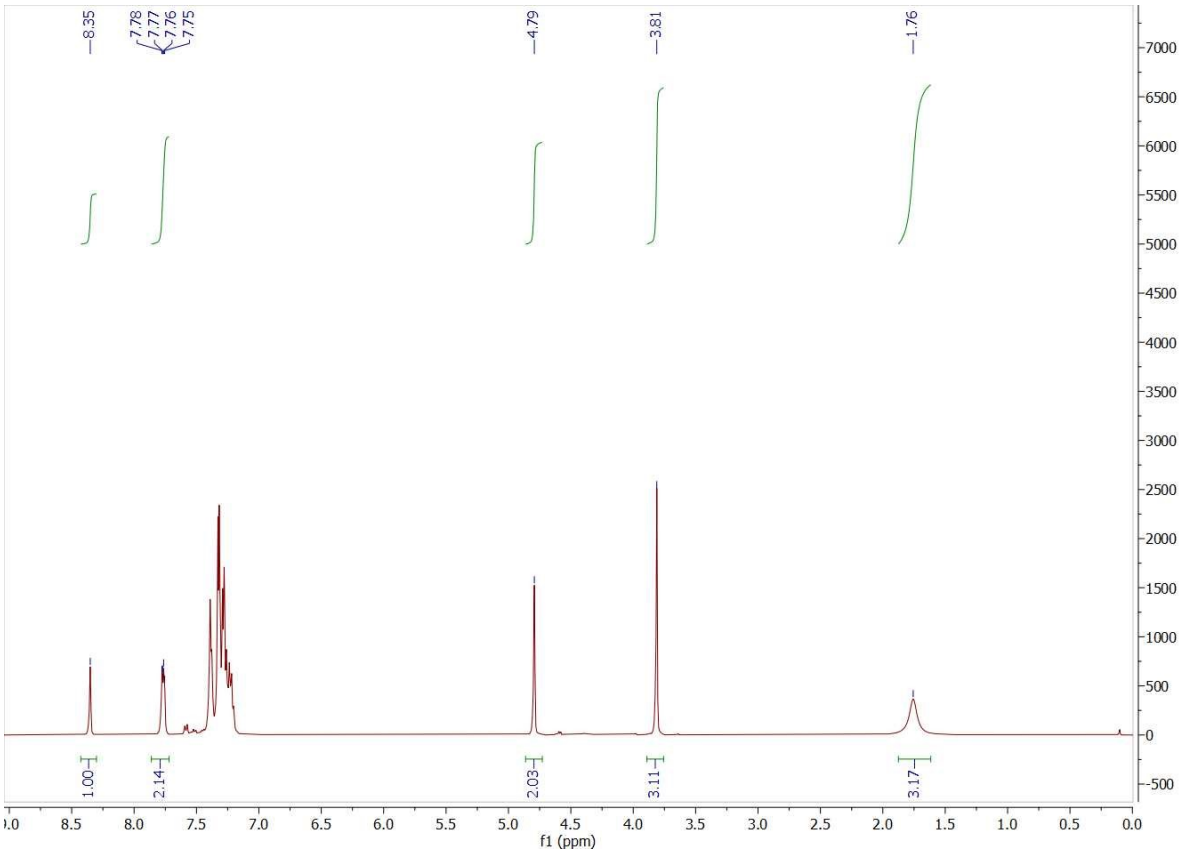


**Figure S45.** $^{1}$H NMR ($CDCl_3$, 500MHz) of the reaction mixture *of the aerobic oxidation of benzylamine catalysed by 1 % mmol of* $[\{RuCl_2(\eta^5\text{-}C_5Me_5)\}_2]$ + 1-$PPh_2$-8-Br-$C_{10}H_6$.

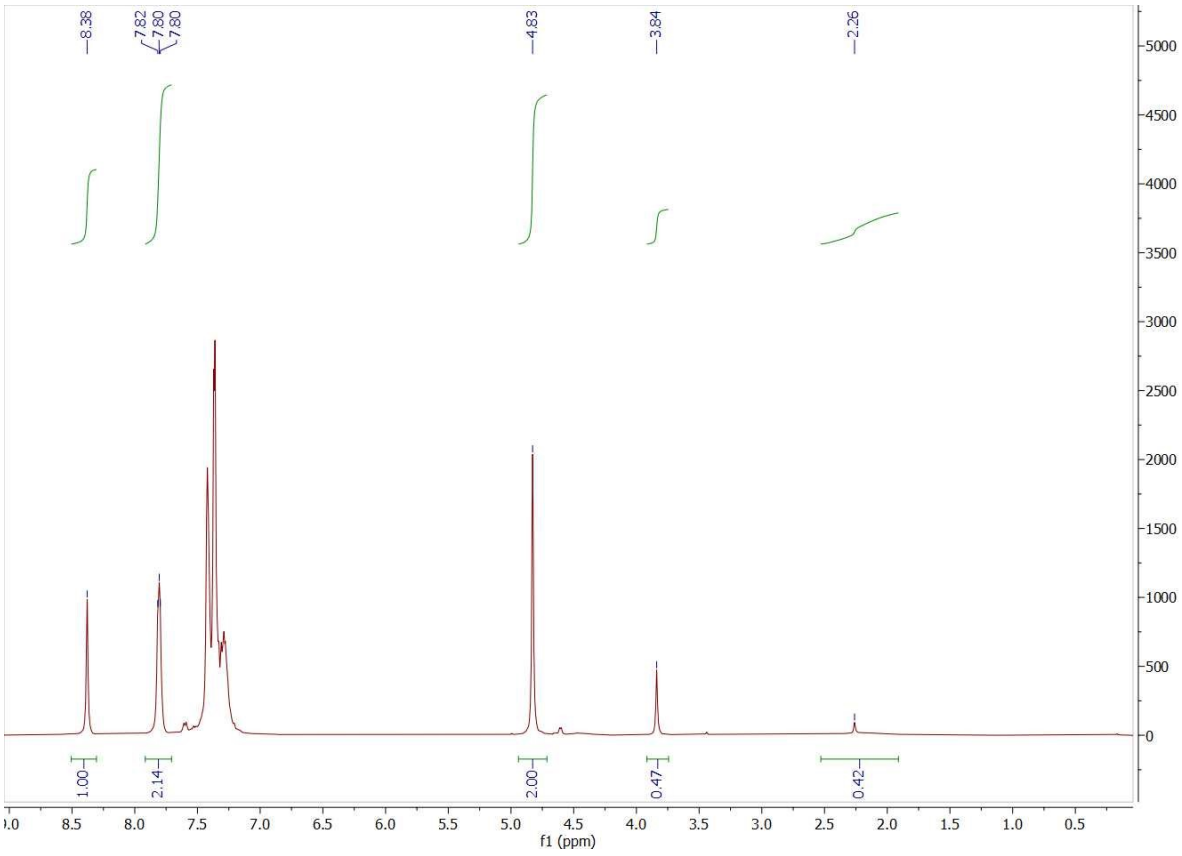


**Figure S46.** $^{1}H$ NMR ($CDCl_3$, 500MHz) of the reaction mixture *of the aerobic oxidation of benzylamine catalysed by 1 % mmol of* $[\{RuCl_2(\eta^5\text{-}C_5Me_5)\}_2]$ + L + 1-$PPh_2$-8-Br-$C_{10}H_6$.

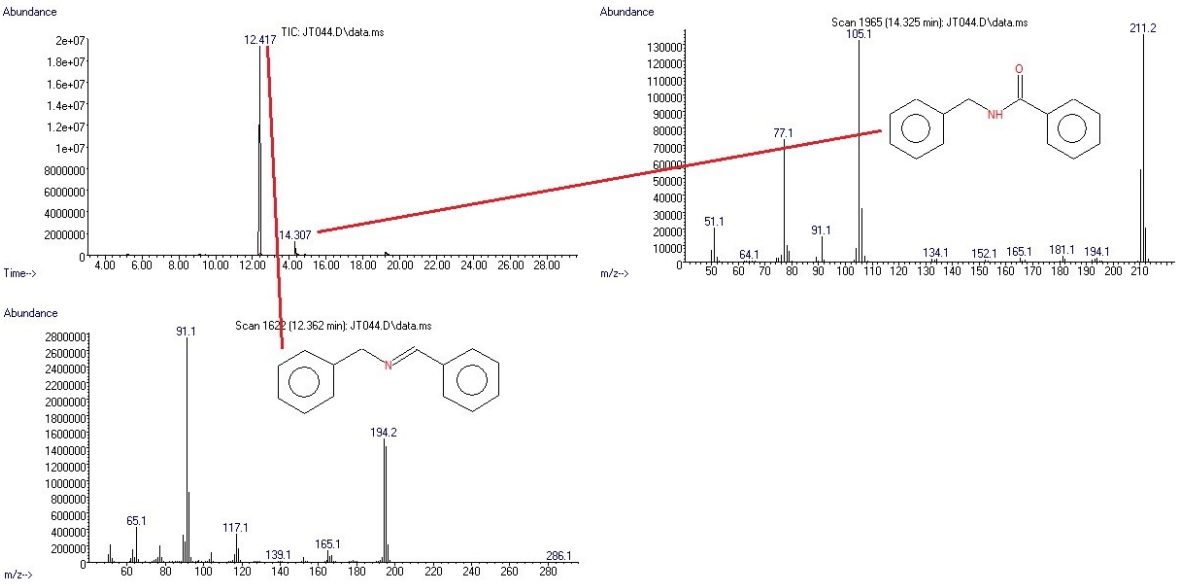


**Figure S47.** A) GC chromatograph of the reaction mixture obtained by the *aerobic oxidation of benzylamine catalysed by 1 % mmol of* $[\{RuCl_2(\eta^5\text{-}C_5Me_5)\}_2]$ + L + 1-$PPh_2$-8-Br-$C_{10}H_6$ after 24 h; B) EI-MS spectrum of $\{(C_6H_5CH_2)N{=}CH\}\text{-}C_6H_5$ ($R_t$ ~ 12.3-12.4 min); C) EI-MS spectrum of $\{(C_6H_5CHO)NHCH_2\}\text{-}C_6H_5$ ($R_t$ ~ 14.3-14.4 min).

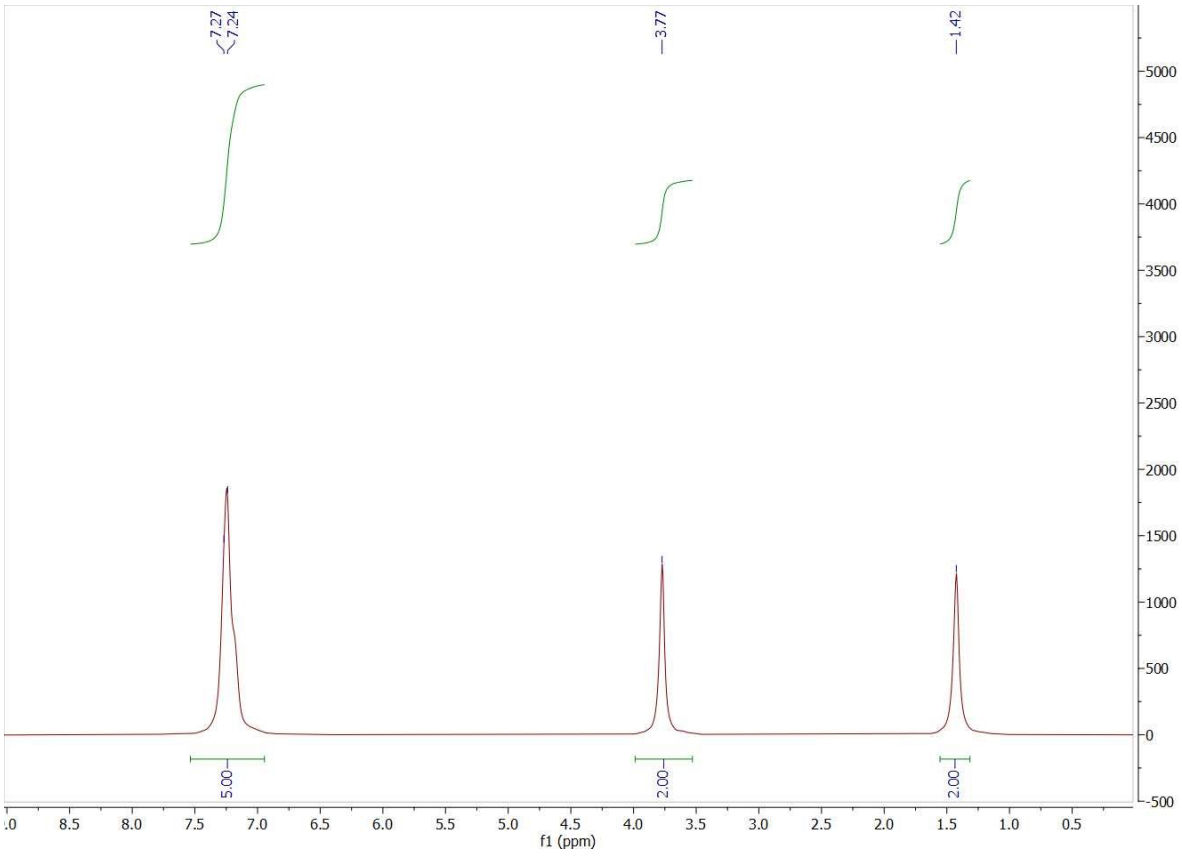


**Figure S48.** $^{1}$H NMR ($CDCl_3$, 500MHz) of the reaction mixture *of the aerobic oxidation of benzylamine catalysed by 1 % mmol of* ***1.***

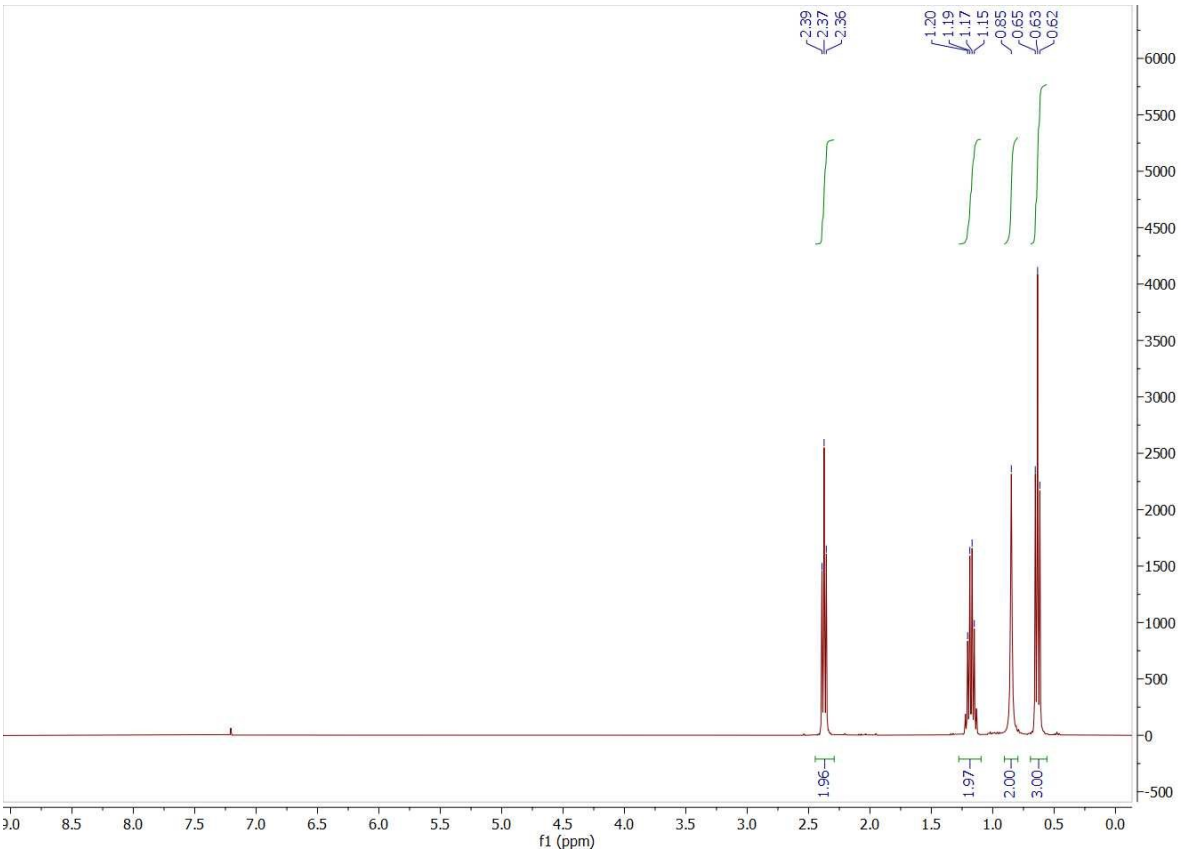


**Figure S49.** $^{1}H$ NMR ($CDCl_3$, 500MHz) of the reaction mixture *of the aerobic oxidation of propylamine catalysed by 1 % mmol of* ***2.***

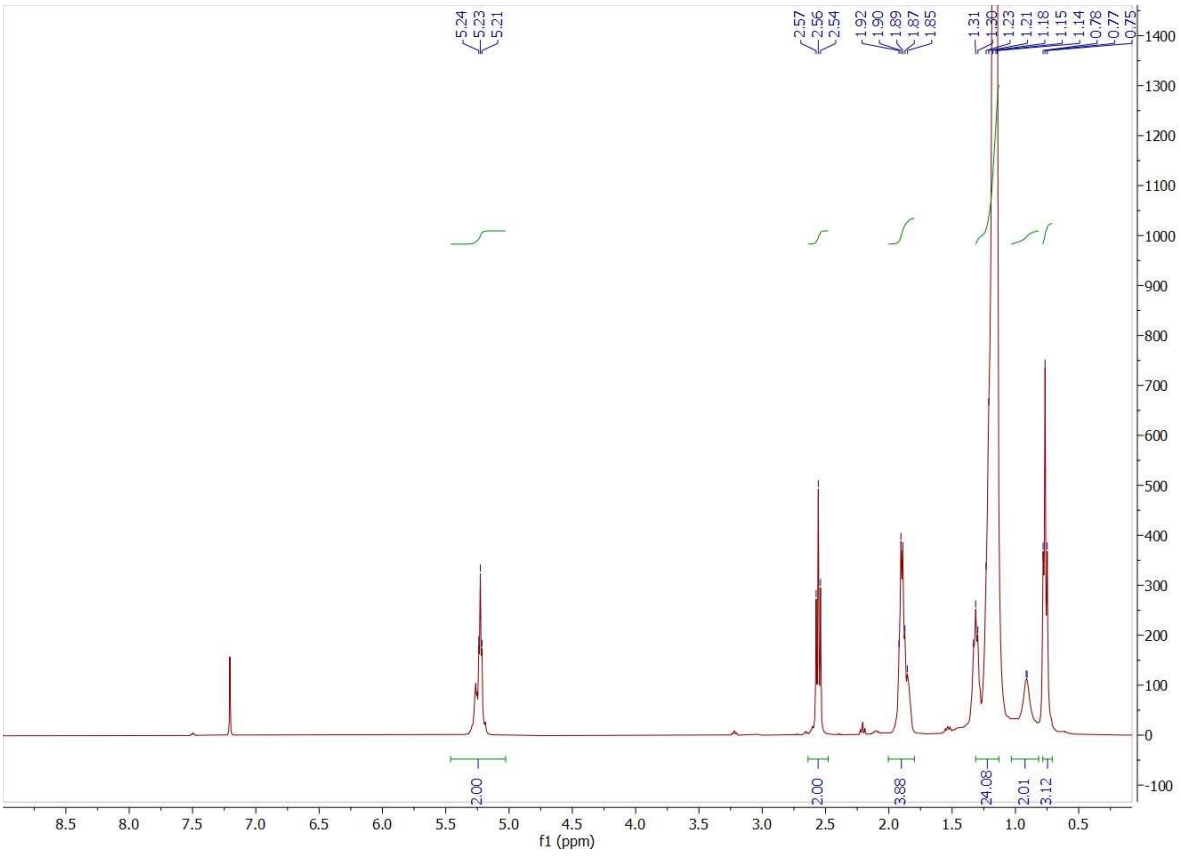


**Figure S50.** $^{1}H$ NMR ($CDCl_3$, 500MHz) of the reaction mixture *of the aerobic oxidation of oleylamine catalysed by 1 % mmol of* ***2.***

## 6. Kinetic and mechanistic studies

**Table S7.** Kinetic studies for the oxidation of benzylamine with 0.005 mol% of **2.**

| time (h) | Conversion of benzylamine | |
|---|---|---|
| | Oxidant | |
| | Air | Oxygen |
| 1 | 2 | 5 |
| 2 | 4 | 15 |
| 3 | 5 | 64 |
| 6 | 28 | 82 |
| 10 | 60 | 94 |
| 12 | 72 | 99 |
| 16 | 100 | |

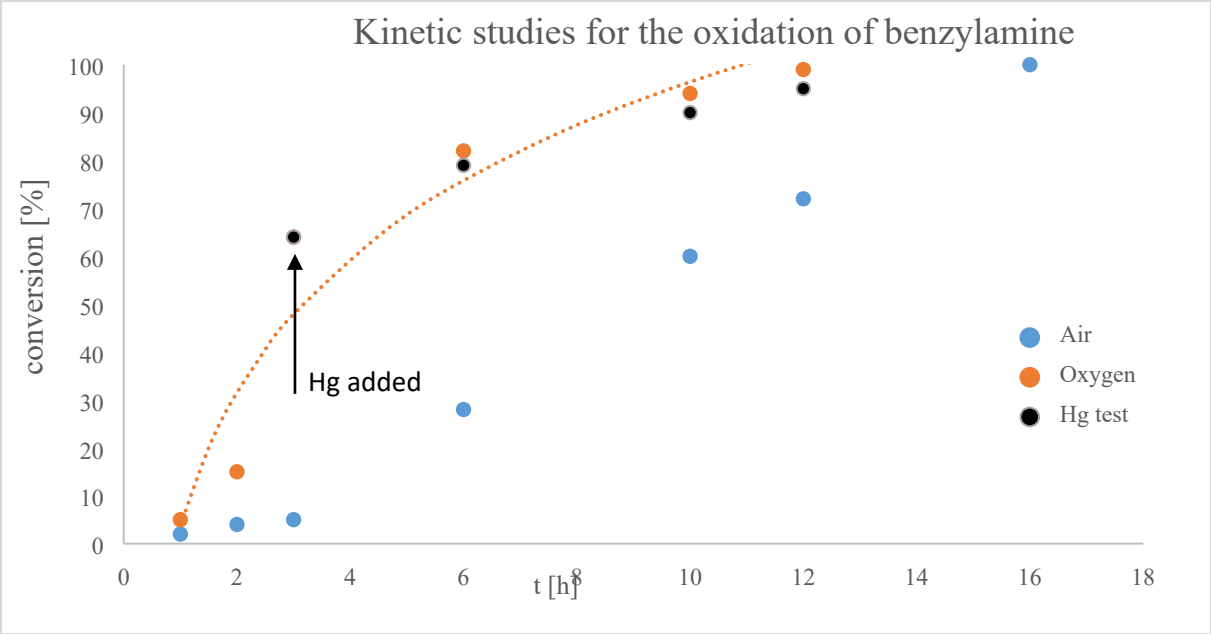


**Figure S51.** Kinetic studies for the oxidation of benzylamine with 0.005 mol% of **2.**

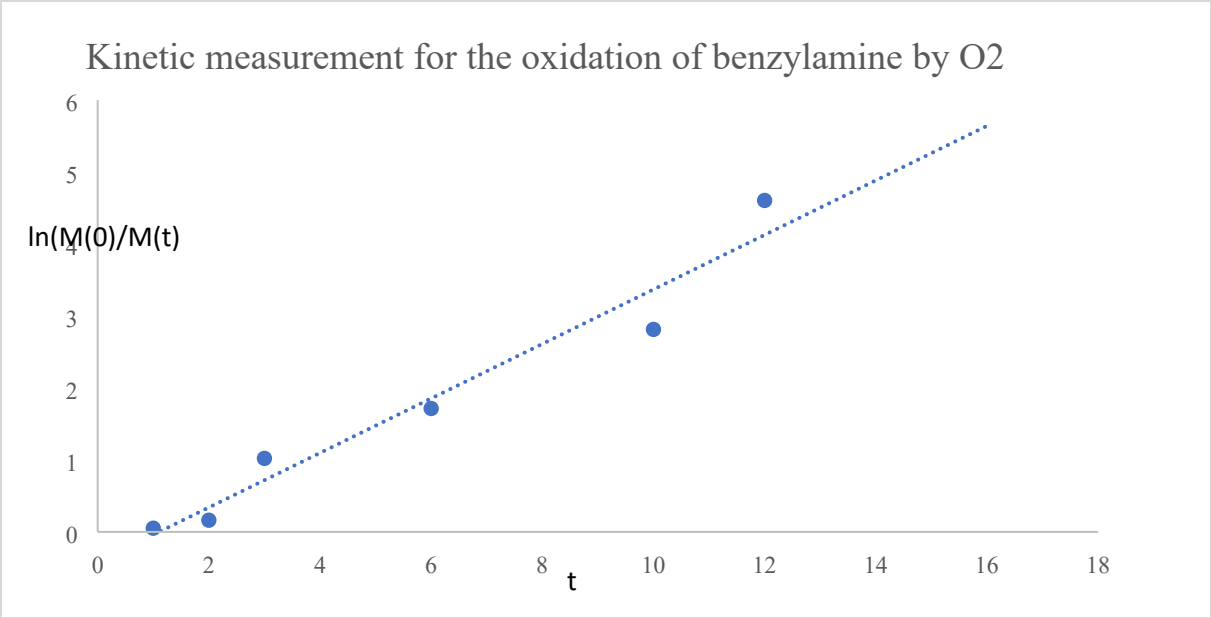


**Figure S52.** Kinetic studies for the oxidation of benzylamine with 0.005 mol% of **2**, oxygen is used as an oxidant.

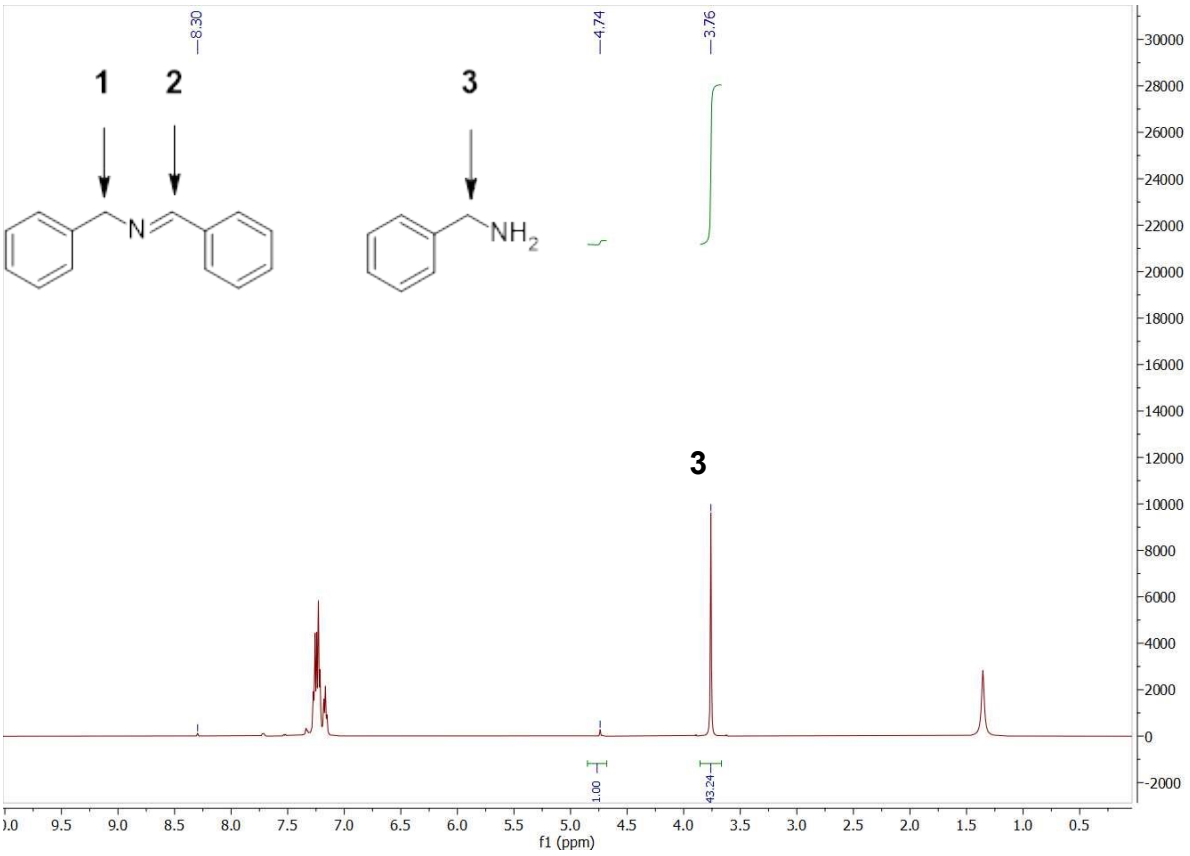


**Figure S53.** Kinetic studies for the oxidation of benzylamine with 0.005 mol% of **2,** air is used as an oxidant, time 1 h.

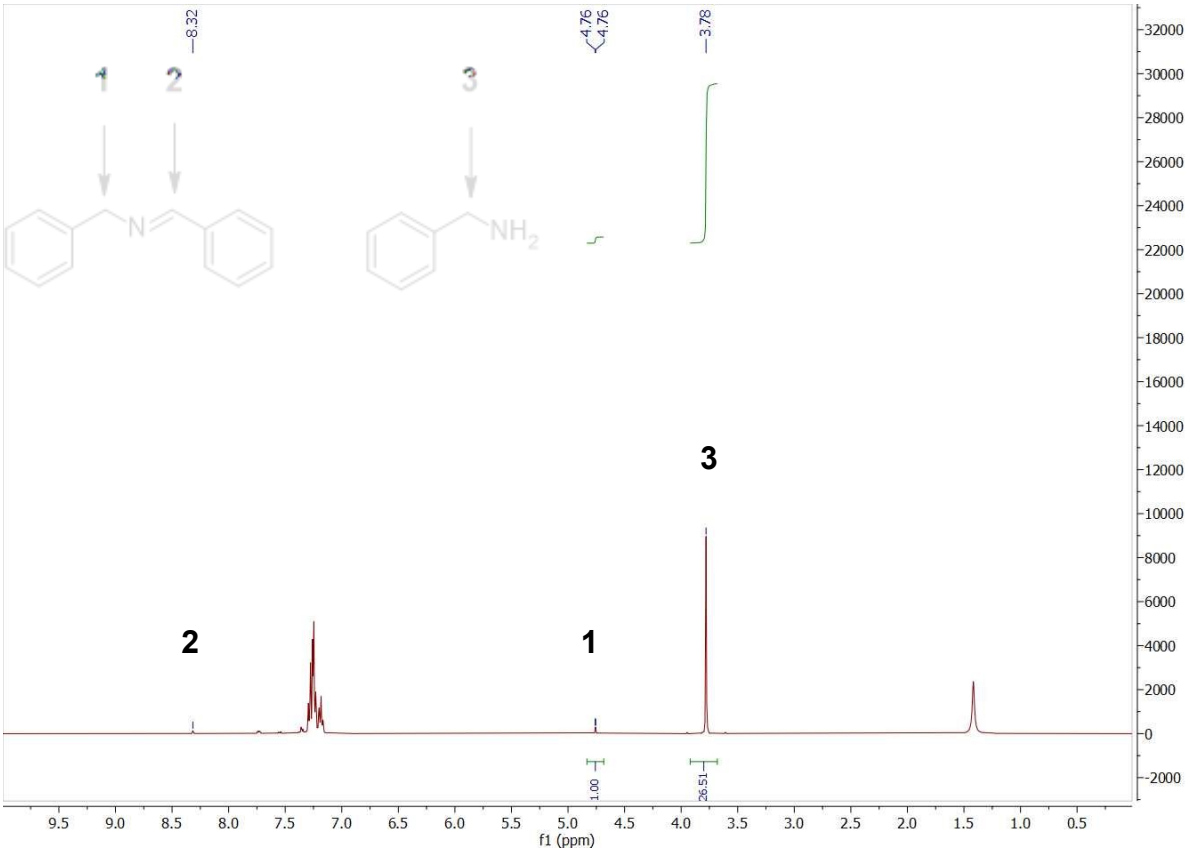


**Figure S54.** Kinetic studies for the oxidation of benzylamine with 0.005 mol% of **2,** air is used as an oxidant, time 2 h.

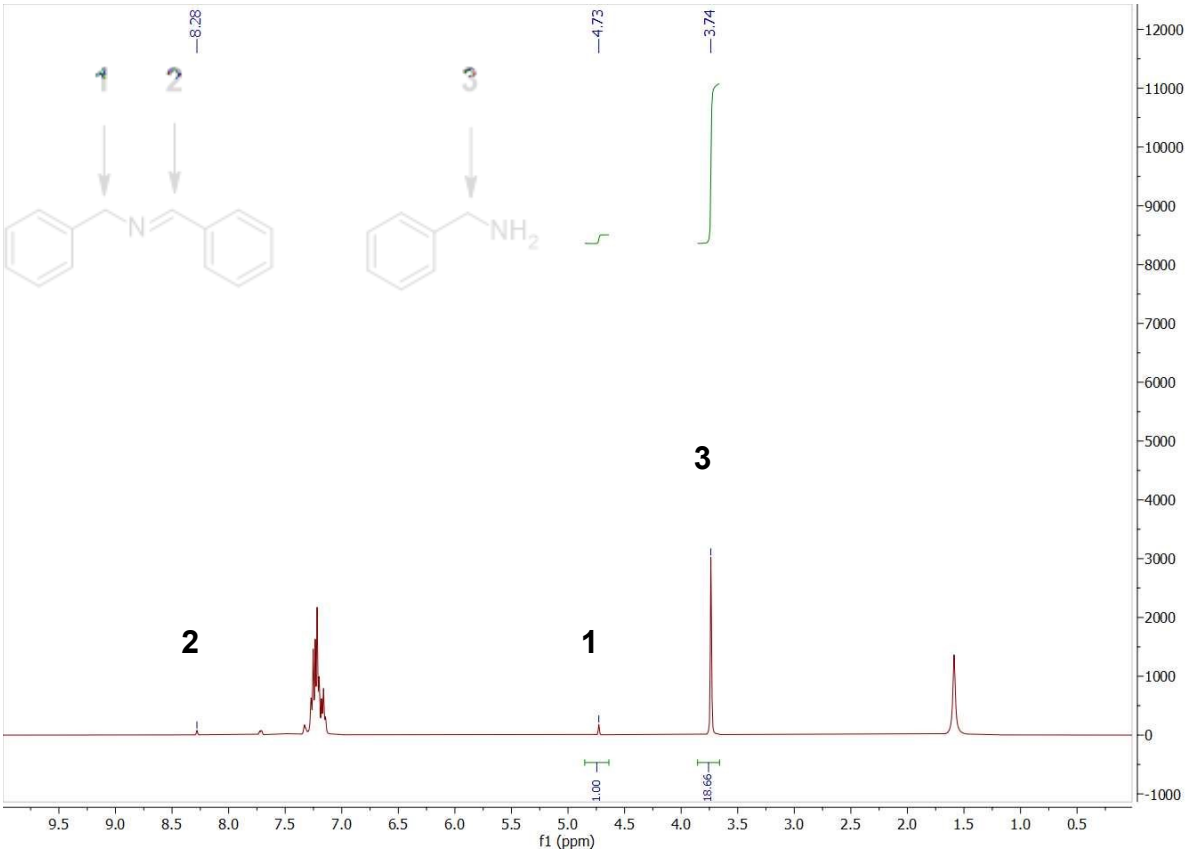


**Figure S55.** Kinetic studies for the oxidation of benzylamine with 0.005 mol% of **2,** air is used as an oxidant, time 3 h.

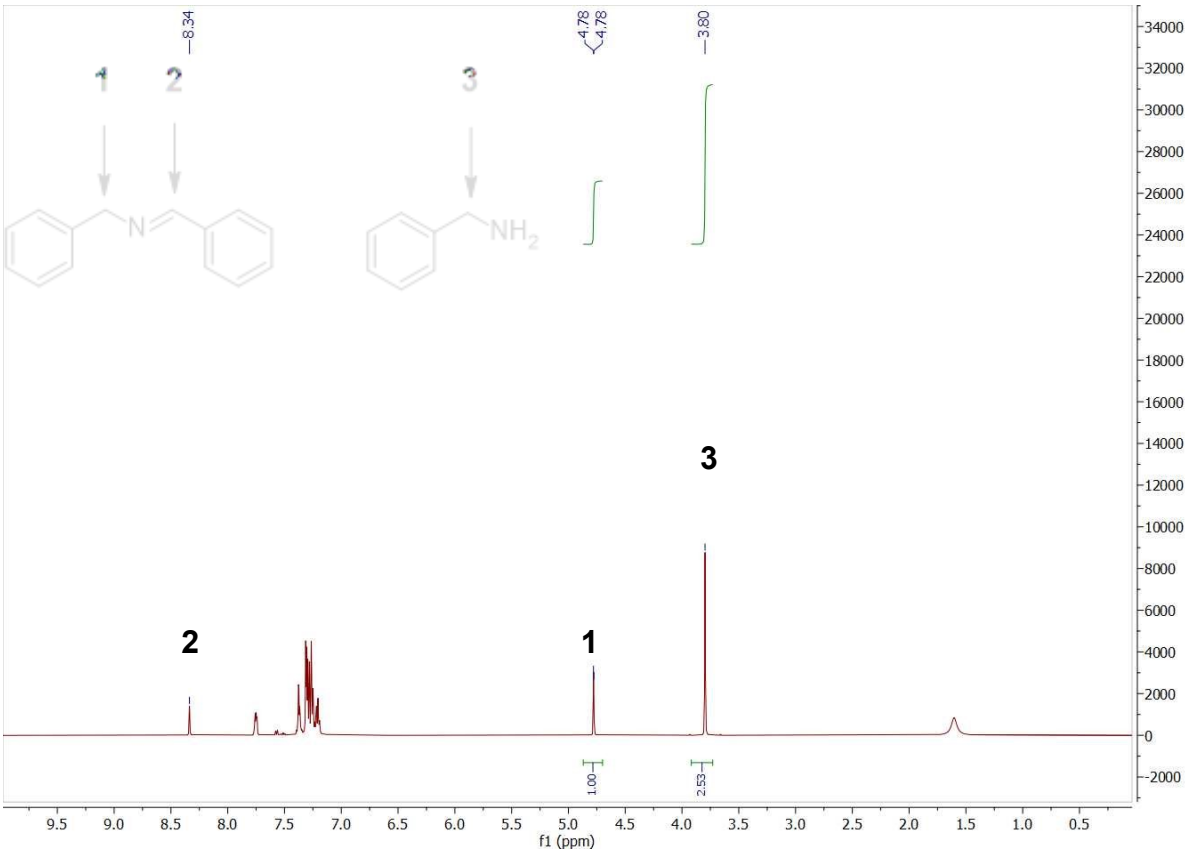


**Figure S56.** Kinetic studies for the oxidation of benzylamine with 0.005 mol% of **2,** air is used as an oxidant, time 6 h.

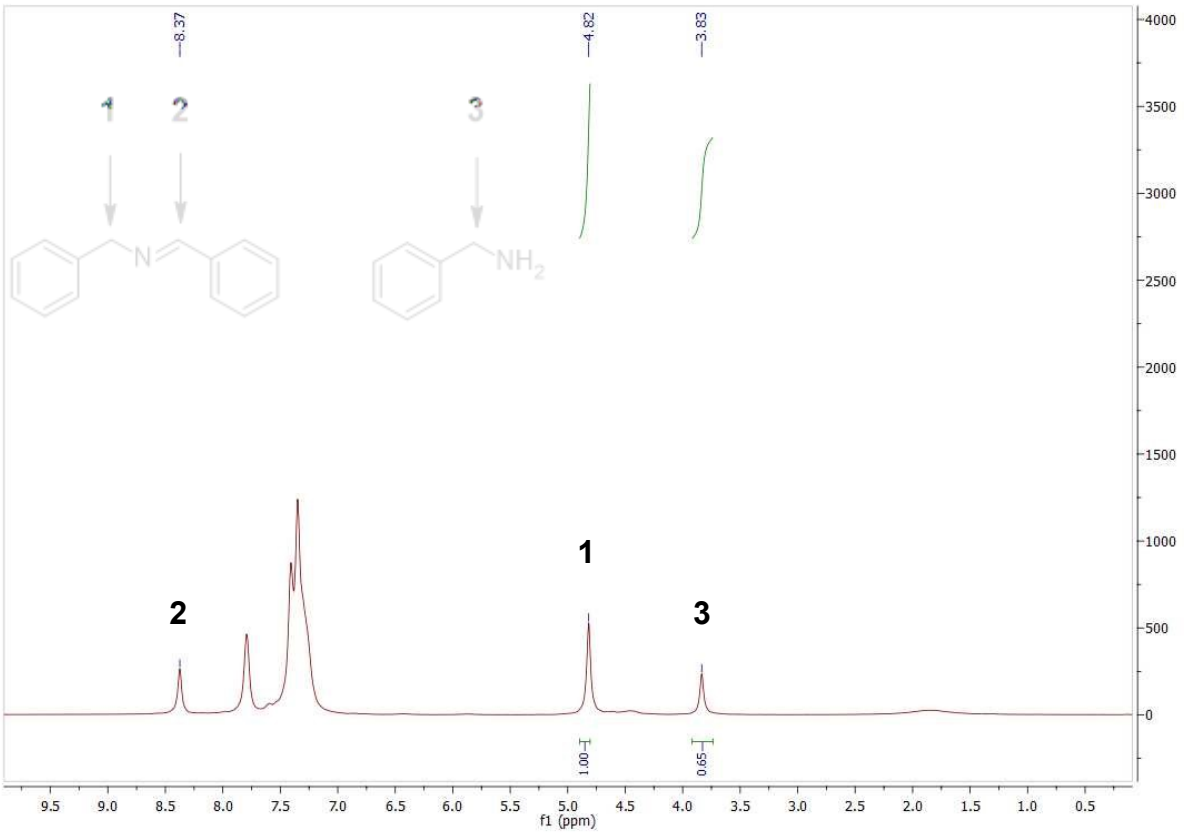


**Figure S57.** Kinetic studies for the oxidation of benzylamine with 0.005 mol% of **2,** air is used as an oxidant, time 10 h.

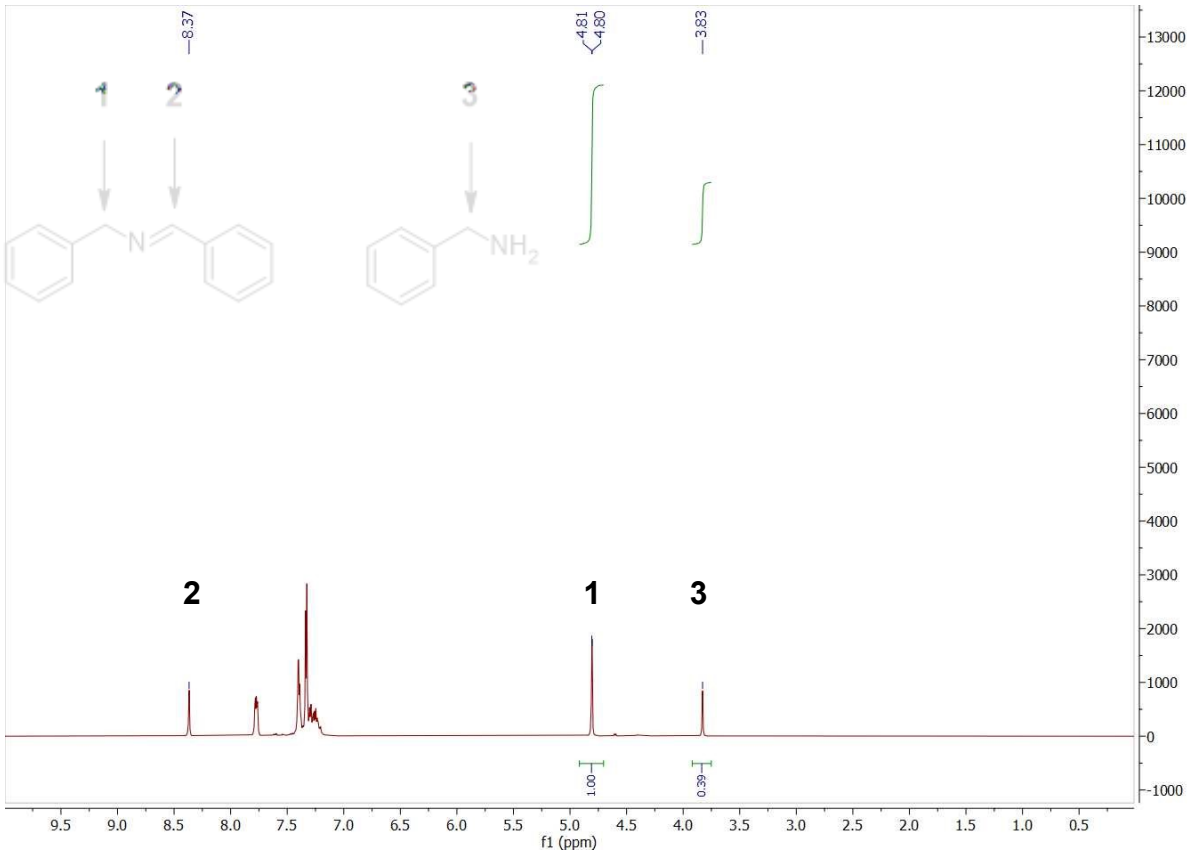


**Figure S58.** Kinetic studies for the oxidation of benzylamine with 0.005 mol% of **2,** air is used as an oxidant, time 12 h.

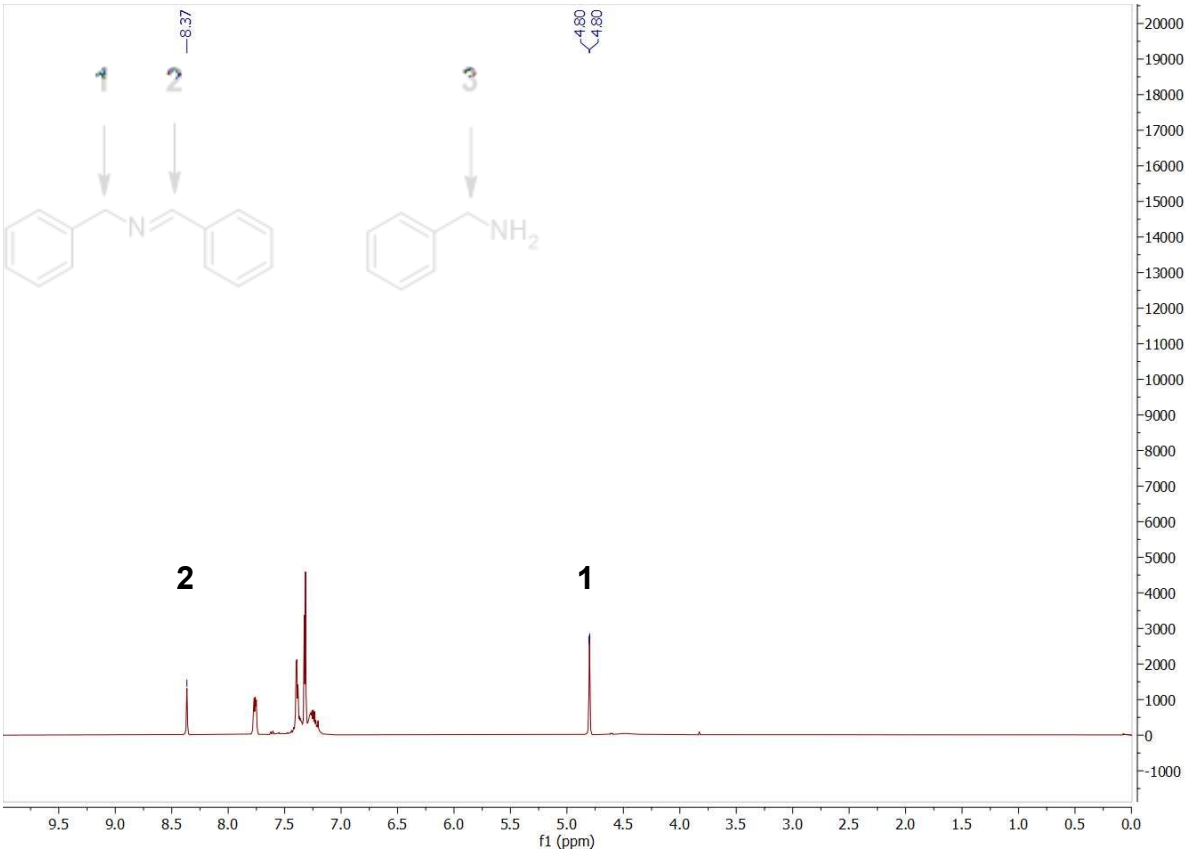


**Figure S59.** Kinetic studies for the oxidation of benzylamine with 0.005 mol% of **2,** air is used as an oxidant, time 16 h.

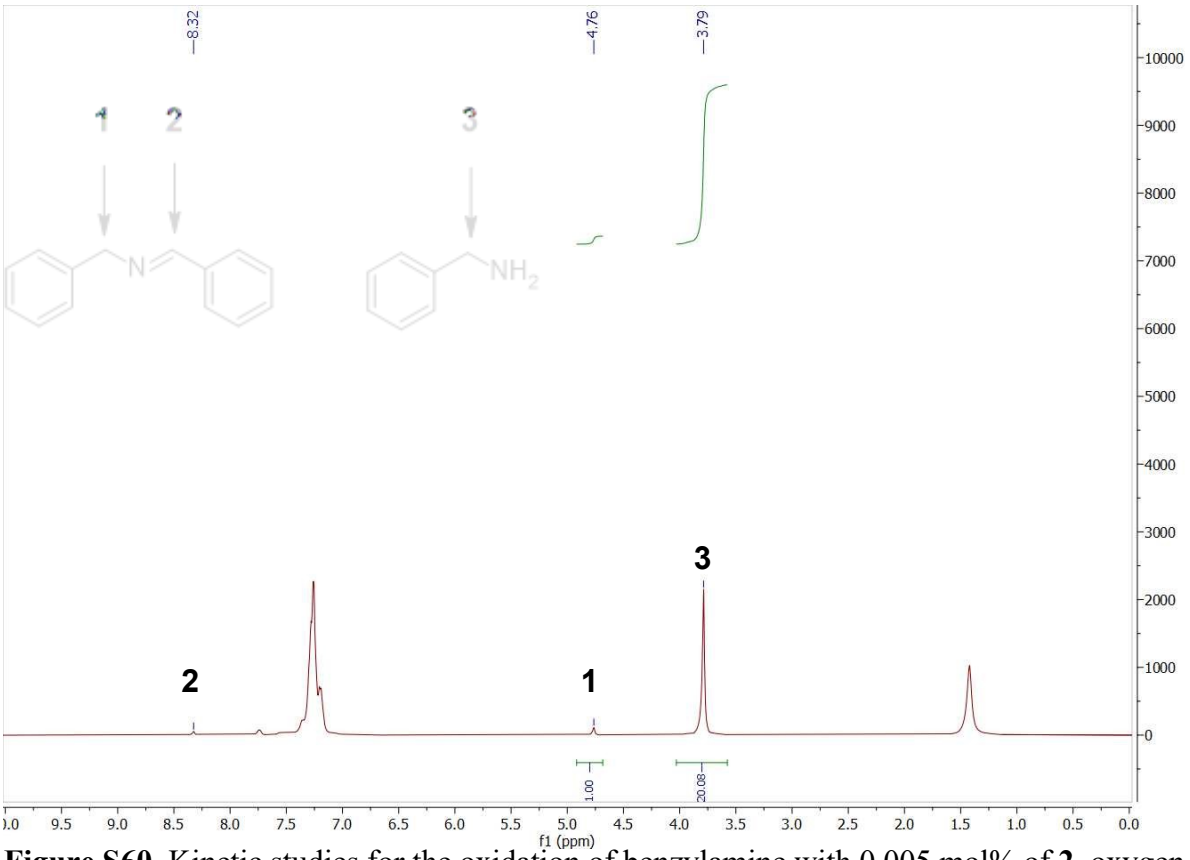


**Figure S60.** Kinetic studies for the oxidation of benzylamine with 0.005 mol% of **2,** oxygen is used as an oxidant, time 1 h.

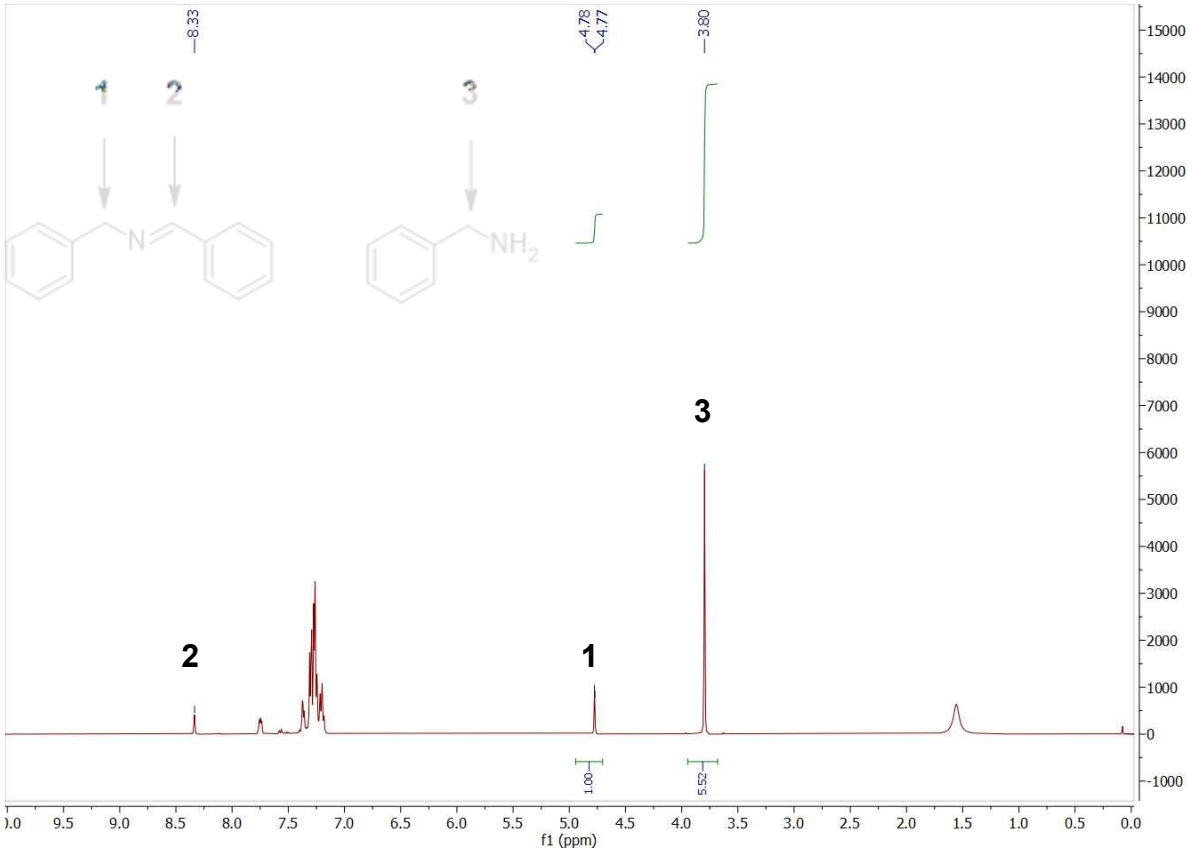


**Figure S61.** Kinetic studies for the oxidation of benzylamine with 0.005 mol% of **2,** oxygen is used as an oxidant, time 2 h.

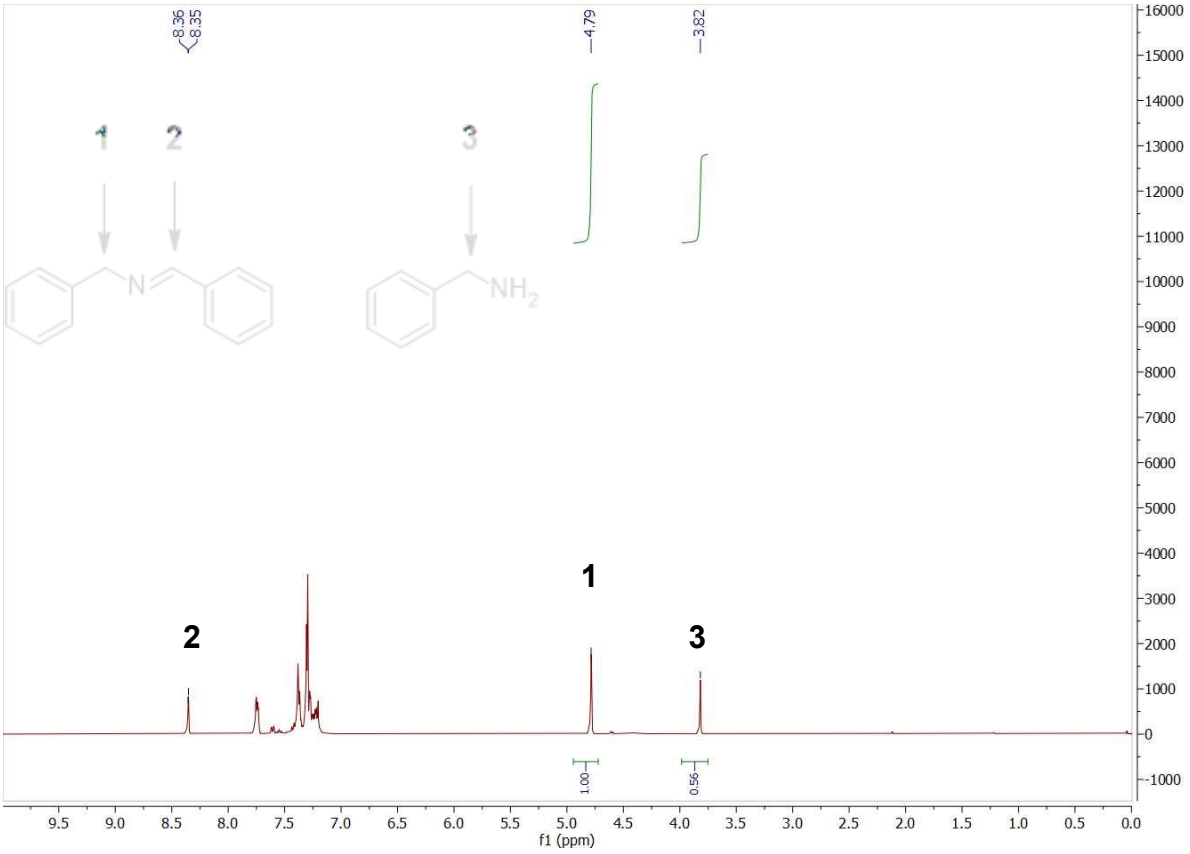


**Figure S62.** Kinetic studies for the oxidation of benzylamine with 0.005 mol% of **2,** oxygen is used as an oxidant, time 3 h.

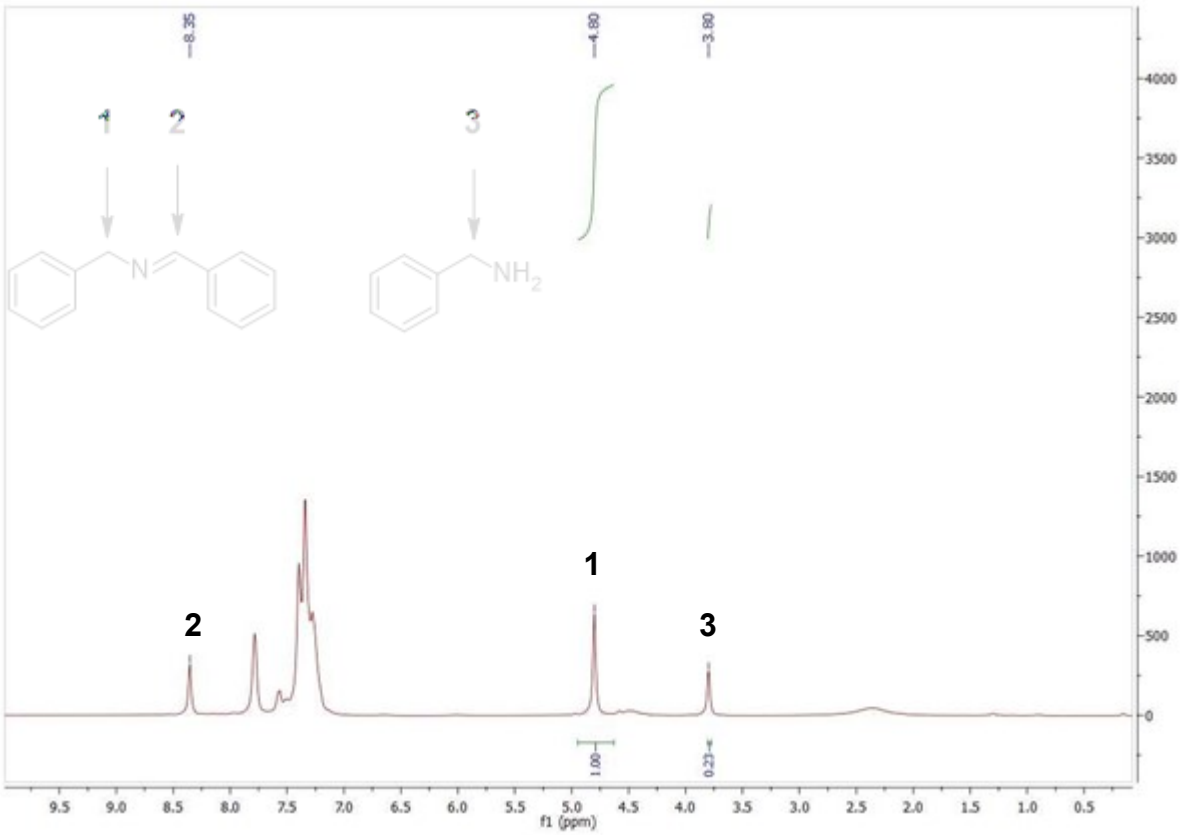


**Figure S63.** Kinetic studies for the oxidation of benzylamine with 0.005 mol% of **2,** oxygen is used as an oxidant, time 6 h.

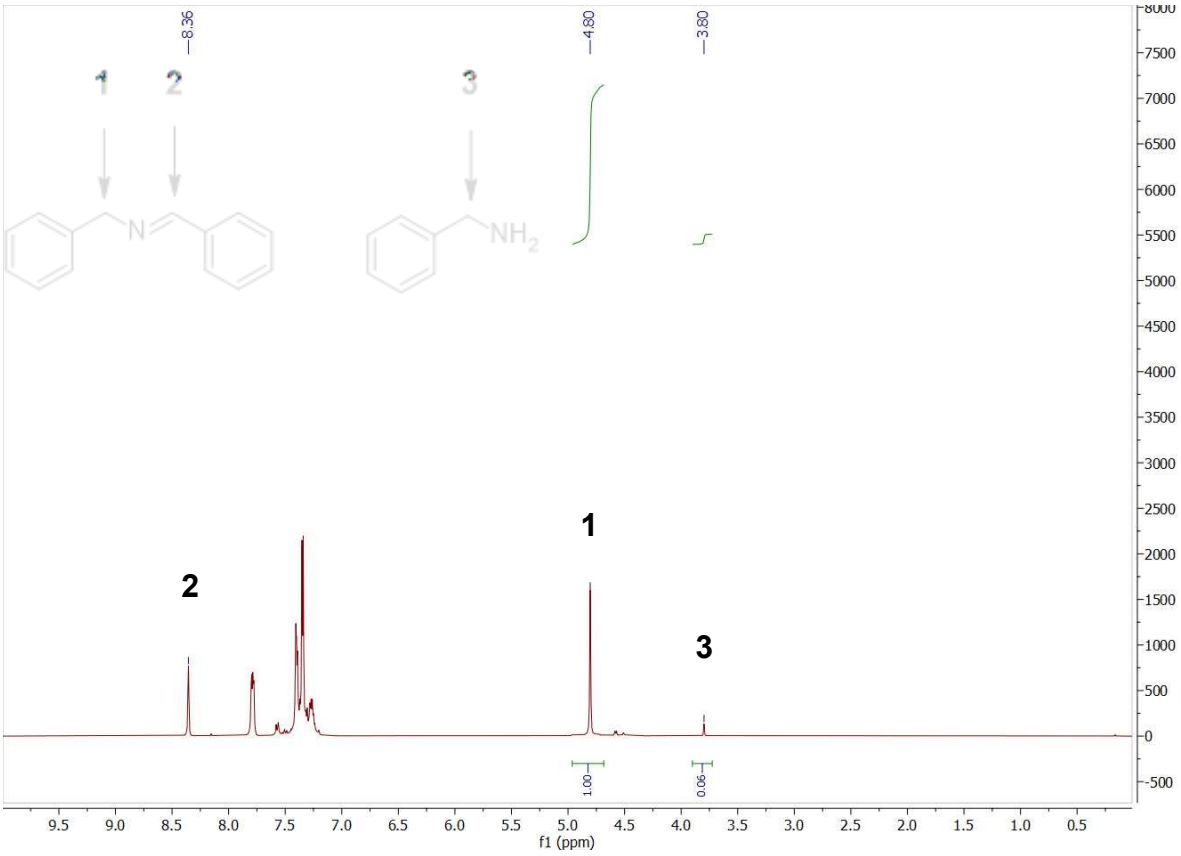


**Figure S64.** Kinetic studies for the oxidation of benzylamine with 0.005 mol% of **2,** oxygen is used as an oxidant, time 10 h.

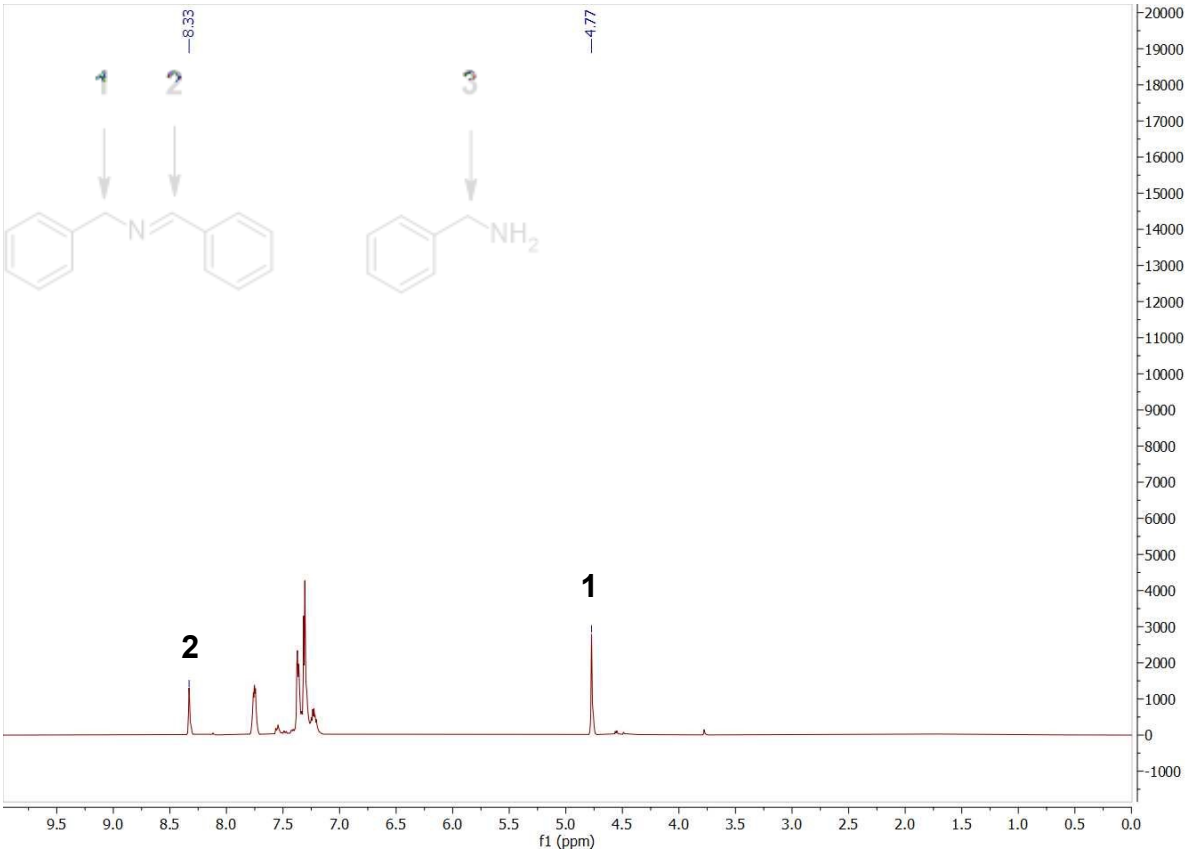


**Figure S65.** Kinetic studies for the oxidation of benzylamine with 0.005 mol% of **2,** oxygen is used as an oxidant, time 12 h.

**Table S8.** Kinetic studies: concentration and solvent dependence for the oxidation of benzylamine by oxygen.

| | Conversion of benzylamine | | |
|---|---|---|---|
| Condition/ time (h) | neat, 0.001% mol of **2** | toluene solution, [benzylamine]/[**2**] = 100/1 ratio | toluene solution, [benzylamine]/[**2**] = 20000/1 ratio (0.001% mol of **2**) |
| 8 | | 22 | 6 |
| 10 | | 36 | 7 |
| 12 | 5 | 47 | 8 |
| 14 | 15 | 59 | 9 |
| 16 | 64 | 72 | 10 |
| 18 | 82 | 86 | 12 |
| 20 | 94 | | |
| 22 | 99 | | |

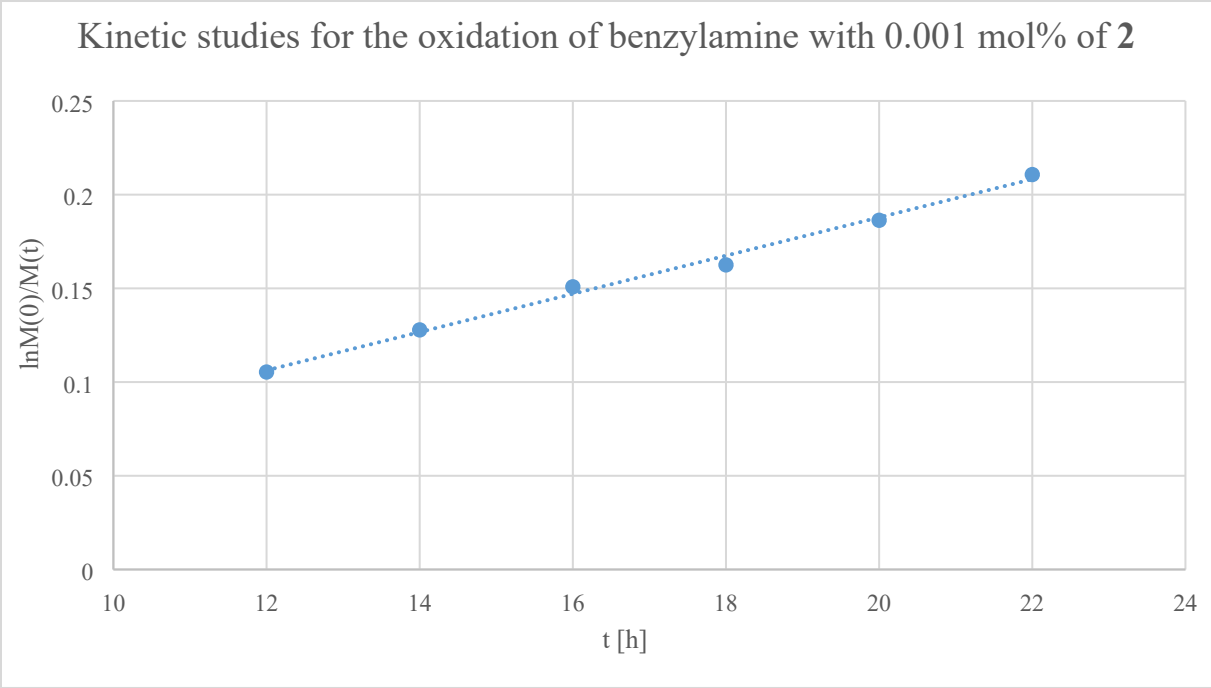


**Figure S66.** Kinetic studies for the oxidation of benzylamine with 0.001 mol% of **2.**

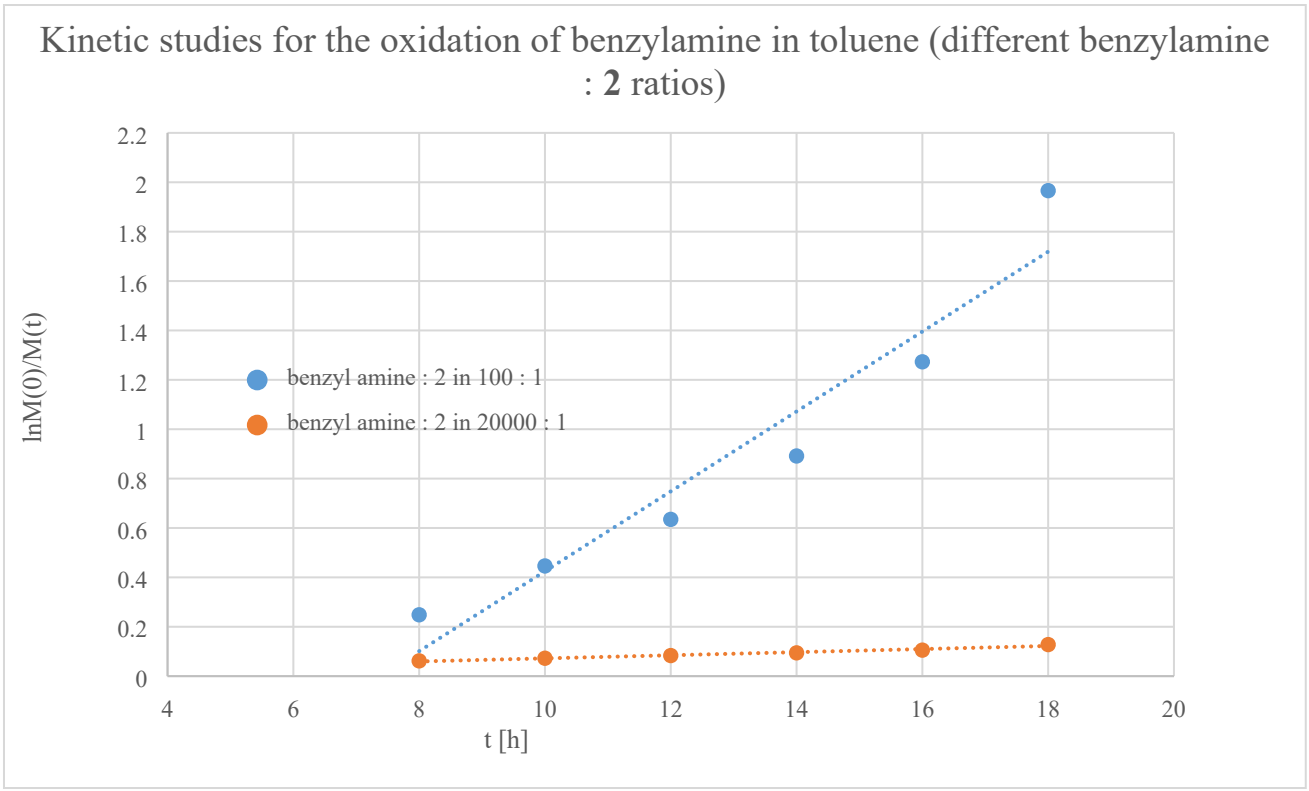


**Figure S67.** Kinetic studies for the oxidation of benzylamine in toluene, oxygen is used as an oxidant, different ratios of benzylamine and **2**.

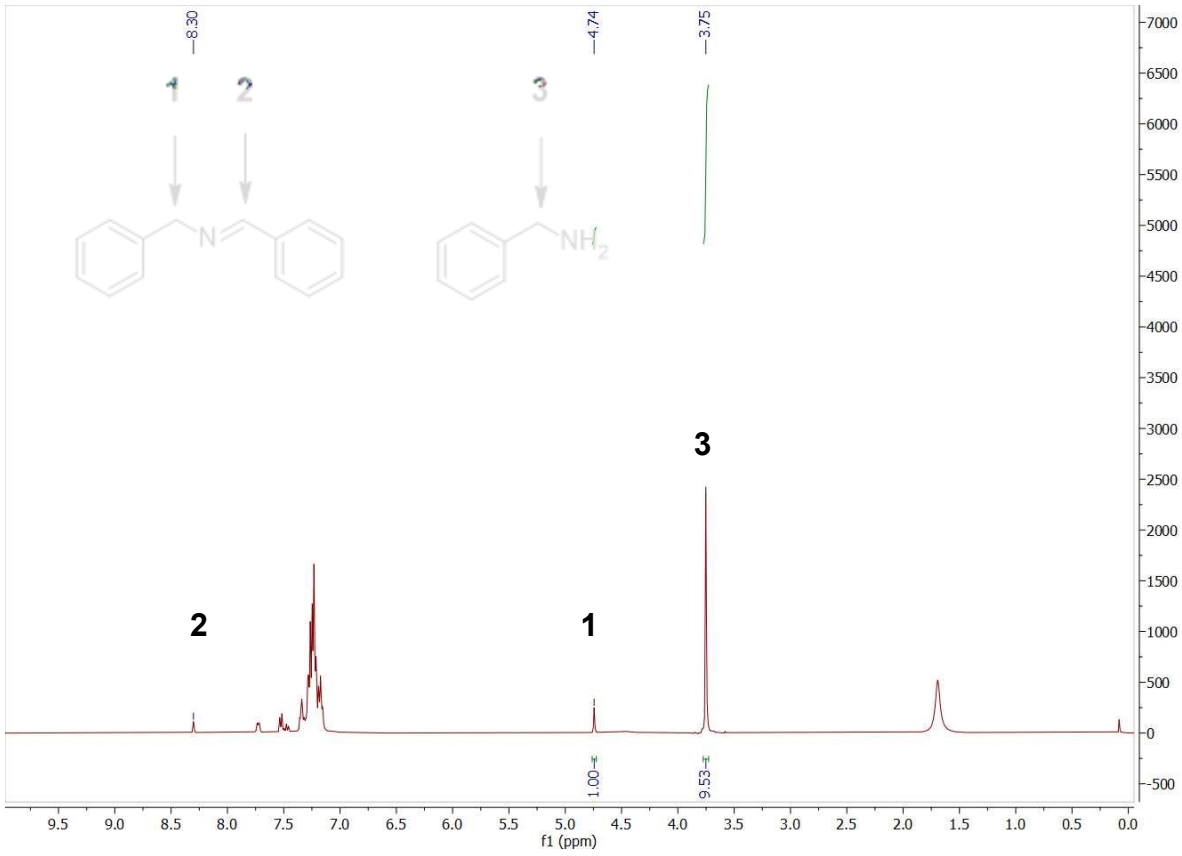


**Figure S68.** Kinetic studies for the oxidation of benzylamine with 0.001 mol% of **2**, oxygen is used as an oxidant, time 12 h.

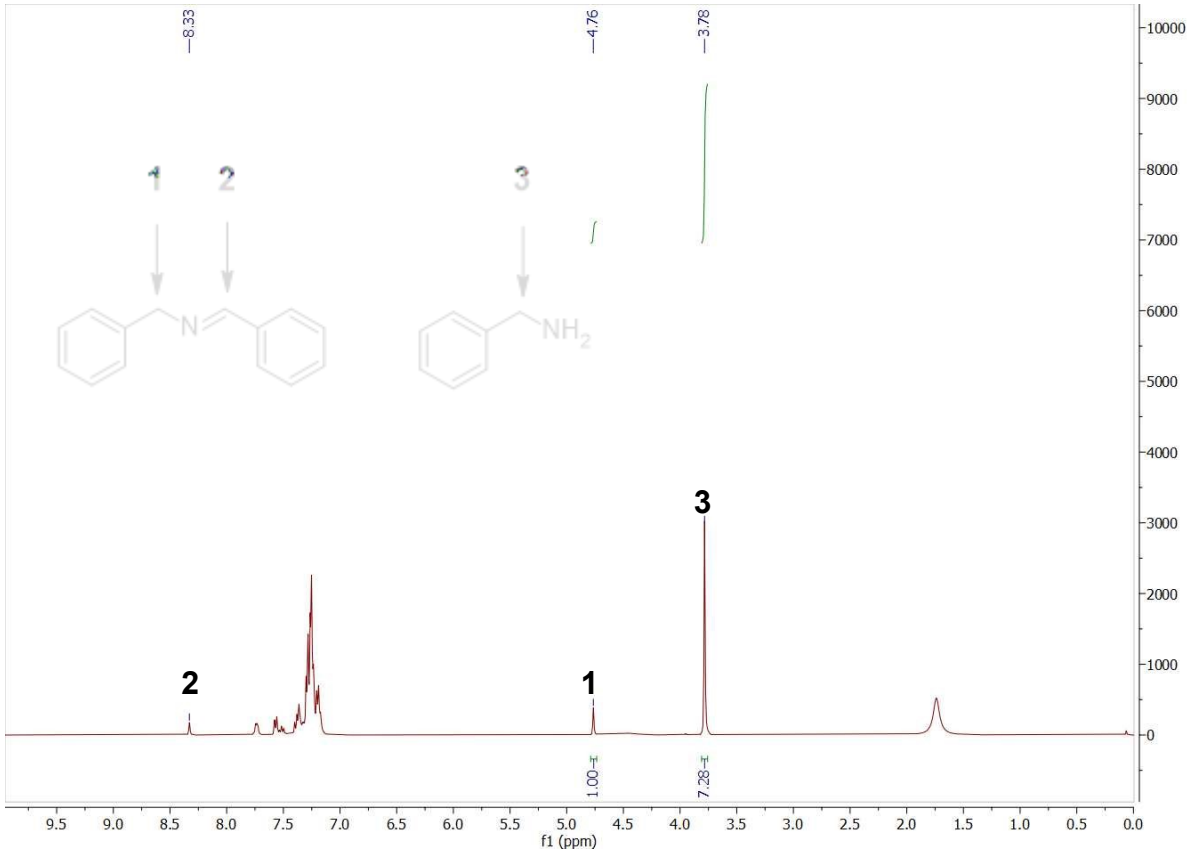


**Figure S69.** Kinetic studies for the oxidation of benzylamine with 0.001 mol% of **2**, oxygen is used as an oxidant, time 14 h.

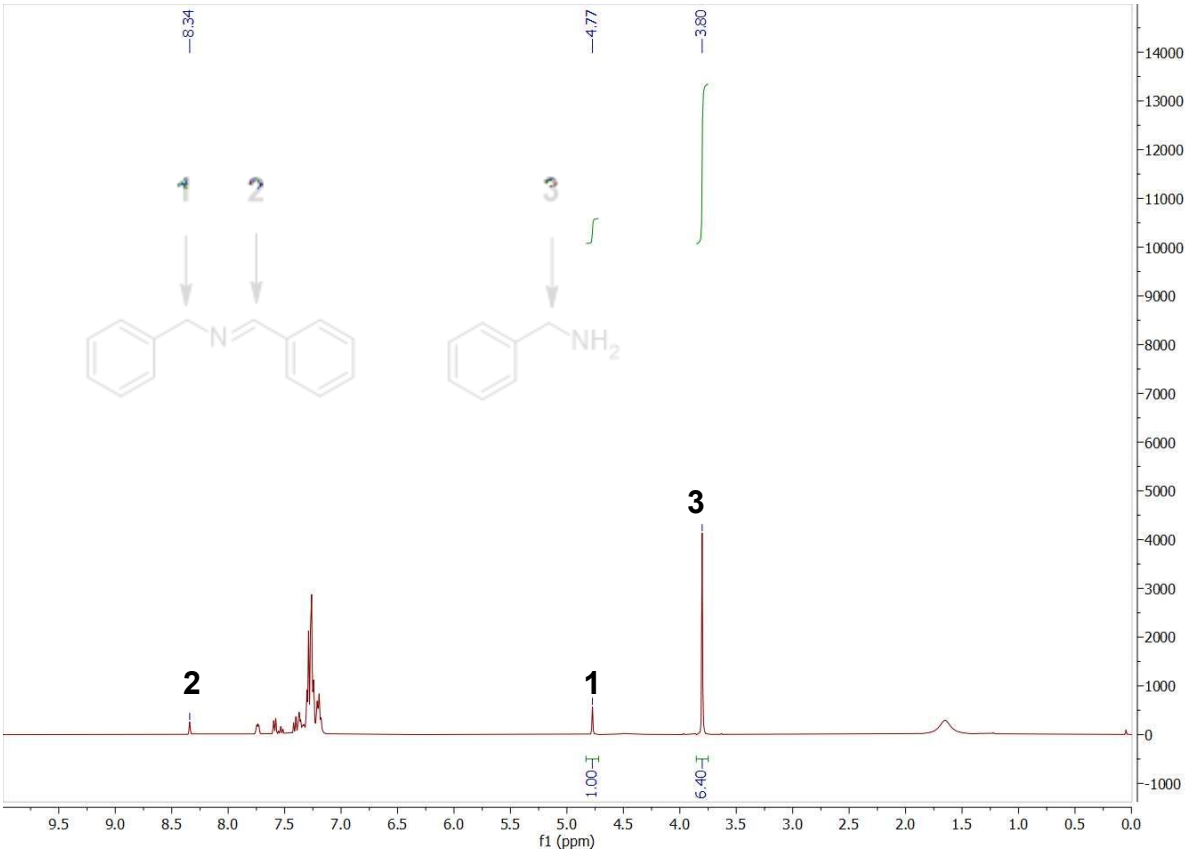


**Figure S70.** Kinetic studies for the oxidation of benzylamine with 0.001 mol% of **2**, oxygen is used as an oxidant, time 16 h.

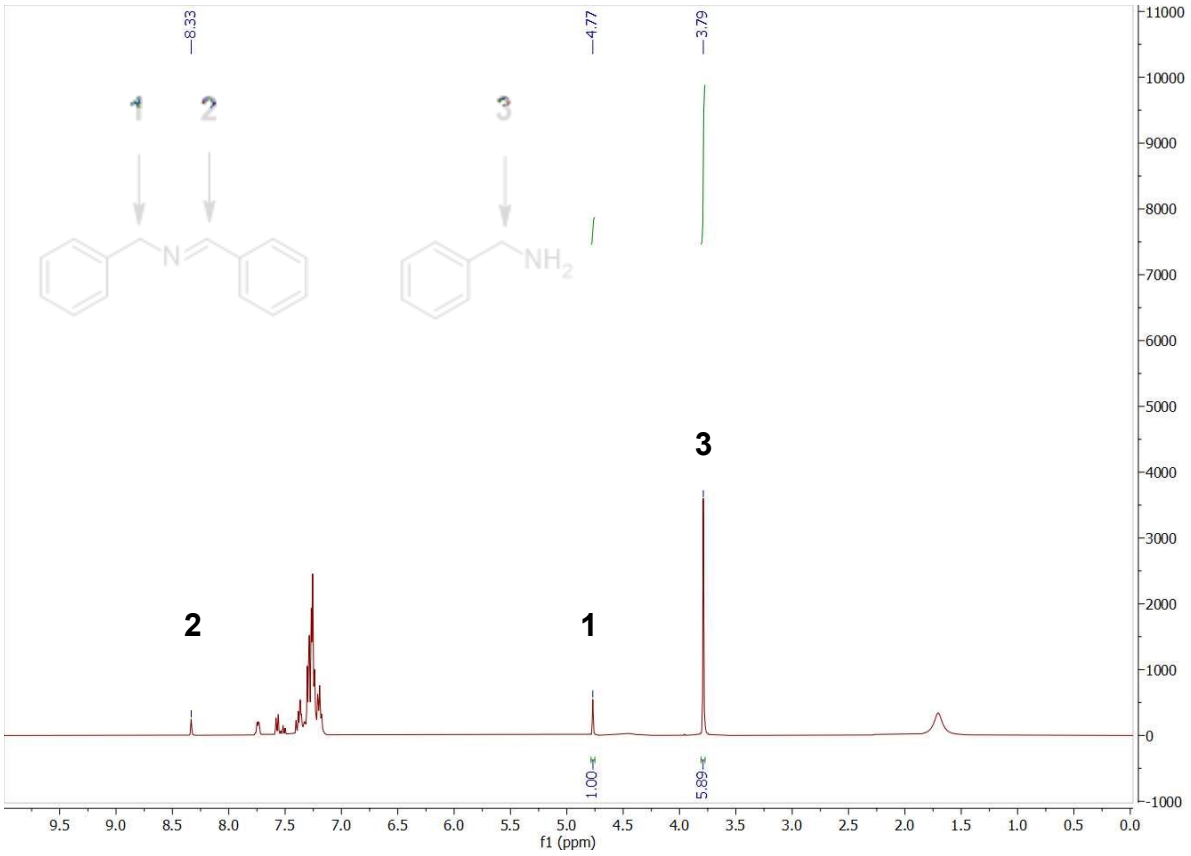


**Figure S71.** Kinetic studies for the oxidation of benzylamine with 0.001 mol% of **2**, oxygen is used as an oxidant, time 18 h.

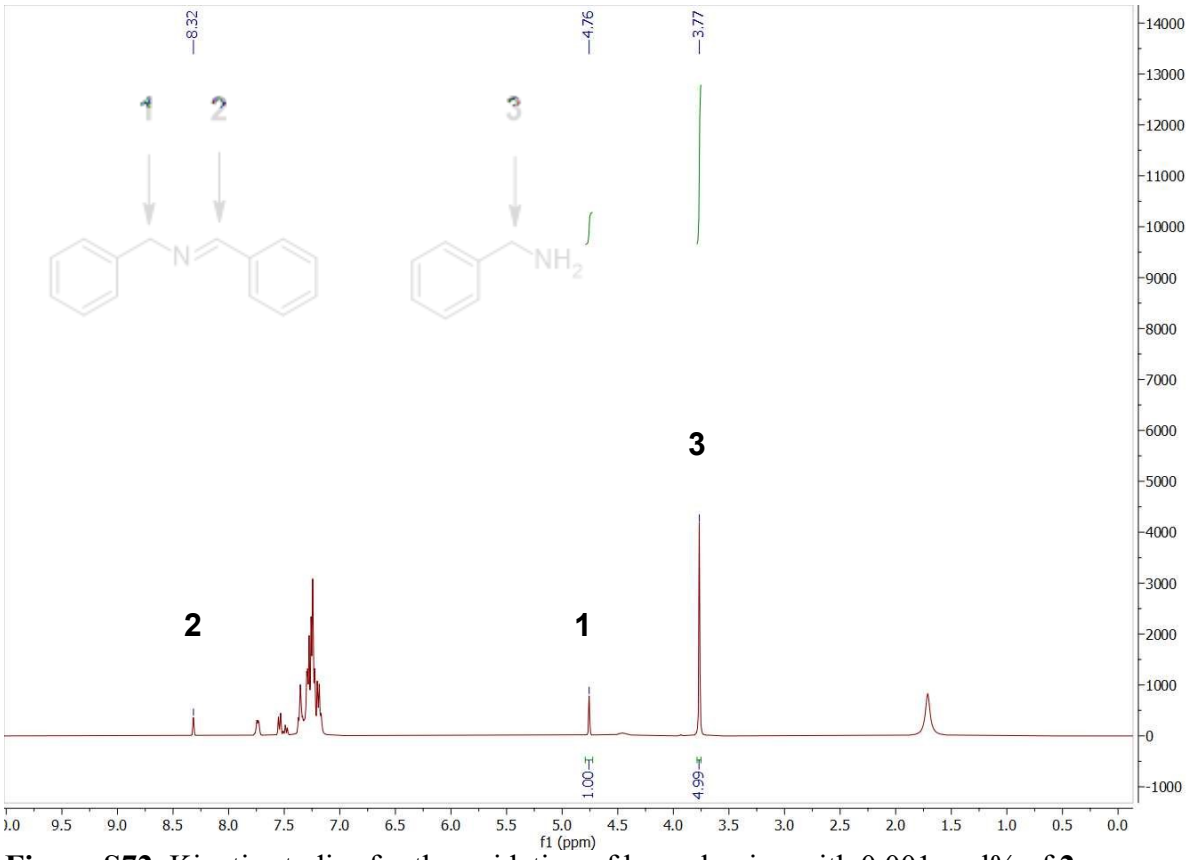


**Figure S72.** Kinetic studies for the oxidation of benzylamine with 0.001 mol% of **2**, oxygen is used as an oxidant, time 20 h.

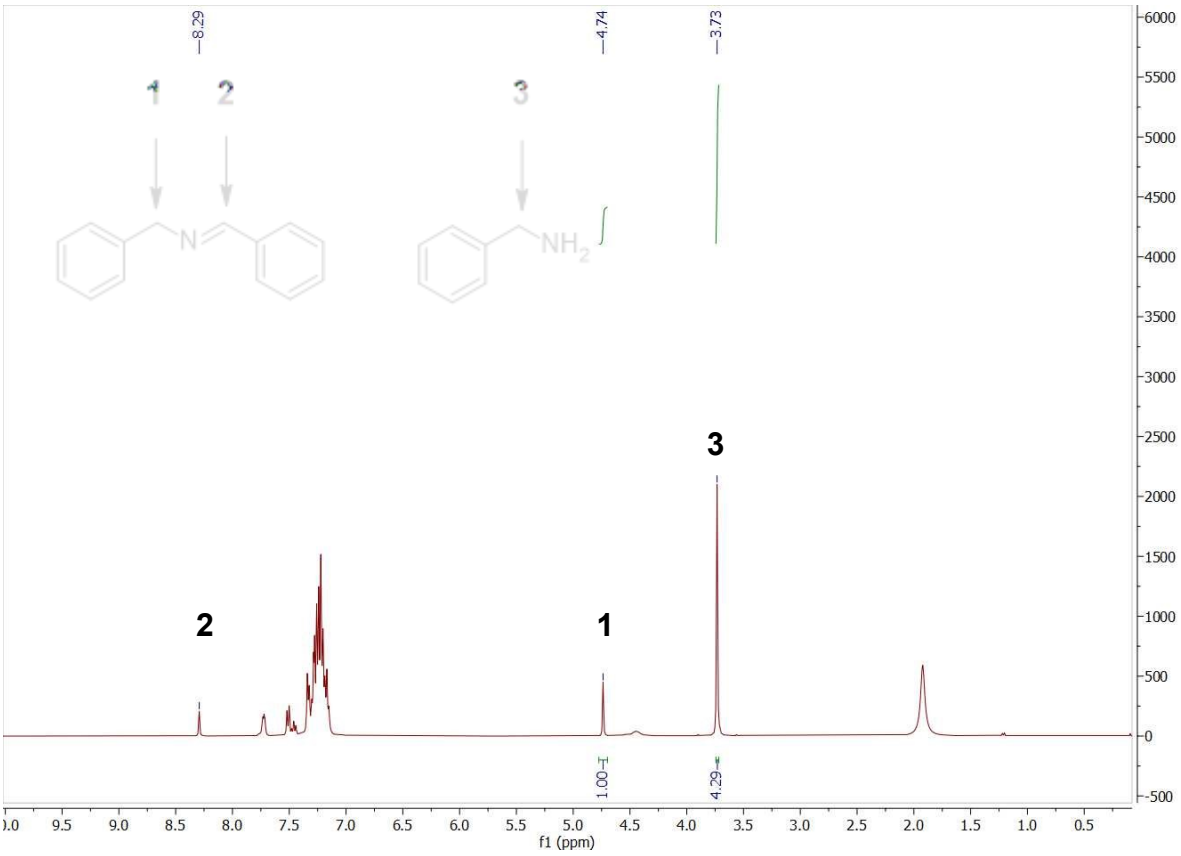


**Figure S73.** Kinetic studies for the oxidation of benzylamine with 0.001 mol% of **2**, oxygen is used as an oxidant, time 22 h.

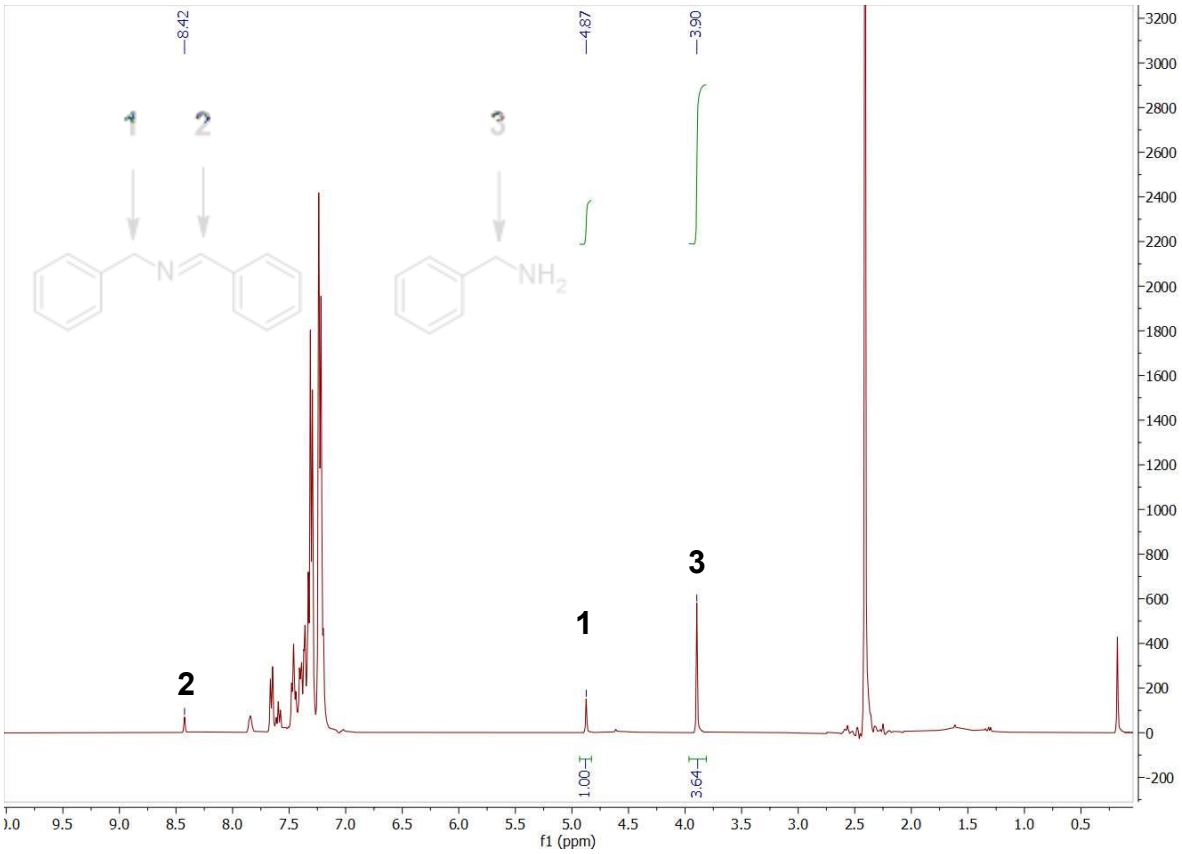


**Figure S74.** Kinetic studies for the oxidation of benzylamine with **2** (100:1 ratio) in toluene, oxygen is used as an oxidant, time 8 h.

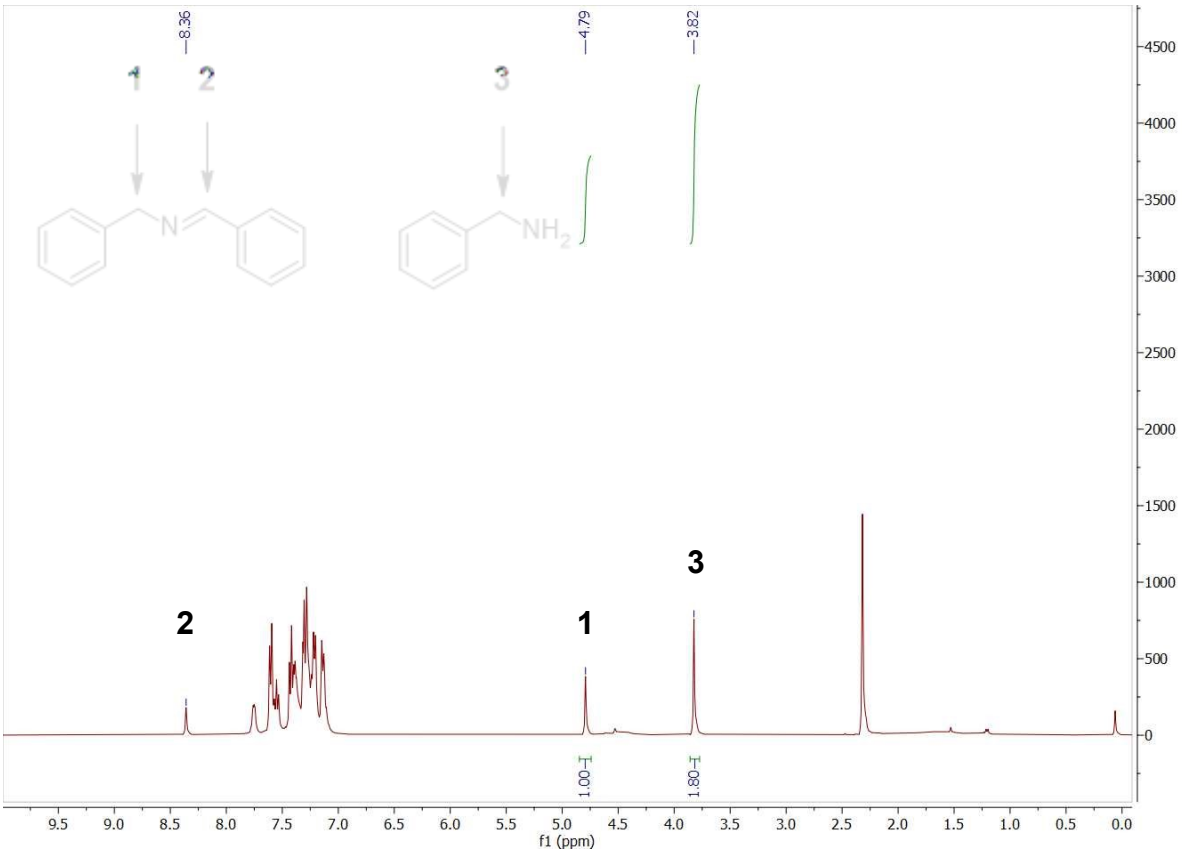


**Figure S75.** Kinetic studies for the oxidation of benzylamine with **2** (100:1 ratio) in toluene, oxygen is used as an oxidant, time 10 h.

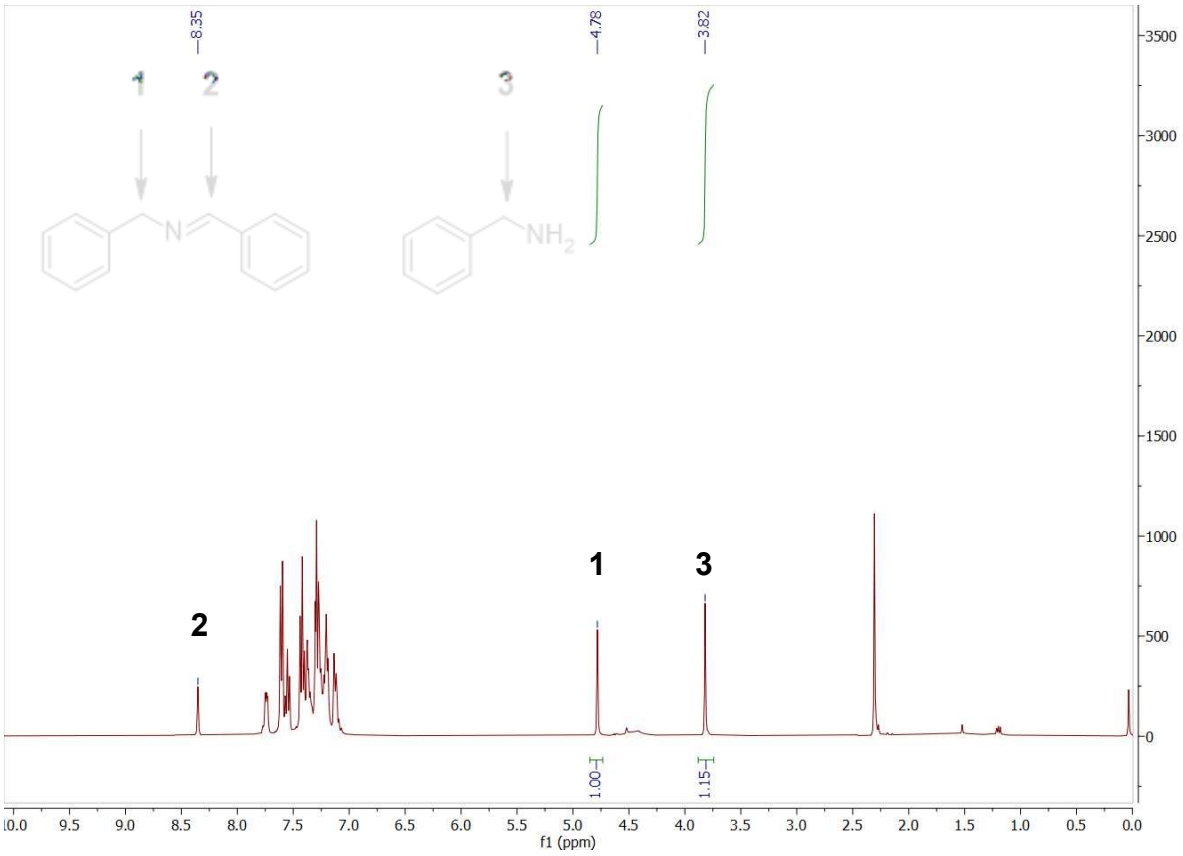


**Figure S76.** Kinetic studies for the oxidation of benzylamine with **2** (100:1 ratio) in toluene, oxygen is used as an oxidant, time 12 h.

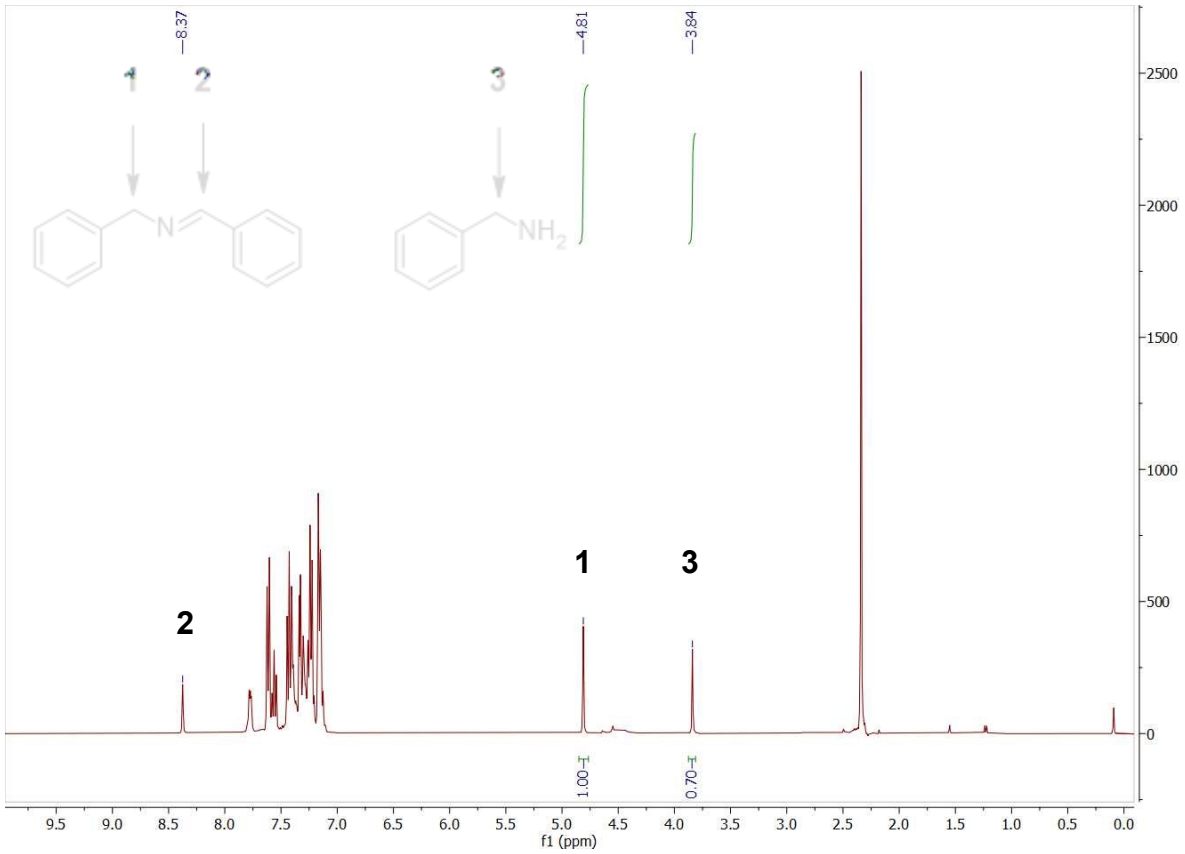


**Figure S77.** Kinetic studies for the oxidation of benzylamine with **2** (100:1 ratio) in toluene, oxygen is used as an oxidant, time 14 h.

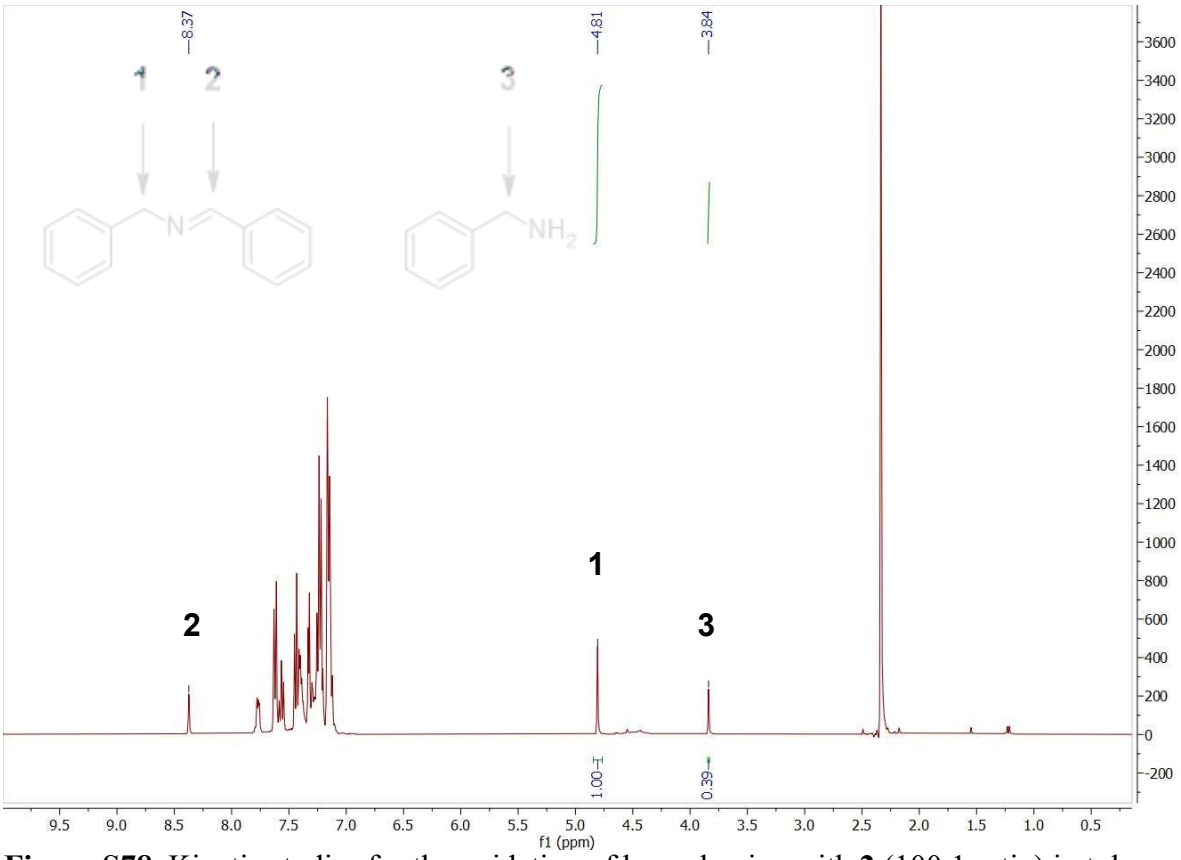


**Figure S78.** Kinetic studies for the oxidation of benzylamine with **2** (100:1 ratio) in toluene, oxygen is used as an oxidant, time 16 h.

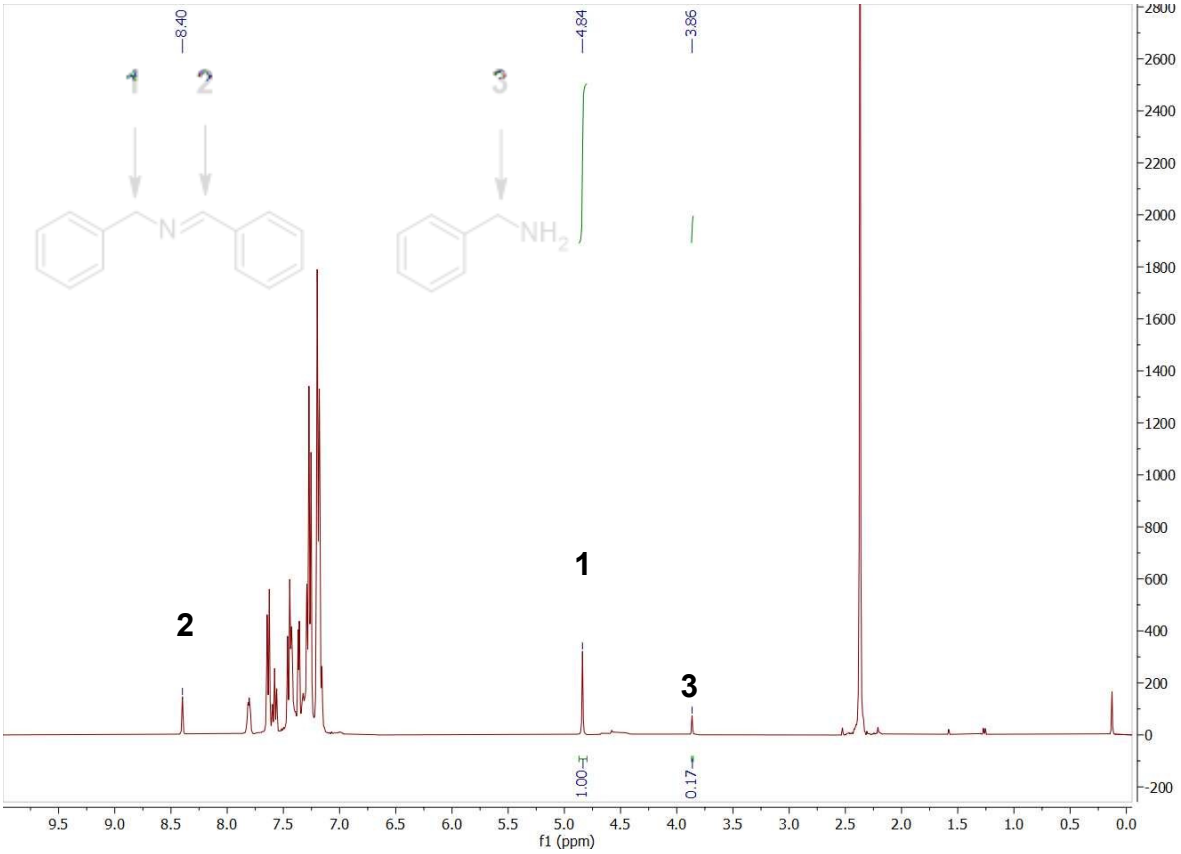


**Figure S79.** Kinetic studies for the oxidation of benzylamine with **2** (100:1 ratio) in toluene, oxygen is used as an oxidant, time 18 h.

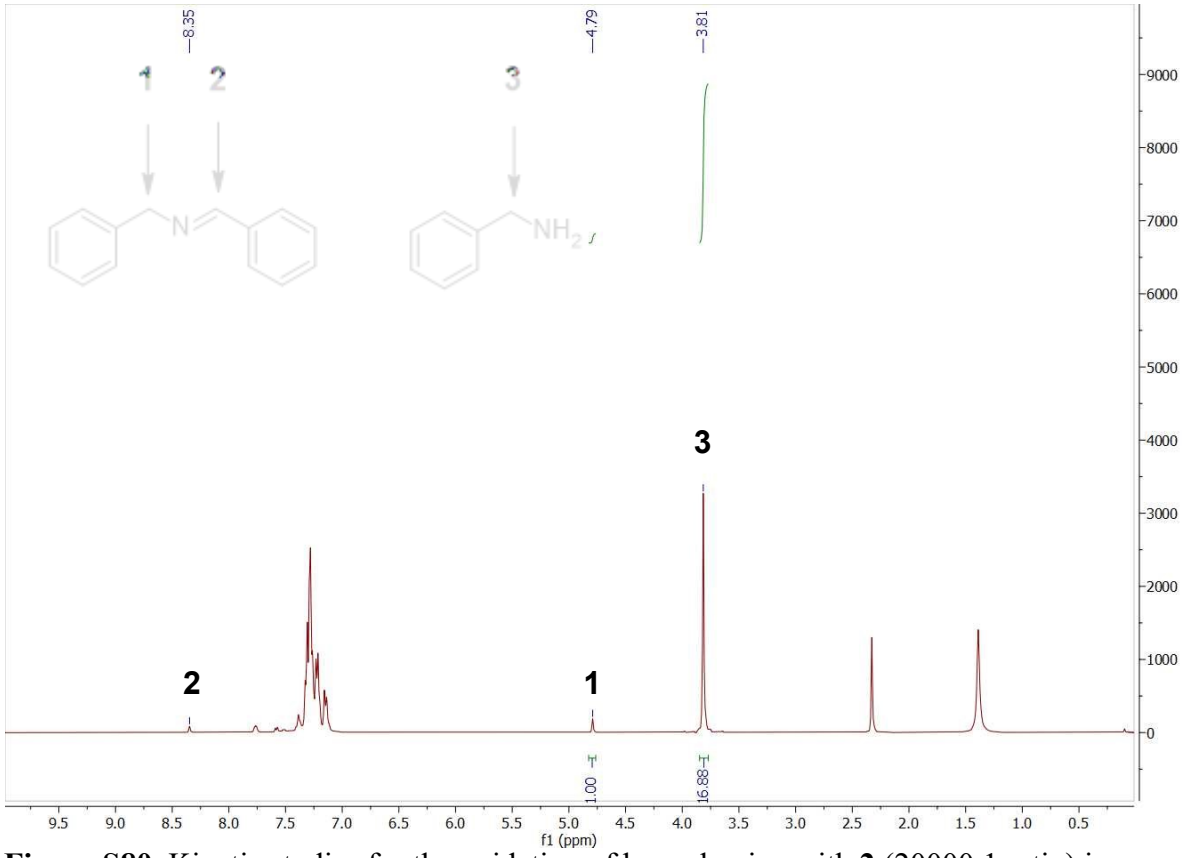


**Figure S80.** Kinetic studies for the oxidation of benzylamine with **2** (20000:1 ratio) in toluene, oxygen is used as an oxidant, time 8 h.

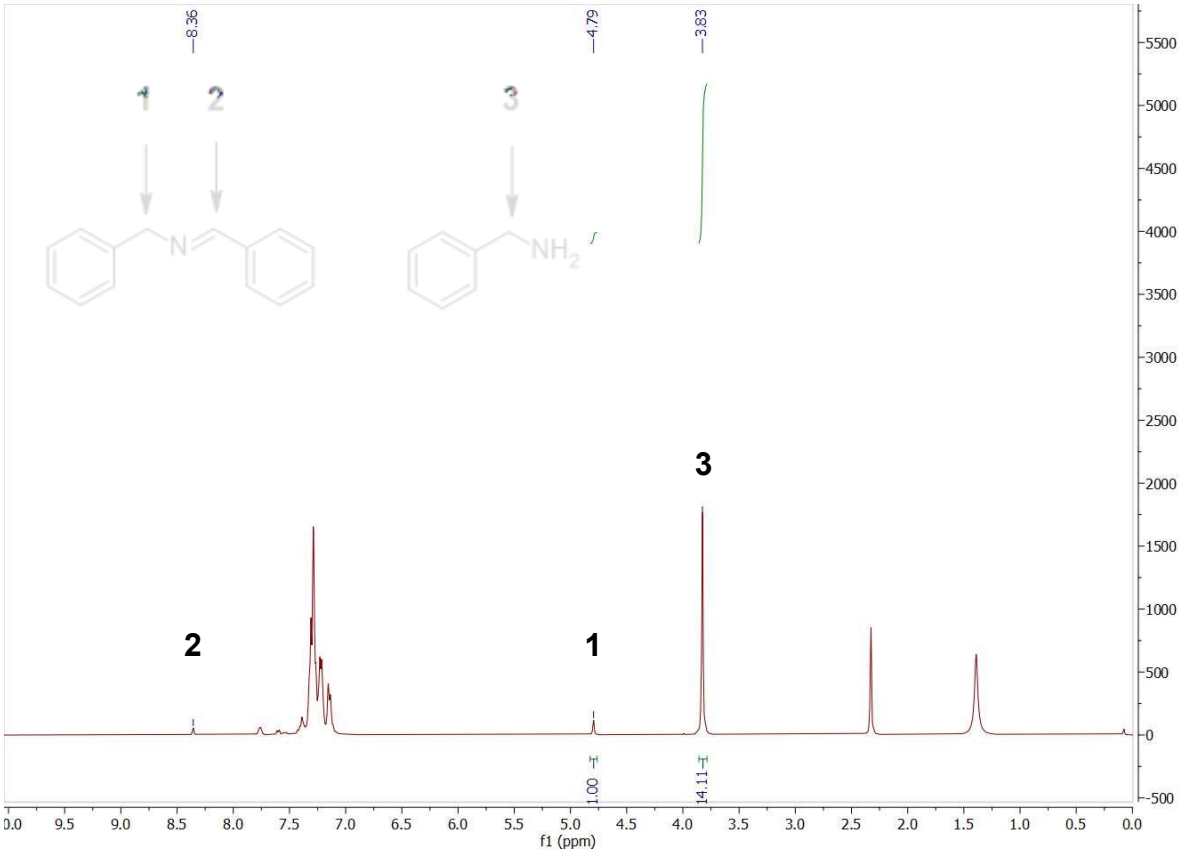


**Figure S81.** Kinetic studies for the oxidation of benzylamine with **2** (20000:1 ratio) in toluene, oxygen is used as an oxidant, time 10 h.

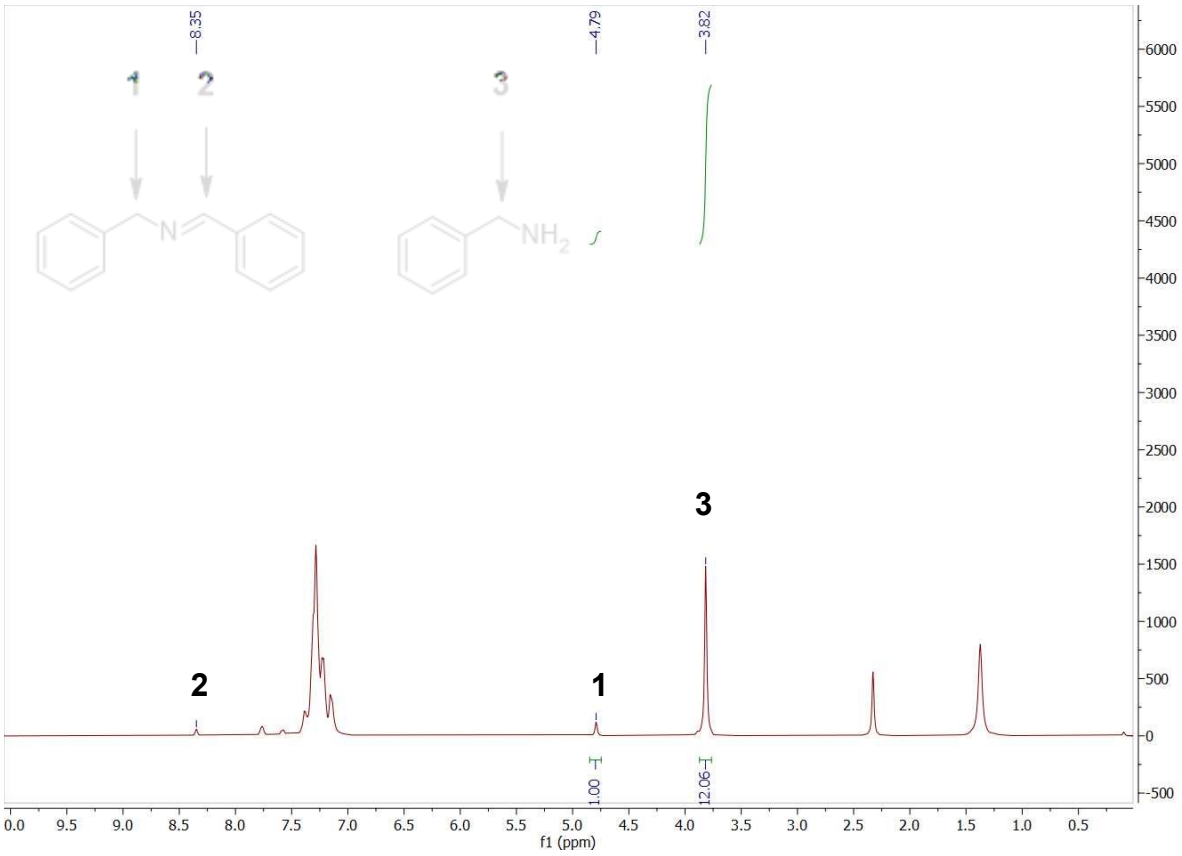


**Figure S82.** Kinetic studies for the oxidation of benzylamine with **2** (20000:1 ratio) in toluene, oxygen is used as an oxidant, time 12 h.

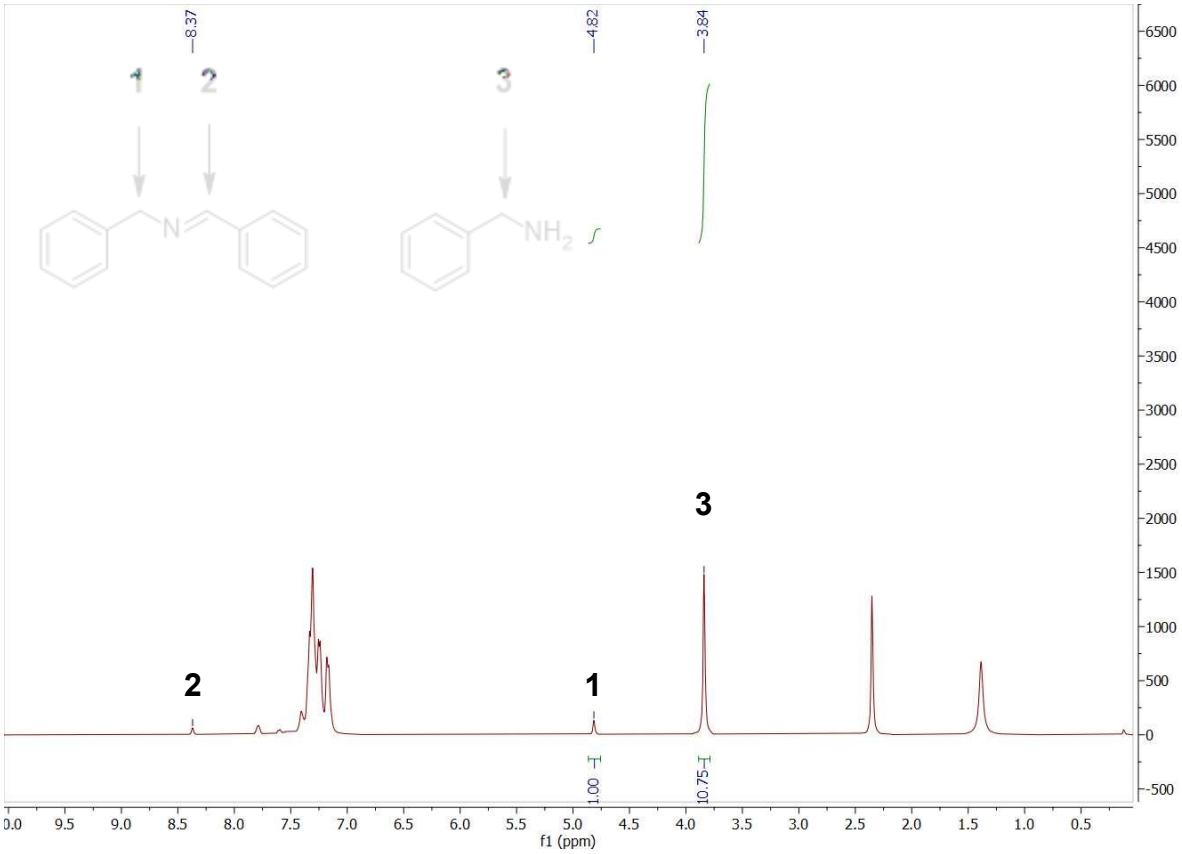


**Figure S83.** Kinetic studies for the oxidation of benzylamine with **2** (20000:1 ratio) in toluene, oxygen is used as an oxidant, time 14 h.

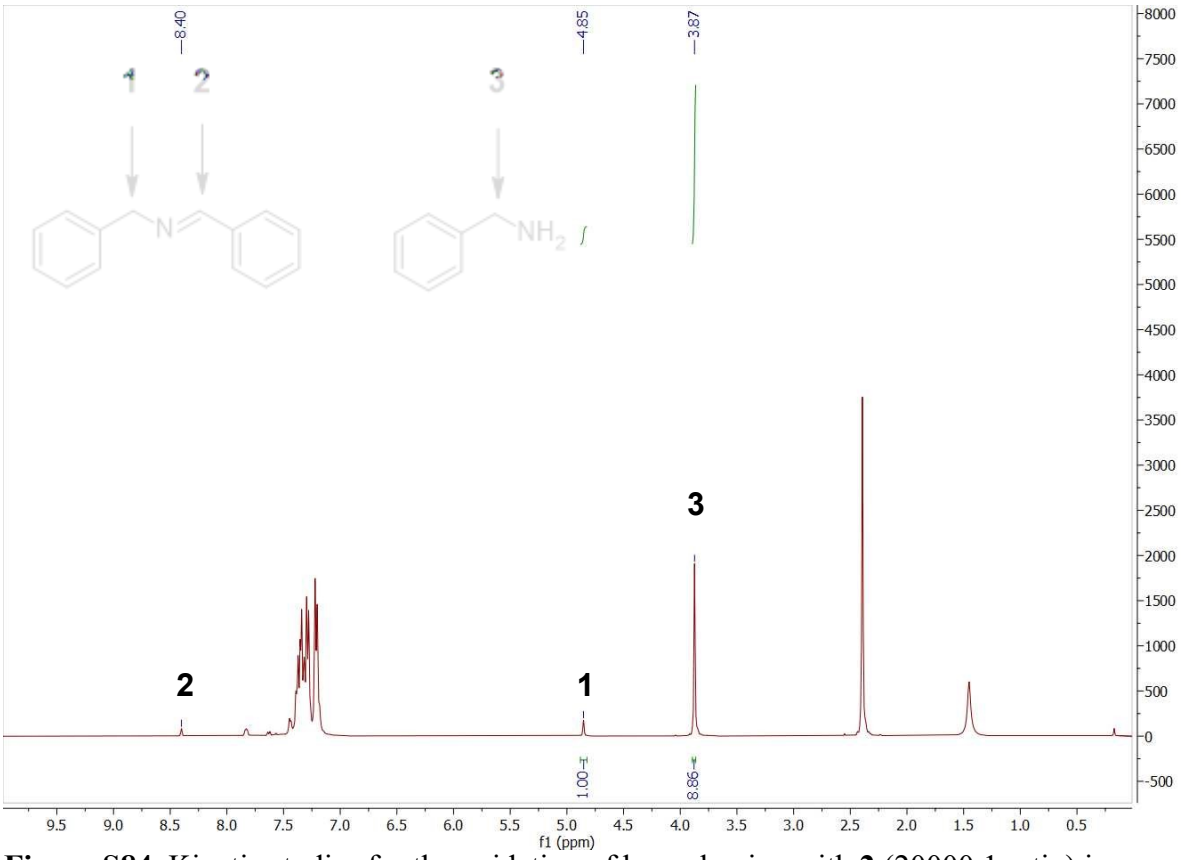


**Figure S84.** Kinetic studies for the oxidation of benzylamine with **2** (20000:1 ratio) in toluene, oxygen is used as an oxidant, time 16 h.

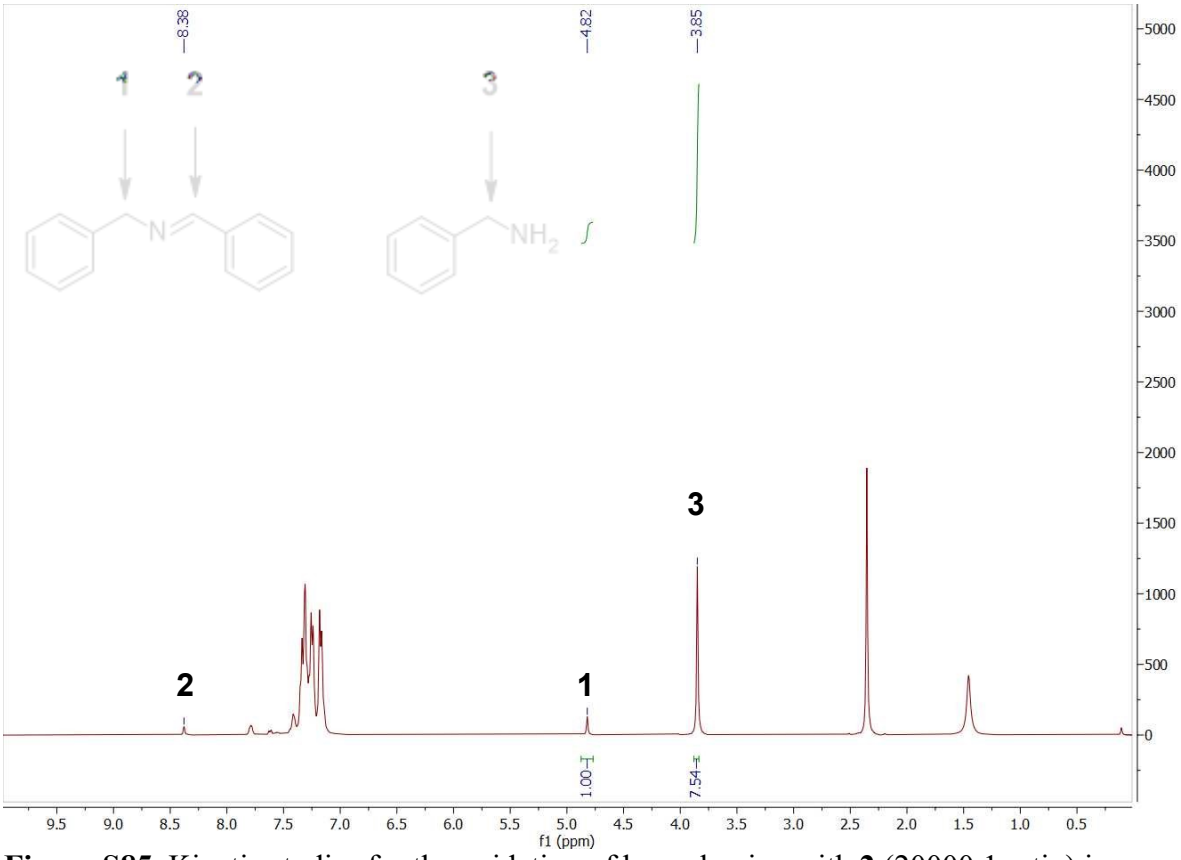


**Figure S85.** Kinetic studies for the oxidation of benzylamine with **2** (20000:1 ratio) in toluene, oxygen is used as an oxidant, time 18 h.

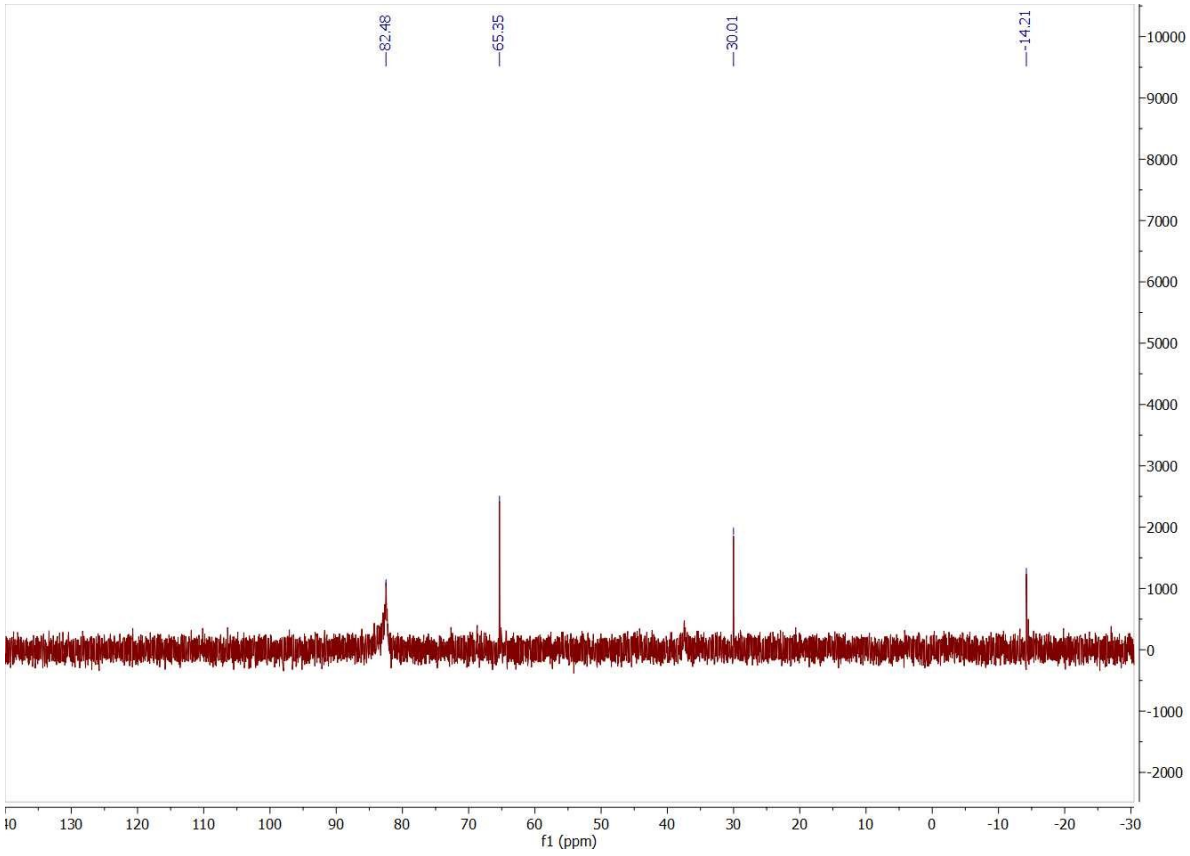


**Figure S86.** $^{31}P\{^{1}H\}$ NMR (toluene-$d_{8,}$ 202 MHz) of the NMR tube experiment for the oxidation of benzylamine with **2** (100:1 ratio), oxygen is used as an oxidant, time 8 h.

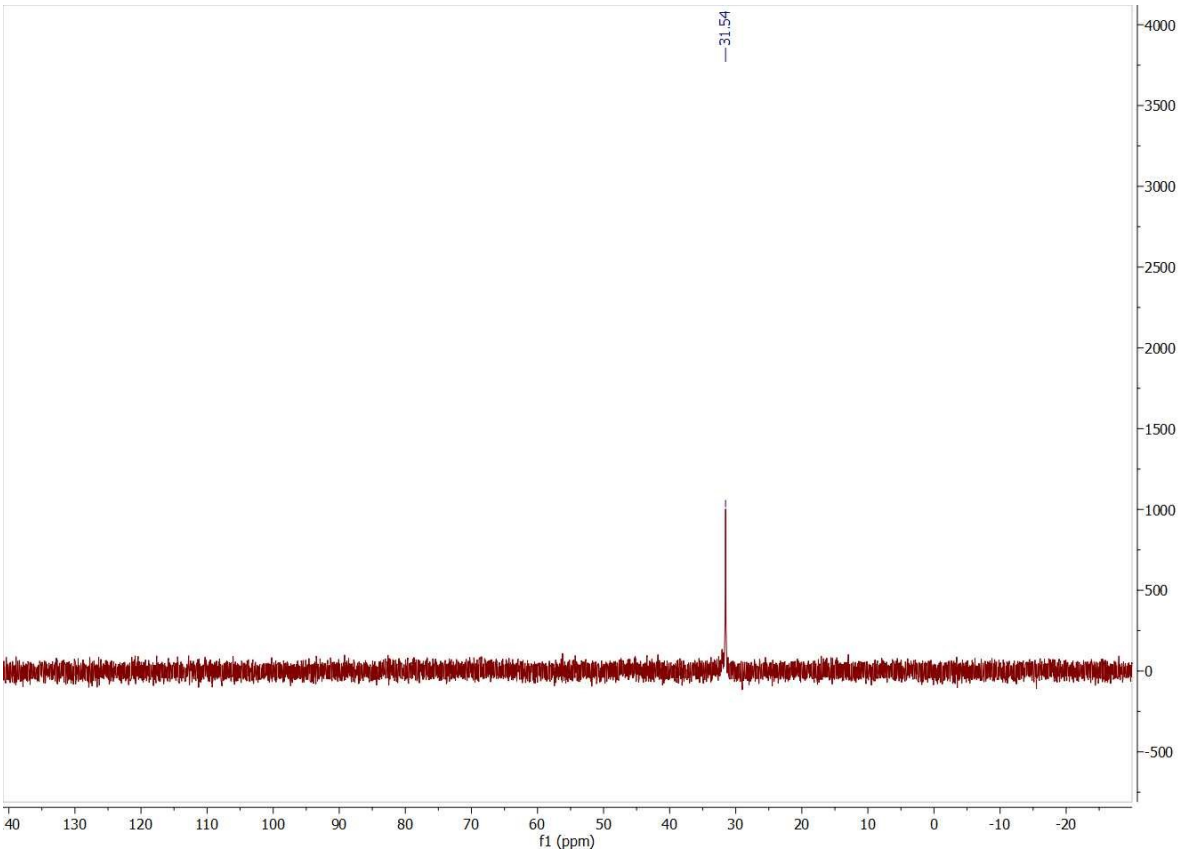


**Figure S87.** $^{31}P\{^{1}H\}$ NMR (toluene-$d_{8,}$ 202 MHz) of the NMR tube experiment for the oxidation of benzylamine with **2** (100:1 ratio), oxygen is used as an oxidant, time 14 h.

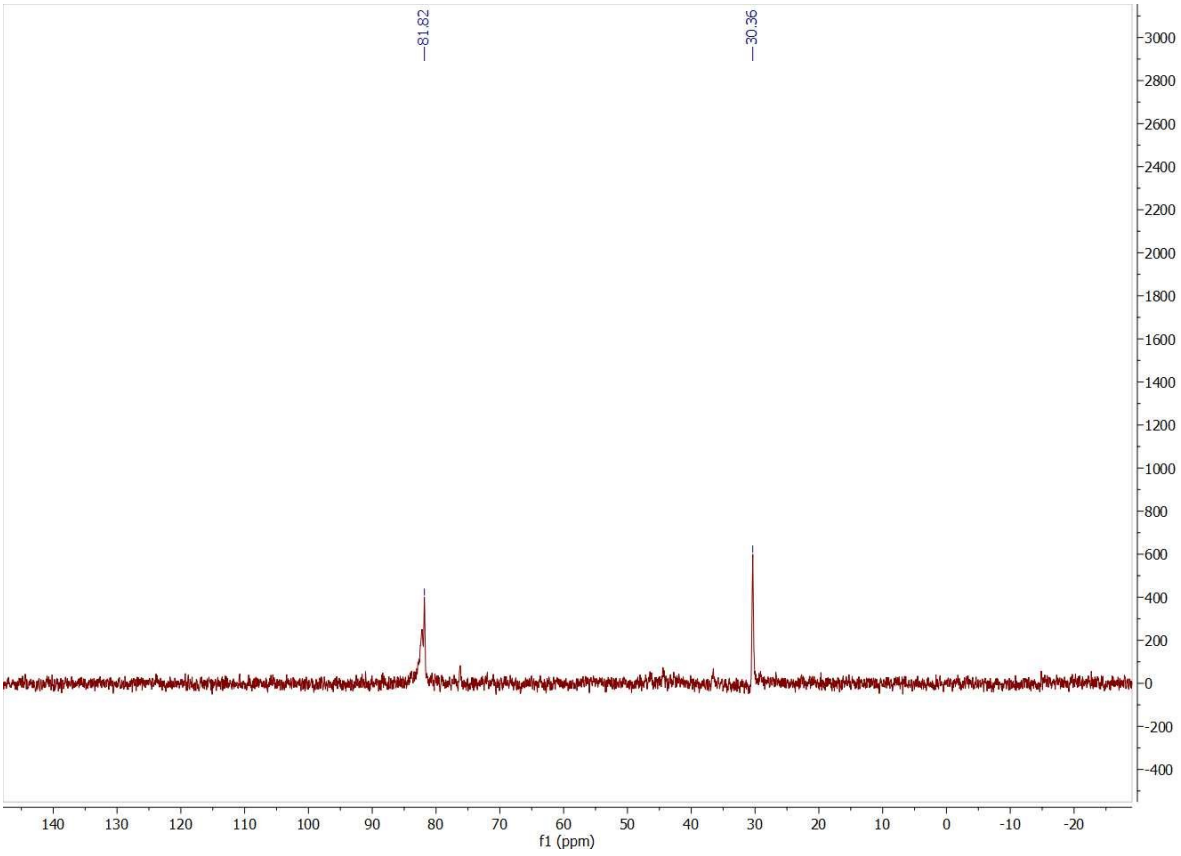


**Figure S88.** $^{31}P\{^{1}H\}$ NMR (toluene-$d_{8,}$ 202 MHz) of the NMR tube experiment for a mixture of benzylamine with **2** (100:1 ratio), argon atmosphere is used to prohibit any oxidation of benzylamine, time 2 h.

## 7. Tests of stability of 2

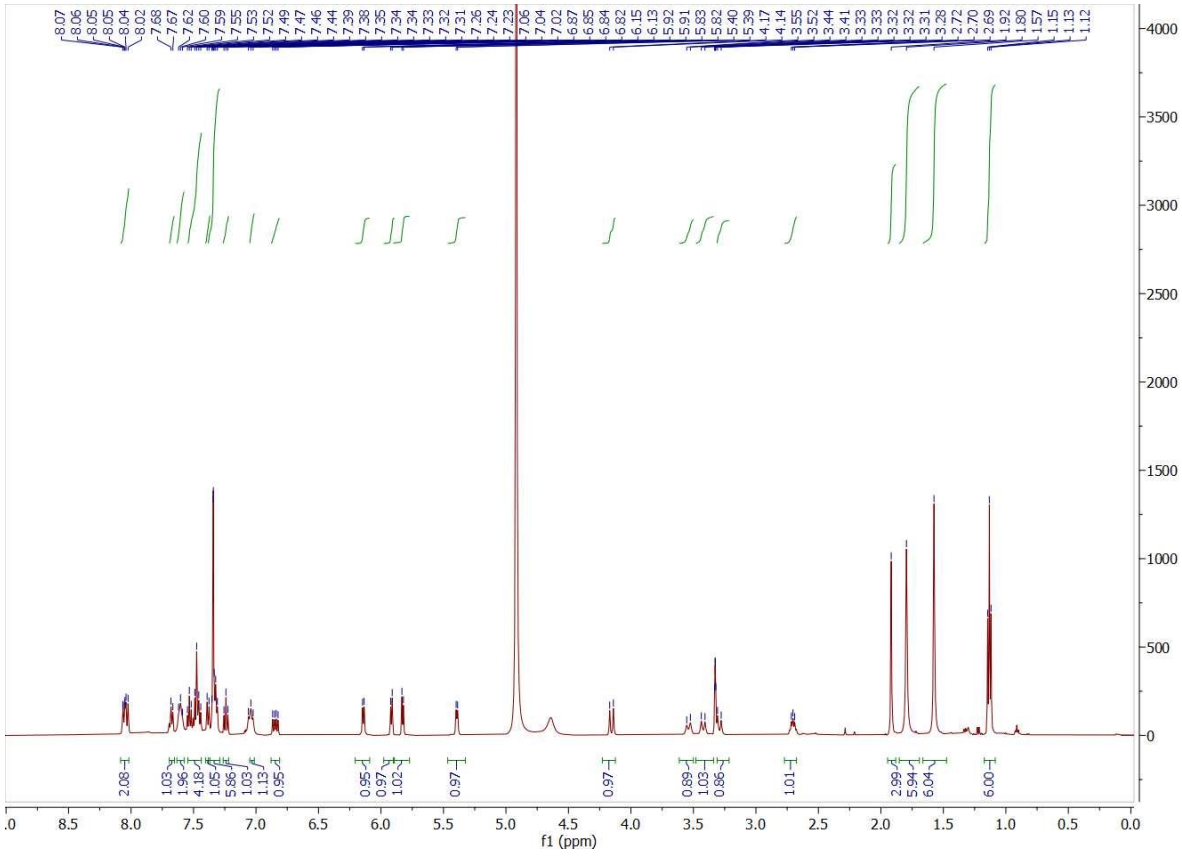


**Figure S89.** $^{1}$H NMR ($CD_3OD$, 500MHz) of compound **2** in $CD_3OD$, measured after 1 h in the air atmosphere at rt.

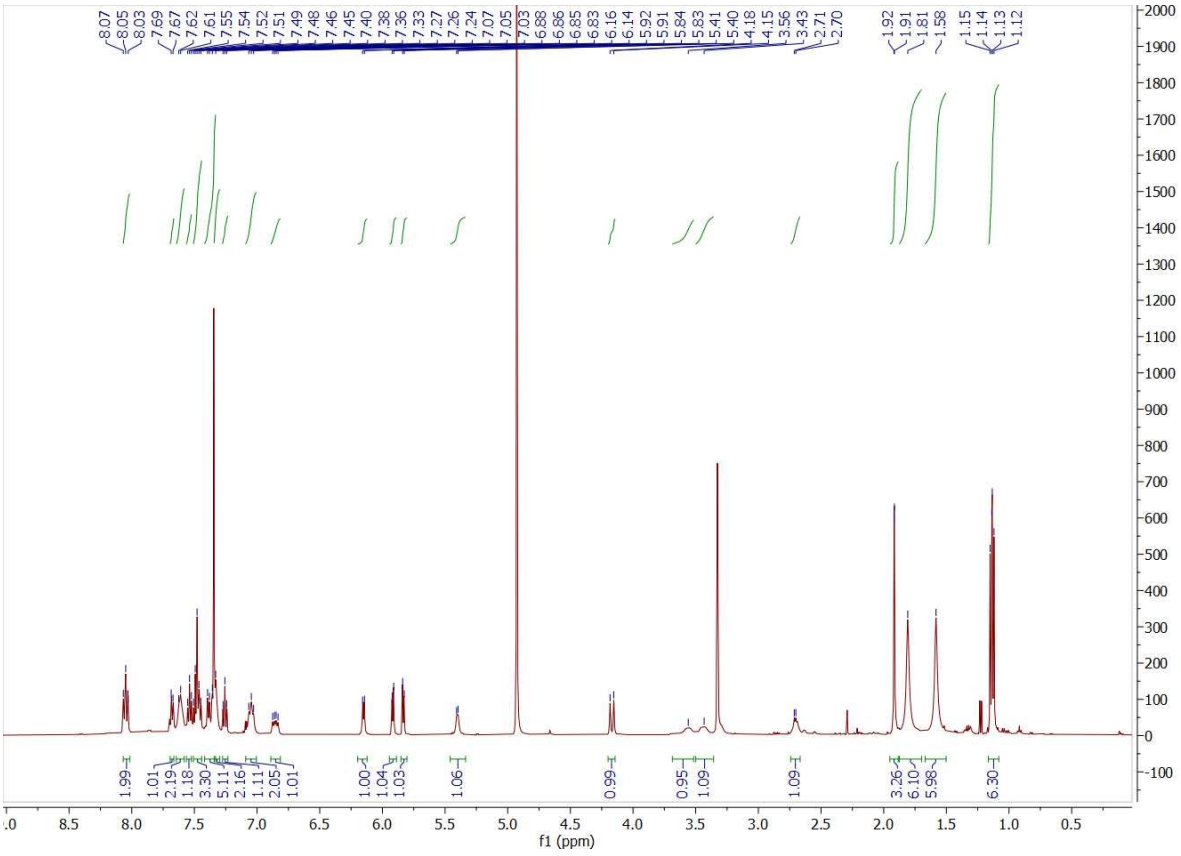


**Figure S90.** $^{1}$H NMR ($CD_3OD$, 500MHz) of compound **2** in $CD_3OD$, measured after 24 h in the air atmosphere at rt.

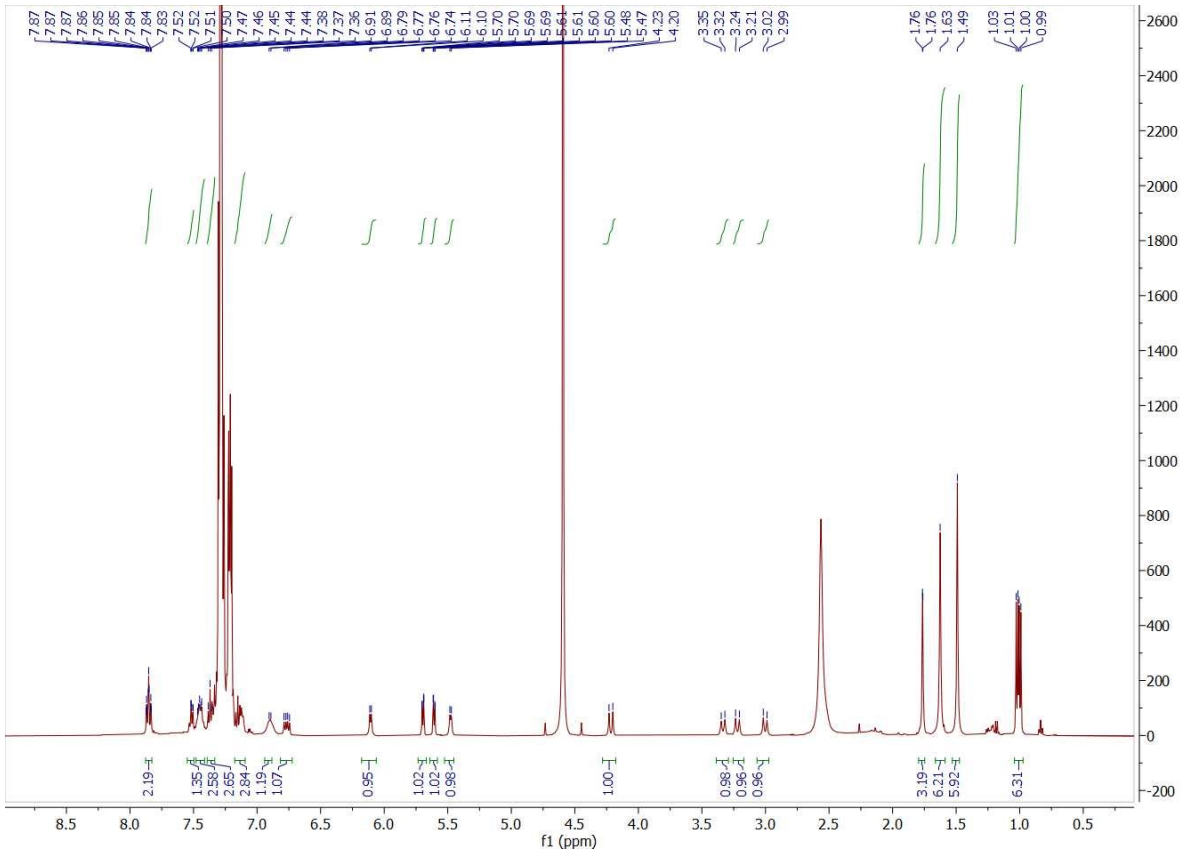


**Figure S91.** $^{1}$H NMR ($CDCl_3$, 500MHz) of compound **2** in the presence of benzyl alcohol, measured after 24 h in the air atmosphere at rt.

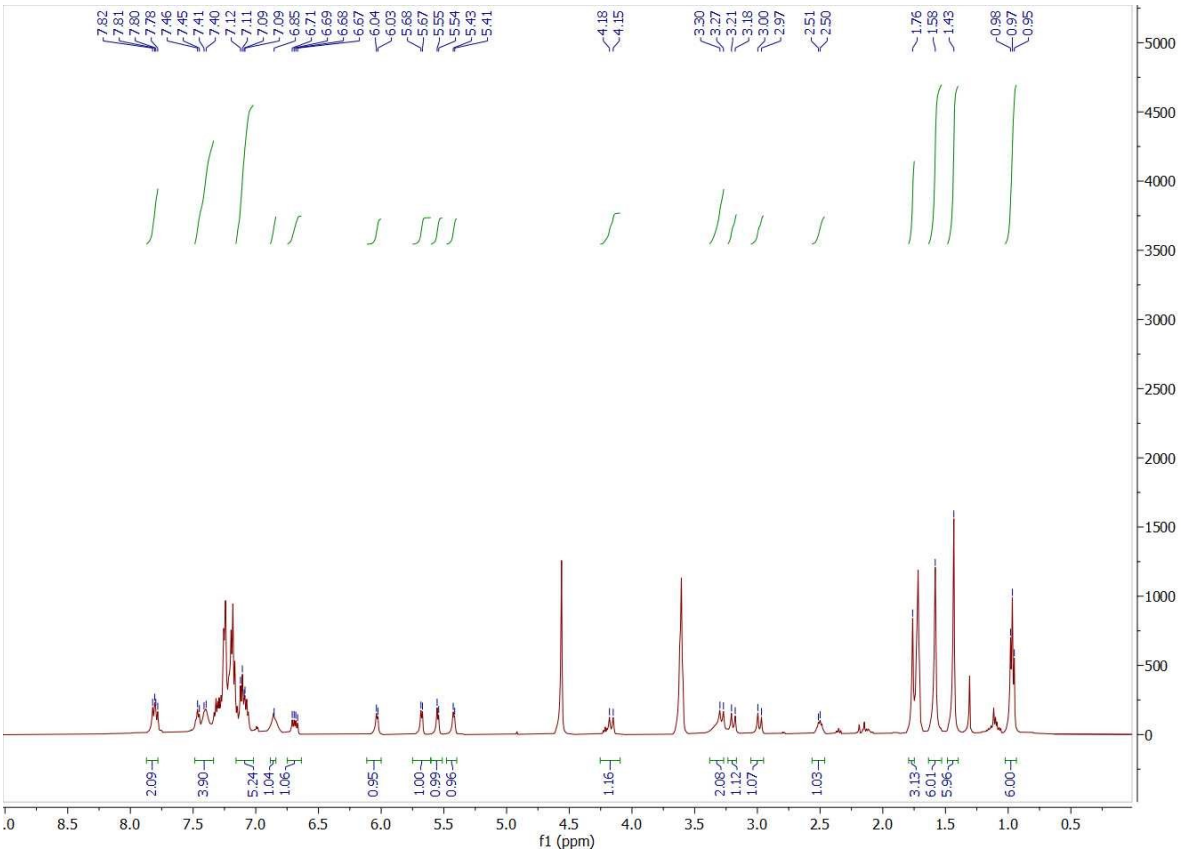


**Figure S92.** $^{1}$H NMR ($CDCl_3$, 500MHz) of compound **2** in the presence of benzyl alcohol, measured in the air atmosphere after heating to 50°C for 2 h.

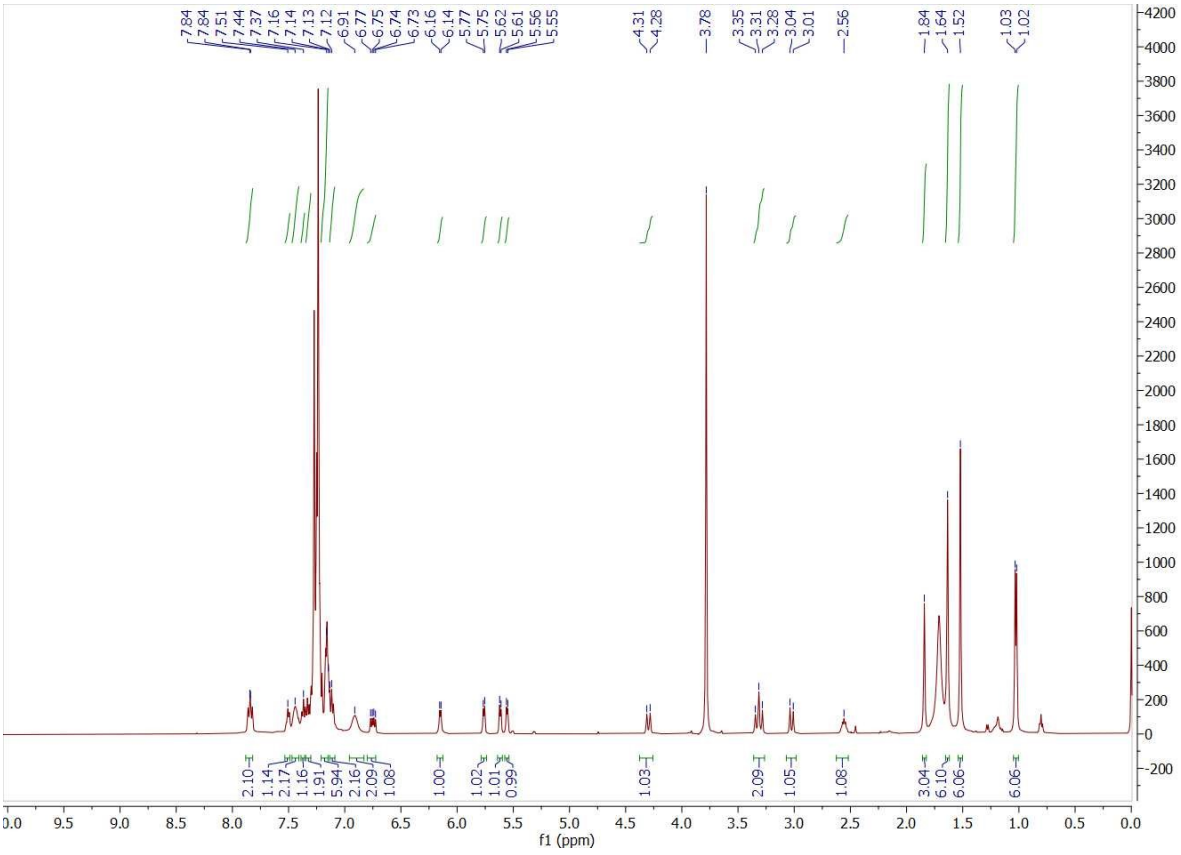


**Figure S93.** $^{1}H$ NMR ($CDCl_3$, 500MHz) of compound **2** in the presence of benzylamine, measured after 24 h in the air atmosphere at rt

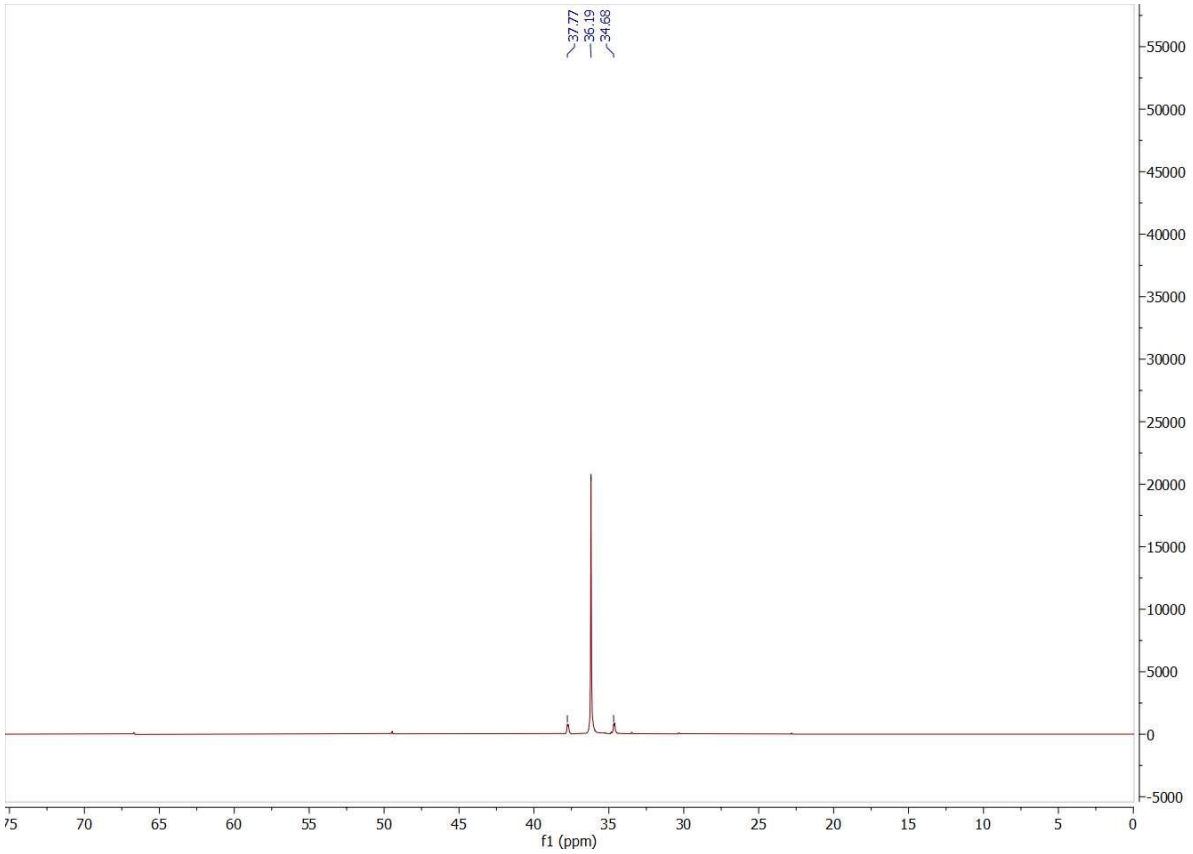


**Figure S94.** $^{31}P\{^{1}H\}$ NMR ($CD_3OD$, 202 MHz) of compound **2** in $CD_3OD$, measured after 1 h in the air atmosphere at rt.

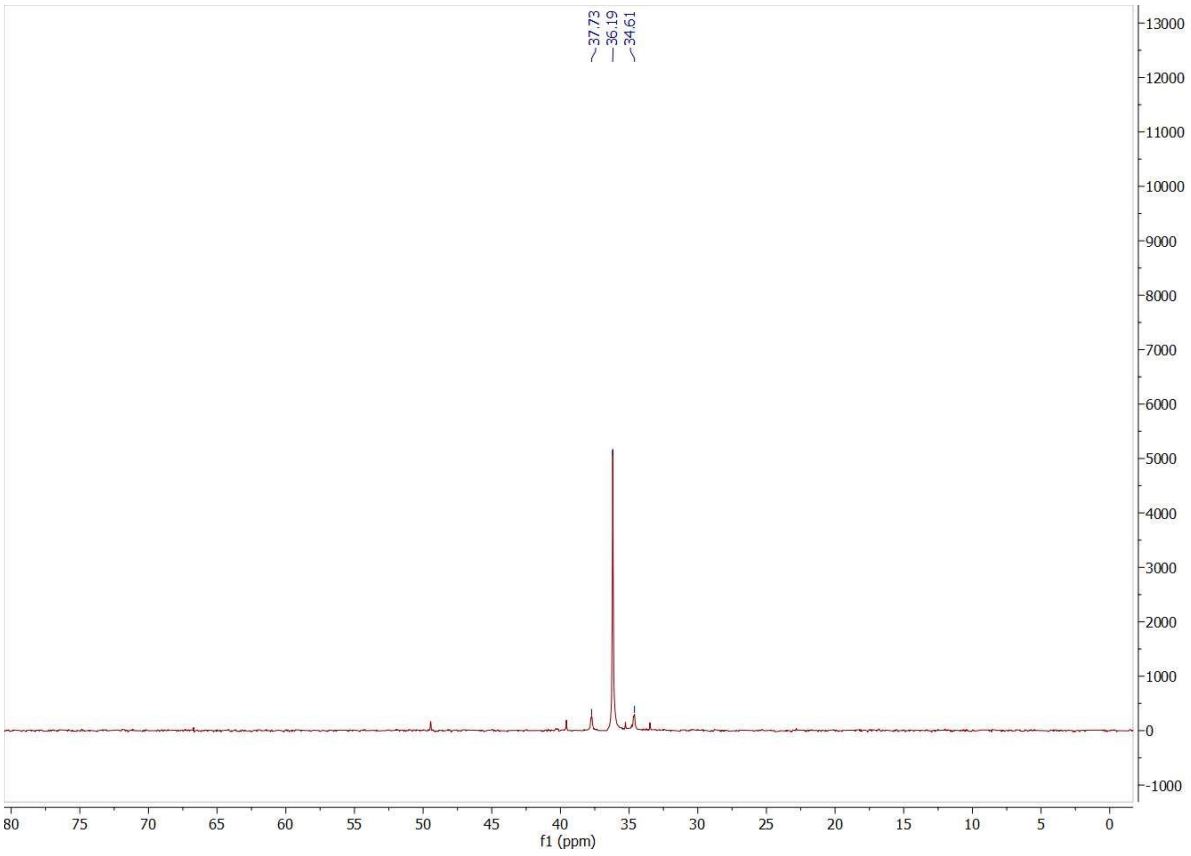


**Figure S95.** $^{31}P\{^{1}H\}$ NMR ($CD_3OD$, 202 MHz) of compound **2** in $CD_3OD$, measured after 24 h in the air atmosphere at rt.

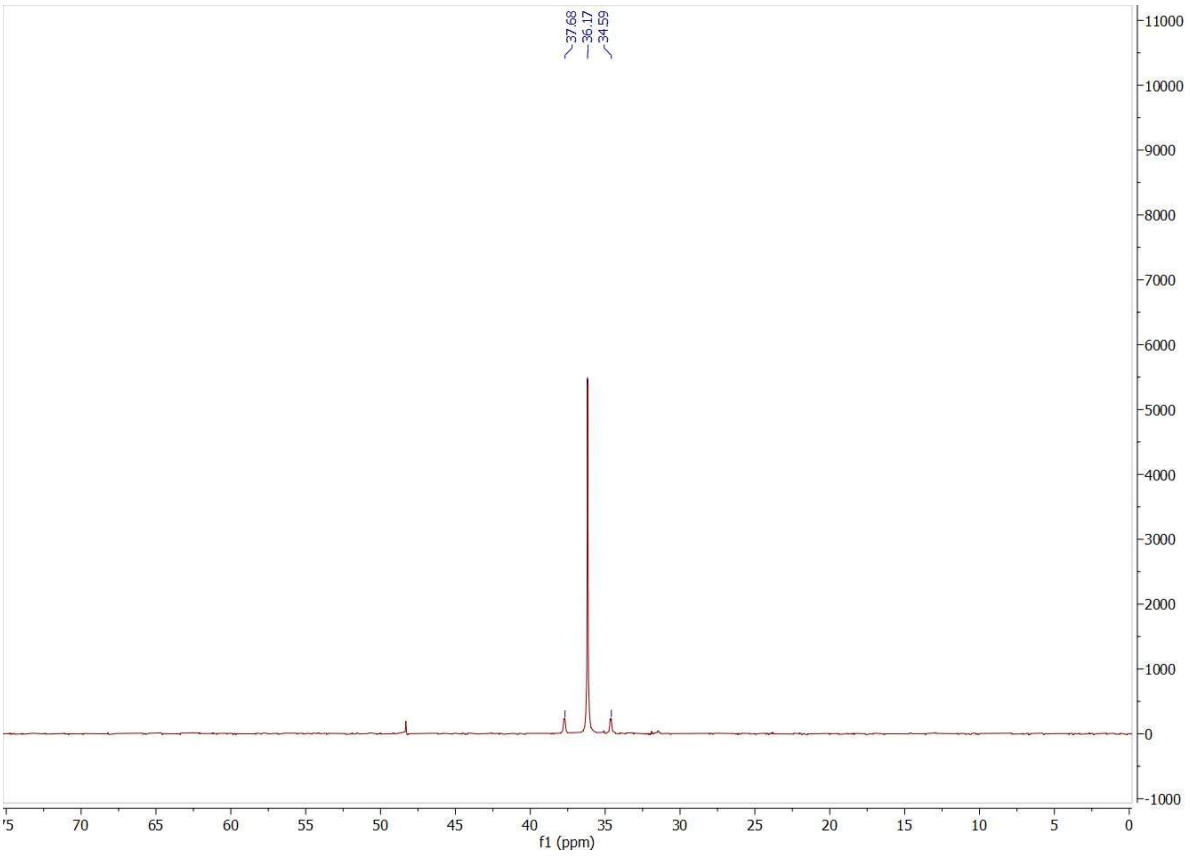


**Figure S96.** $^{31}P\{^{1}H\}$ NMR ($CDCl_3$, 202 MHz) of compound **2** in the presence of benzyl alcohol, measured after 24 h in the air atmosphere at rt.

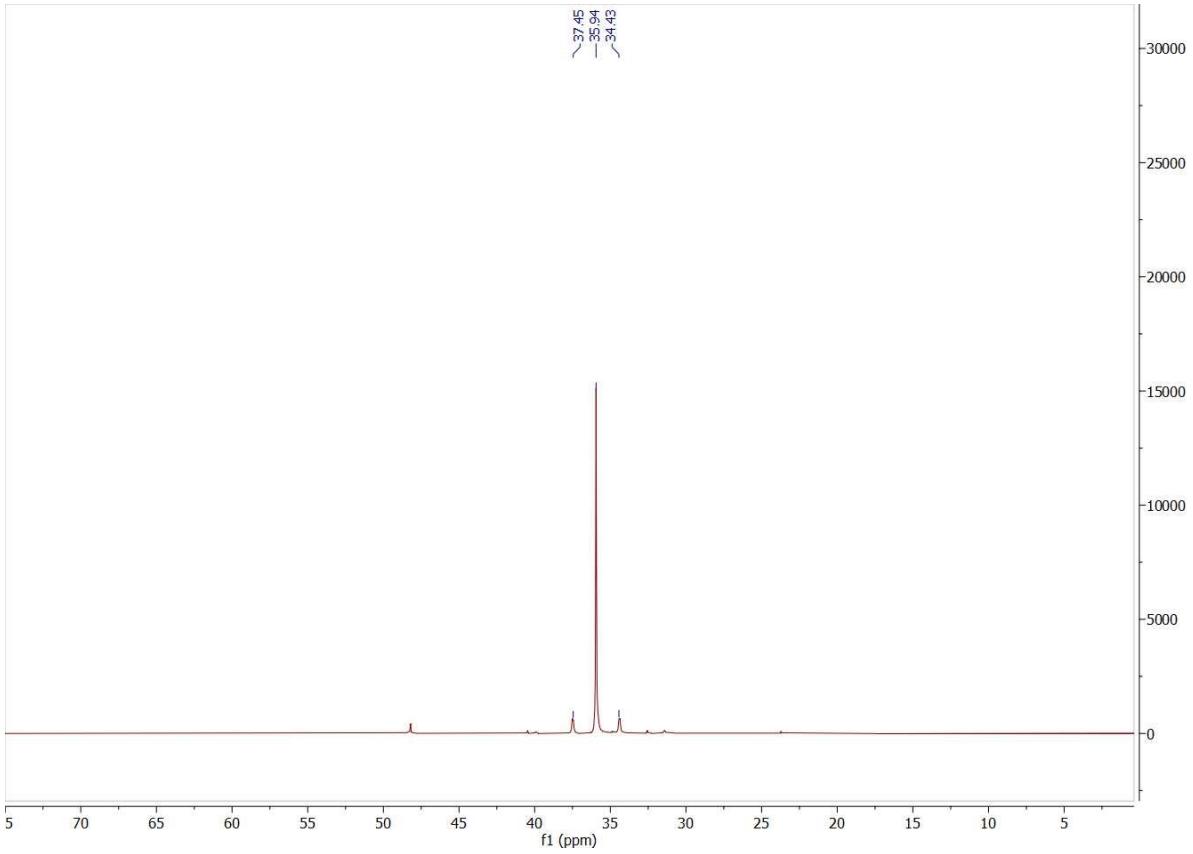


**Figure S97.** $^{31}P\{^{1}H\}$ NMR ($CDCl_3$, 202 MHz) of compound **2** in the presence of benzyl alcohol, measured after 24 h in the air atmosphere after heating to 50°C for 2 h.

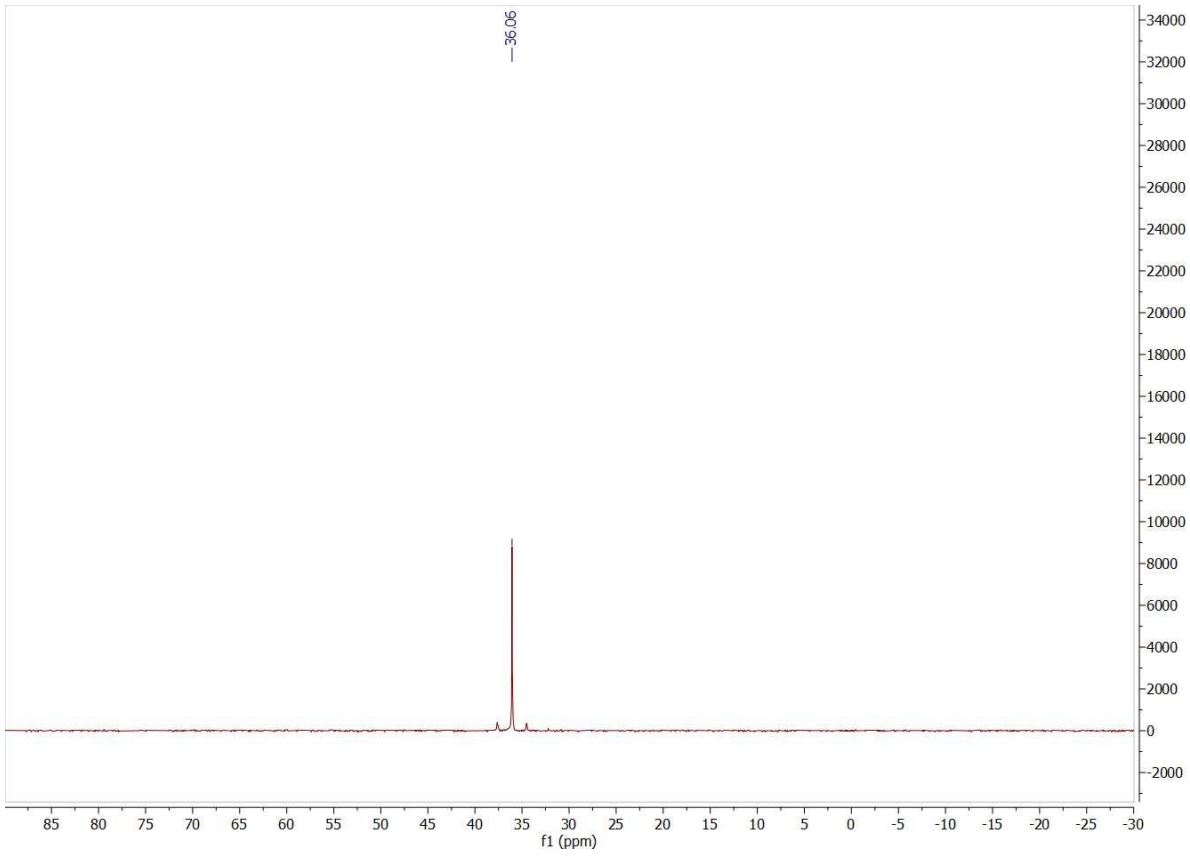


**Figure S98.** $^{31}P\{^{1}H\}$ NMR ($CDCl_3$, 202 MHz) of compound **2** in the presence of benzylamine, measured after 24 h in the air atmosphere at rt.

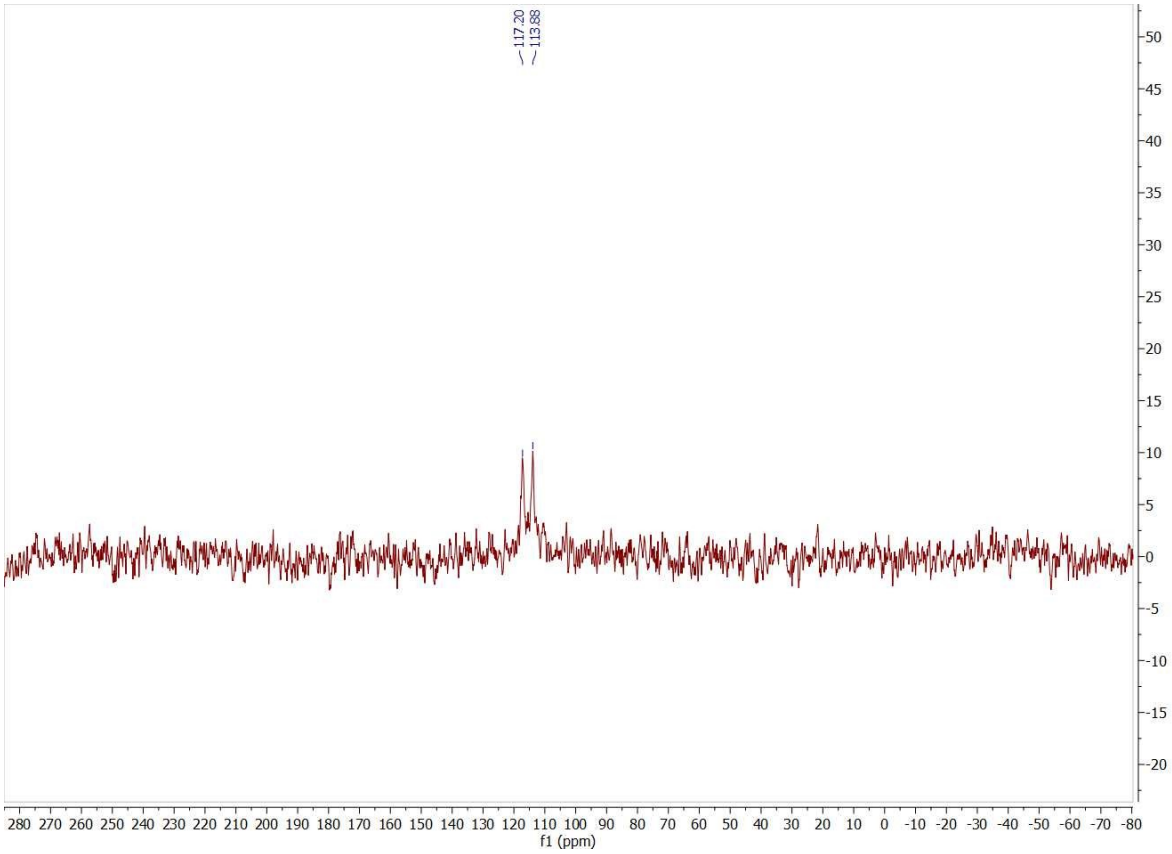


**Figure S99.** $^{119}Sn\{^{1}H\}$ NMR ($CD_3OD$, 186 MHz) of compound **2** in $CD_3OD$, measured after 1 h in the air atmosphere at rt.

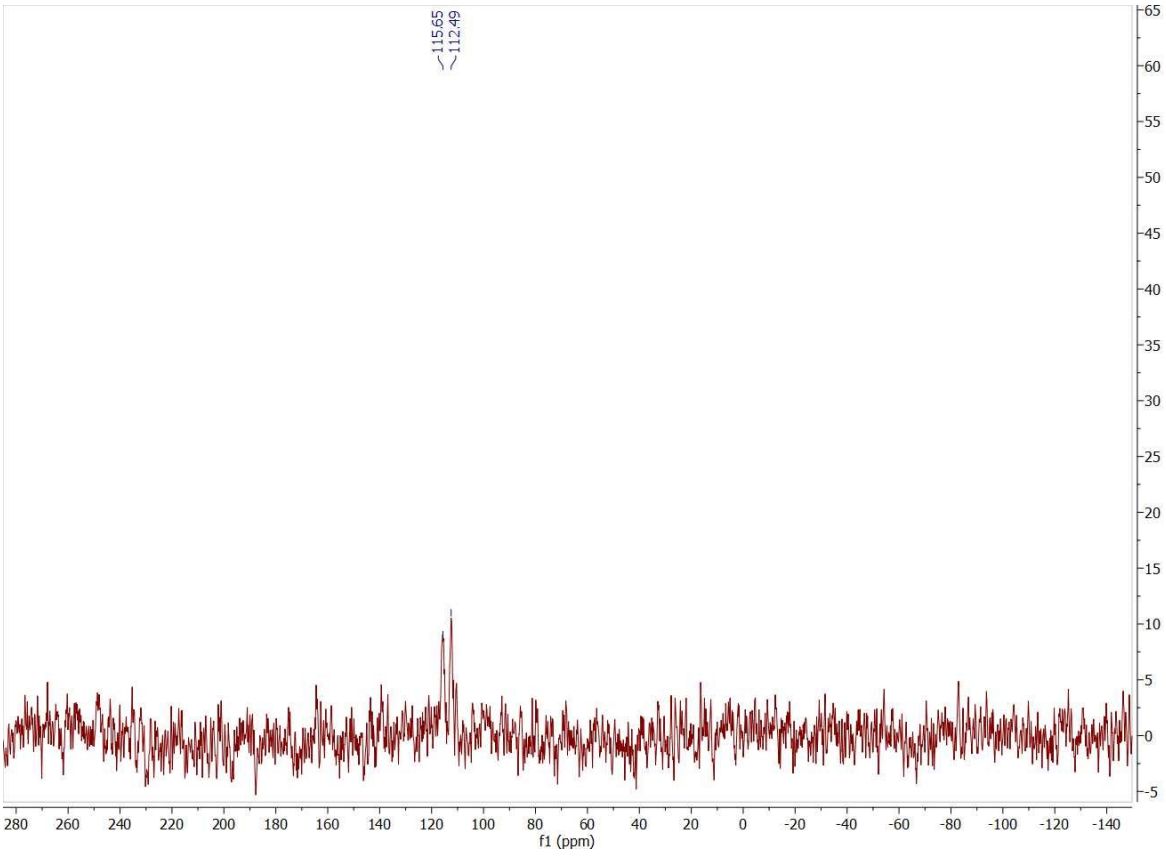


**Figure S100.** $^{119}Sn\{^{1}H\}$ NMR ($CD_3OD$, 186 MHz) of compound **2** in $CD_3OD$, measured after 24 h in the air atmosphere at rt.

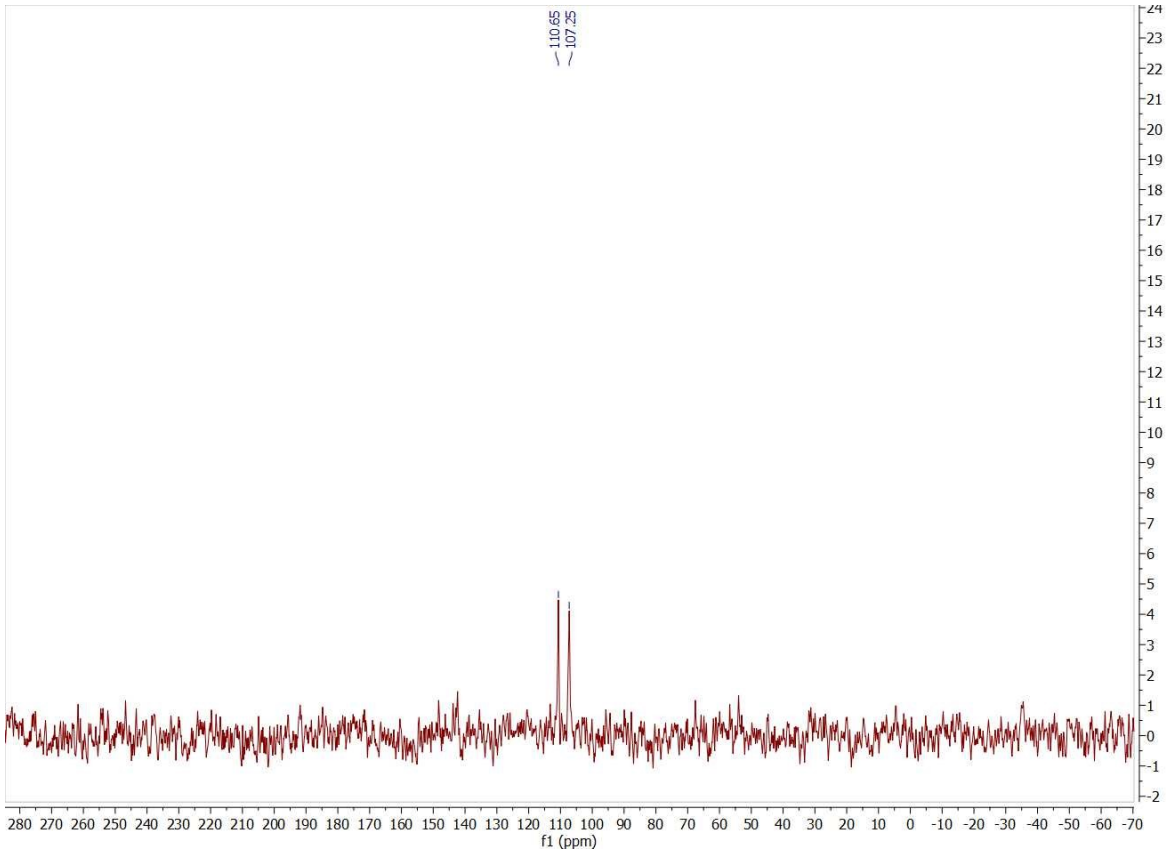


**Figure S101.** $^{119}Sn\{^{1}H\}$ NMR ($CDCl_3$, 186 MHz) of compound **2** in the presence of benzyl alcohol, measured after 24 h in the air atmosphere at rt.

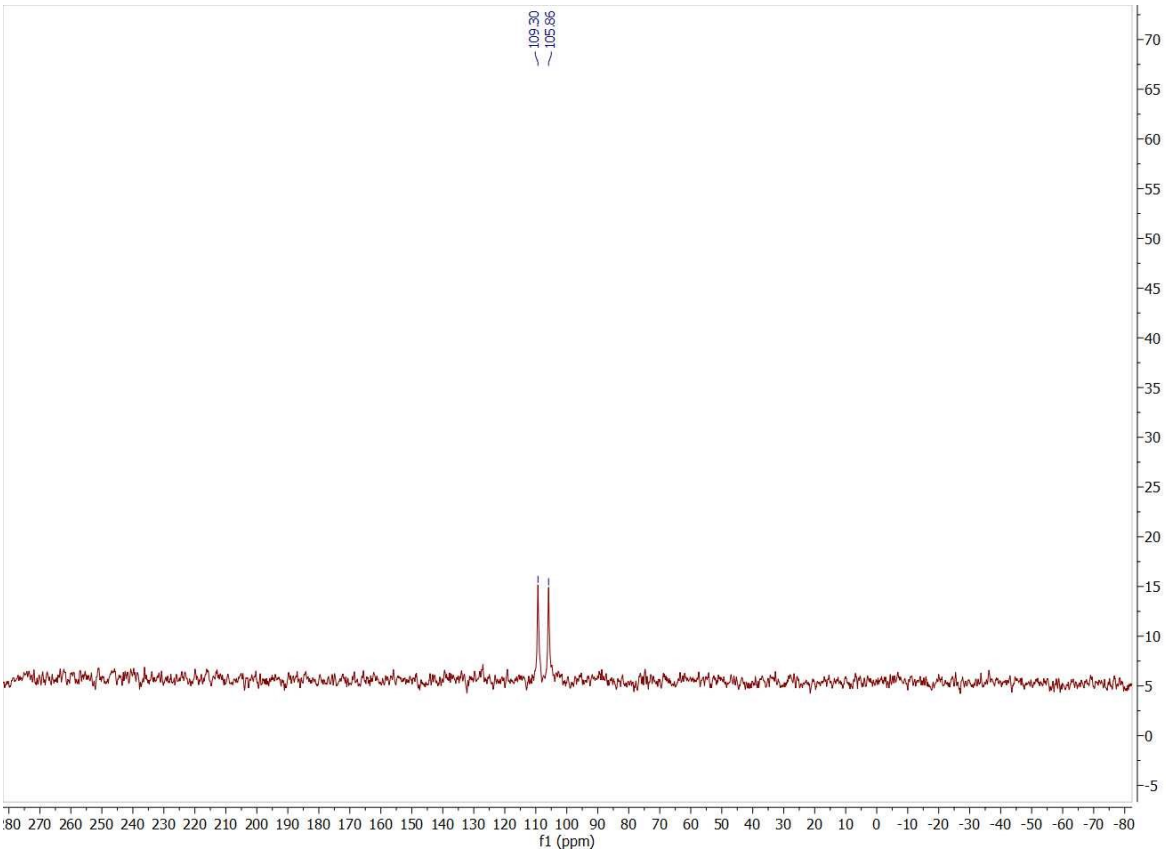


**Figure S102.** $^{119}Sn\{^{1}H\}$ NMR ($CDCl_3$, 186 MHz) of compound **2** in the presence of benzyl alcohol, measured in the air atmosphere after heating to 50°C for 2 h.

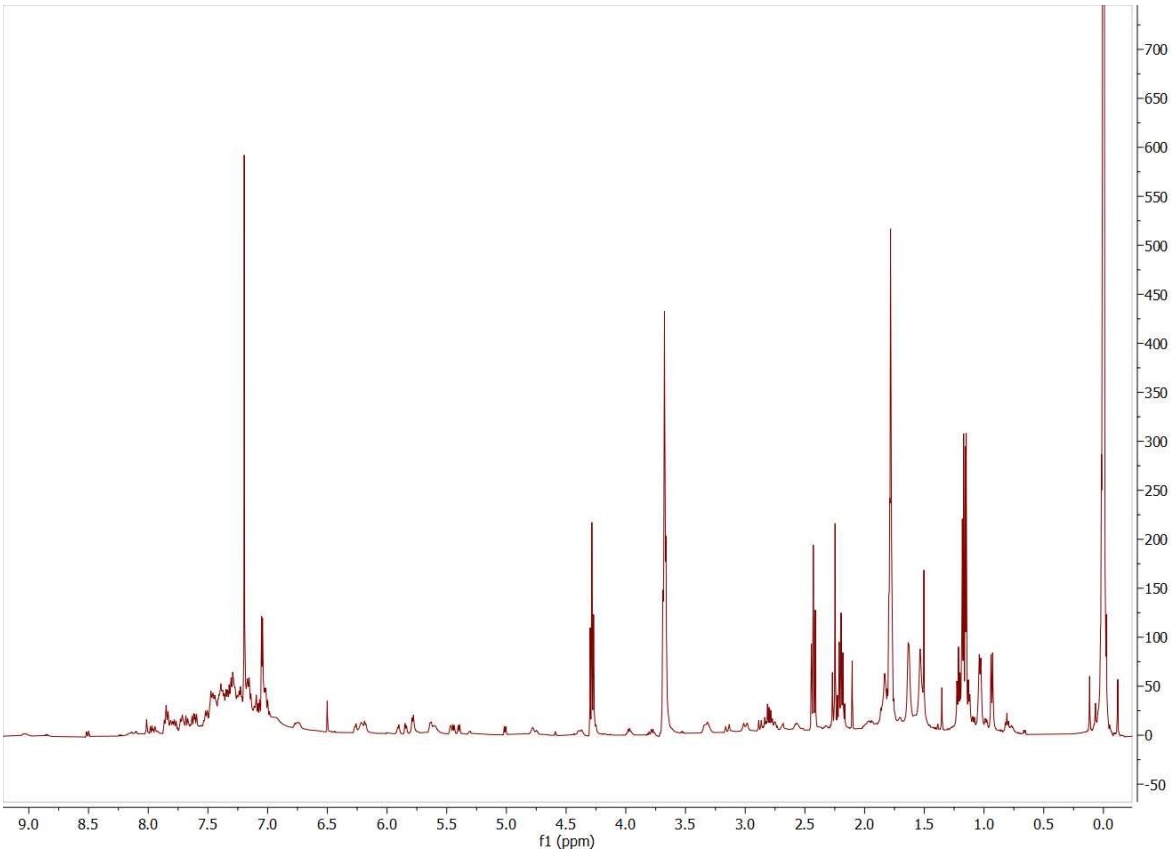


**Figure S103.** $^{1}H$ NMR ($CDCl_3$, 500MHz) spectrum of the reaction mixture received after reaction of **2** with $O_2$ in THF (heating at 60 °C for 24 h).

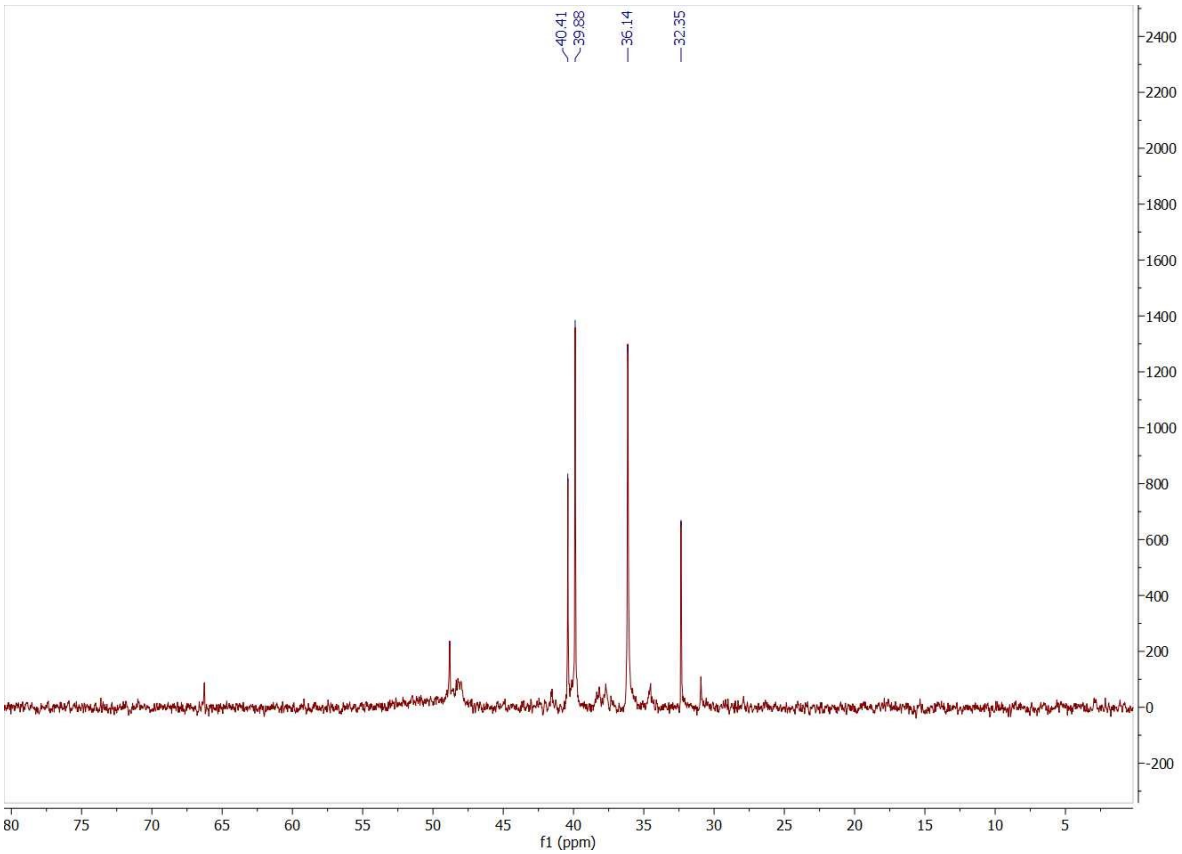


**Figure S104.** $^{31}P\{^{1}H\}$ NMR ($CDCl_3$, 202MHz) spectrum of the reaction mixture received after reaction of **2** with $O_2$ in THF (heating at 60 °C for 24 h).

## 8. Crystallographic data

**Table S9.** Crystallographic data of **2.**2($H_2O$).

| | |
|---|---|
| Crystal data | |
| Chemical formula | $C_{56}H_{65}Cl_2N_2O_2PRuSn$ |
| $M_r$ | 1119.73 |
| Crystal system, space group | Triclinic, *P*-1 |
| Temperature (K) | 150 |
| *a*, *b*, *c* (Å) | 9.5879 (4), 15.9384 (7), 17.1123 (7) |
| α, β, γ (°) | 96.625 (2), 103.202 (2), 94.788 (2) |
| *V* (Å$^3$) | 2512.56 (19) |
| *Z* | 2 |
| Radiation type | Mo *K*α |
| μ (mm$^{-1}$) | 0.98 |
| Crystal size (mm) | 0.14 × 0.11 × 0.07 |
| Data collection | |
| Diffractometer | Bruker D8 - Venture |
| Absorption correction | Multi-scan<br>*SADABS2016*/2 - Bruker AXS area detector scaling and absorption correction |
| $T_{min}$, $T_{max}$ | 0.561, 0.746 |
| No. of measured, independent and observed [$I > 2\sigma(I)$] reflections | 74530, 11568, 10146 |
| $R_{int}$ | 0.041 |
| $(\sin \theta/\lambda)_{max}$ (Å$^{-1}$) | 0.651 |
| Refinement | |
| $R[F^2 > 2\sigma(F^2)]$, $wR(F^2)$, *S* | 0.024, 0.054, 1.10 |
| No. of reflections | 11568 |
| No. of parameters | 625 |
| No. of restraints | 582 |
| H-atom treatment | H atoms treated by a mixture of independent and constrained refinement |
| $\Delta\rho_{max}$, $\Delta\rho_{min}$ (e Å$^{-3}$) | 0.43, −0.75 |

Computer programs: Bruker Instrument Service vV6.2.3, *APEX3* v2016.5-0 (Bruker AXS), *SAINT* V8.37A (Bruker AXS Inc., 2015), XT, VERSION 2014/5, *SHELXL2017*/1 (Sheldrick, 2017), *PLATON* (Spek, 2009).

**Table S10.** Crystallographic details for **4**

| Crystal data | |
|---|---|
| Chemical formula | $C_{44}H_{50}ClN_2PRuSn$ |
| $M_r$ | 893.04 |
| Crystal system, space group | Orthorhombic, $Pna2_1$ |
| Temperature (K) | 150 |
| $a$, $b$, $c$ (Å) | 32.4751 (11), 11.7571 (4), 10.4836 (3) |
| $V$ (Å$^3$) | 4002.8 (2) |
| $Z$ | 4 |
| Radiation type | Mo $K\alpha$ |
| μ (mm$^{-1}$) | 1.14 |
| Crystal size (mm) | 0.30 × 0.23 × 0.20 |
| **Data collection** | |
| Diffractometer | Bruker D8 - Venture |
| Absorption correction | Multi-scan<br>*SADABS2016*/2 - Bruker AXS area detector scaling and absorption correction |
| $T_{min}$, $T_{max}$ | 0.660, 0.746 |
| No. of measured, independent and observed [$I > 2\sigma(I)$] reflections | 52302, 10755, 8611 |
| $R_{int}$ | 0.061 |
| $(\sin \theta/\lambda)_{max}$ (Å$^{-1}$) | 0.745 |
| **Refinement** | |
| $R[F^2 > 2\sigma(F^2)]$, $wR(F^2)$, $S$ | 0.041, 0.059, 1.03 |
| No. of reflections | 10755 |
| No. of parameters | 460 |
| No. of restraints | 1 |
| H-atom treatment | H-atom parameters constrained |
| $\Delta\rho_{max}$, $\Delta\rho_{min}$ (e Å$^{-3}$) | 0.78, −0.73 |
| Absolute structure | Flack x determined using 2877 quotients [(I+)-(I-)]/[(I+)+(I-)] (Parsons, Flack and Wagner, Acta Cryst. B69 (2013) 249-259). |
| Absolute structure parameter | −0.009 (10) |

Computer programs: Bruker Instrument Service vV6.2.3, *APEX3* v2016.5-0 (Bruker AXS), *SAINT* V8.37A (Bruker AXS Inc., 2015), XT, VERSION 2014/5, *SHELXL2017*/1 (Sheldrick, 2017), *PLATON* (Spek, 2009).

**Table S11.** Crystallographic details for **3**·2($C_6H_6$)

| | |
|---|---|
| Crystal data | |
| Chemical formula | $C_{44}H_{49}I_2N_2PRuSn·2(C_6H_6)$ |
| $M_r$ | 1266.59 |
| Crystal system, space group | Triclinic, *P*-1 |
| Temperature (K) | 150 |
| *a*, *b*, *c* (Å) | 13.6053 (8), 18.8739 (10), 20.0434 (12) |
| α, β, γ (°) | 85.037 (3), 79.518 (3), 85.220 (3) |
| *V* (Å$^3$) | 5030.0 (5) |
| *Z* | 4 |
| Radiation type | Mo *K*α |
| μ (mm$^{-1}$) | 2.10 |
| Crystal size (mm) | 0.59 × 0.42 × 0.13 |
| Data collection | |
| Diffractometer | Bruker D8 - Venture |
| Absorption correction | Multi-scan<br>*SADABS2016*/2 - Bruker AXS area detector scaling and absorption correction |
| $T_{min}$, $T_{max}$ | 0.462, 0.747 |
| No. of measured, independent and observed [$I > 2\sigma(I)$] reflections | 199430, 35932, 19899 |
| $R_{int}$ | 0.107 |
| $(\sin\theta/\lambda)_{max}$ (Å$^{-1}$) | 0.781 |
| Refinement | |
| $R[F^2 > 2\sigma(F^2)]$, $wR(F^2)$, *S* | 0.107, 0.225, 1.05 |
| No. of reflections | 35932 |
| No. of parameters | 1038 |
| No. of restraints | 1127 |
| H-atom treatment | H-atom parameters constrained<br>$w = 1/[\sigma^2(F_o^2) + (0.0142P)^2 + 159.3859P]$<br>where $P = (F_o^2 + 2F_c^2)/3$ |
| $\Delta\rho_{max}$, $\Delta\rho_{min}$ (e Å$^{-3}$) | 4.06, −7.20 |

Computer programs: Bruker Instrument Service vV6.2.3, *APEX3* v2016.5-0 (Bruker AXS), *SAINT* V8.37A (Bruker AXS Inc., 2015), XT, VERSION 2014/5, *SHELXL2017*/1 (Sheldrick, 2017), *PLATON* (Spek, 2009).

## References

[S1] see for example (a) T. J. Colacot and S. F. Neelamkavil, in Handbook of Reagents for Organic Synthesis: Catalytic Oxidation Reagents, ed. P. L. Fuchs, Viley-VCH, Weinheim, 2013, 546–549; (b) H. Brunner, M. Weber and M. Zabel, Coord. Chem. Rev., 2003, 242, 3; (c) M. A. Bennett, in Comprehensive Organometallic Chemistry II, ed. E. E. Abel, F. G. A. Stone and G. Wilkinson, Elsevier, Amsterdam, 1995, vol. 7, pp. 549–602.
[S2] J. Brugos, J. A. Cabeza, P. García-Álvarez, E. Pérez-Carreño and D. Polo, *Dalton Trans.*, 2018, **47**, 4534
[S3] (a) L. Alvarez-Rodriguez, J. A. Cabeza, P. Garcia-Alvarez and E. Perez-Carreno, *Organometallics*, 2018, **37**, 3399; (b) G. Albertin, S. Antoniutti, A. Bacchi, G. Pelizzi and G. Zanardo, *Organometallics*, 2008, **27**, 4407; (c) J. Brugos, J. A. Cabeza, P. García-Álvarez, E. Pérez-Carreño and D. Polo, *Dalton Trans.*, 2018, **47**, 4534; (d) T. Güadt, K. Eichele and L. Wesemann, *Dalton Trans.*, 2006, 2706; (e) J. Martincova, R. Dostalova, L. Dostal, A. Ruzicka and R. Jambor, *Organometallics,* 2009, **28**, 4823; (f) M. Novák, M. Bouška, L. Dostál, M. Lutter, K. Jurkschat, J. Turek, F. De Proft, Z. Růžičková and R. Jambor, *Eur. J. Inorg. Chem.*, 2017, **9**, 1292; (g) P. W. Smith, R. C. Handford and T. D. Tilley, *Organometallics* 2019, **38**, 4060.
[S4] (a) J. A. Cabeza, P. Garcia-Alvarez, C. J. Laglera-Gandara and E. Perez-Carreno, *Dalton. Trans.* 2020, **49,** 8331; (b) J. A. Cabeza, P. Garcia-Alvarez and C. J. Laglera-Gandara, Eur. J. Inorg. Chem., 2020, **10,** 784; (c) S. Freitag, K. M. Krebs, J. Henning, J. Hirdler, H. Schubert, P. Sirsch and L. Wesemann, *Organometallics*, 2013, **32**, 6785; (d) K. M. Krebs, S. Freitag, J.-J. Maudrich, H. Schubert, P. Sirsch and L. Wesemann, *Dalton Trans.*, 2018, **47**, 83; (e) K. M. Krebs, J.-J. Maudrich and L. Wesemann, *Dalton Trans.*, 2016, **45**, 8081; (f) J. Brugos, J. A. Cabeza, P. García-Álvarez, E. Pérez-Carreño and D. Polo, *Dalton Trans.*, 2018, **47**, 4534; (g) M. Balmer, Y. J. Franzke, F. Weigend and C. von Hanisch, *Chem. - A Eur. J.*, 2020, **26**, 192; (h) K. Izod, P. Evans, P. G. Waddell, M. R. Probert, and R. Michael, *Inorg. Chem*., 2016, **55,** 10510.
[S5] (a) J. P. Foster and F. Weinhold, *J. Am. Chem. Soc.*, 1980, **102**, 7211; (b) F. Weinhold, *J. Comput. Chem.*, 2012, **33**, 2363, and references therein; (c) C. R. Landis and F. Weinhold, in The Chemical Bond: Fundamental Aspects of Chemical Bonding, eds. G. Frenking and S. Shaik, Wiley-VCH, Weinheim, 2014
[S6] K. B. Wiberg, *Tetrahedron*, 1968, **24**, 1083.
[S7] M. Aman, L. Dostál, Z. Růžičková, S. Mebs, J. Beckmann and R. Jambor, *Organometallics,* 2019, **38**, 816
[S8] Gaussian 16, Revision A.03, M. J. Frisch, G. W. Trucks, H. B. Schlegel, G. E. Scuseria, M. A. Robb, J. R. Cheeseman, G. Scalmani, V. Barone, G. A. Petersson, H. Nakatsuji, X. Li, M. Caricato, A. V. Marenich, J. Bloino, B. G. Janesko, R. Gomperts, B. Mennucci, H. P. Hratchian, J. V. Ortiz, A. F. Izmaylov, J. L. Sonnenberg, D. Williams-Young, F. Ding, F. Lipparini, F. Egidi, J. Goings, B. Peng, A. Petrone, T. Henderson, D. Ranasinghe, V. G. Zakrzewski, J. Gao, N. Rega, G. Zheng, W. Liang, M. Hada, M. Ehara, K. Toyota, R. Fukuda, J. Hasegawa, M. Ishida, T. Nakajima, Y. Honda, O. Kitao, H. Nakai, T. Vreven, K. Throssell, J. A. Montgomery, Jr., J. E. Peralta, F. Ogliaro, M. J. Bearpark, J. J. Heyd, E. N. Brothers, K. N. Kudin, V. N. Staroverov, T. A. Keith, R. Kobayashi, J. Normand, K. Raghavachari, A. P.

Rendell, J. C. Burant, S. S. Iyengar, J. Tomasi, M. Cossi, J. M. Millam, M. Klene, C. Adamo, R. Cammi, J. W. Ochterski, R. L. Martin, K. Morokuma, O. Farkas, J. B. Foresman, and D. J. Fox, Gaussian, Inc., Wallingford CT, 2016.
[S9] (a) S. H. Vosko, L. Wilk and M. Nusair, *Can. J. Phys.*, 1980, **58**, 1200; (b) C. Lee, W. Yang and R. G. Parr, *Phys. Rev. B*, 1988, **37**, 785; (c) A. D. Becke, *J. Chem. Phys.*, 1993, **98**, 5648; (d) P. J. Stephens, F. J. Devlin, C. F. Chabalowski and M. J. Frisch, *J. Phys. Chem.*, 1994, **98**, 11623; (e) S. Grimme, J. Antony, S. Ehrlich and H. Krieg, *J. Chem. Phys.*, 2010, **132**, 154104.
[S10] (a) T. H. Dunning, *J. Chem. Phys.*, 1989, **90**, 1007; (b) D. E. Woon and T. H . Dunning, *J. Chem. Phys.*, 1993, **98**, 1358.
[S11] (a) B. Metz, H. Stoll and M. Dolg, *J. Chem. Phys.*, 2000, **113**, 2563; (b) K. A. Peterson, *J. Chem. Phys.*, 2003, **119**, 11099; (c) K. A. Peterson, D. Figgen, E. Goll, H. Stoll and M. Dolg, *J. Chem. Phys.*, 2003, **119**, 11113; (d) K. A. Peterson, B. C. Shepler, D. Figgen and H. Stoll, *J. Phys. Chem. A*, 2006, **110**, 13877; (e) K. A. Peterson, D. Figgen, M. Dolg and H. Stoll, *J. Chem. Phys.*, 2007, **126**, 124101
[S12] A. V. Marenich, C. J. Cramer and D. G. Truhlar, *J. Phys. Chem. B*, 2009, **113**, 6378
[S13] G.M. Sheldrick, *Acta Crystalllogr., Sect. A,* 2015, **A71**, 3-8.
[S14] P. van der Sluis, A. L. Spek, *Acta Crystalllogr., Sect. A.,* 1990, **46**, 194.